



HAL
open science

A review on electrospun PVDF-based nanocomposites: Recent trends and developments in energy harvesting and sensing applications

Sreelakshmi Moozhiyil Purushothaman, Maïté Fernandes Tronco, Bicy Kottathodi, Isabelle Royaud, Marc Ponçot, Nandakumar Kalarikkal, Sabu Thomas, Didier Rouxel

► To cite this version:

Sreelakshmi Moozhiyil Purushothaman, Maïté Fernandes Tronco, Bicy Kottathodi, Isabelle Royaud, Marc Ponçot, et al.. A review on electrospun PVDF-based nanocomposites: Recent trends and developments in energy harvesting and sensing applications. *Polymer*, 2023, 283, pp.126179. 10.1016/j.polymer.2023.126179 . hal-04243721

HAL Id: hal-04243721

<https://hal.science/hal-04243721>

Submitted on 16 Oct 2023

HAL is a multi-disciplinary open access archive for the deposit and dissemination of scientific research documents, whether they are published or not. The documents may come from teaching and research institutions in France or abroad, or from public or private research centers.

L'archive ouverte pluridisciplinaire **HAL**, est destinée au dépôt et à la diffusion de documents scientifiques de niveau recherche, publiés ou non, émanant des établissements d'enseignement et de recherche français ou étrangers, des laboratoires publics ou privés.



Distributed under a Creative Commons Attribution - NonCommercial - NoDerivatives 4.0 International License

A review on electrospun PVDF-based nanocomposites: Recent trends and developments in energy harvesting and sensing applications

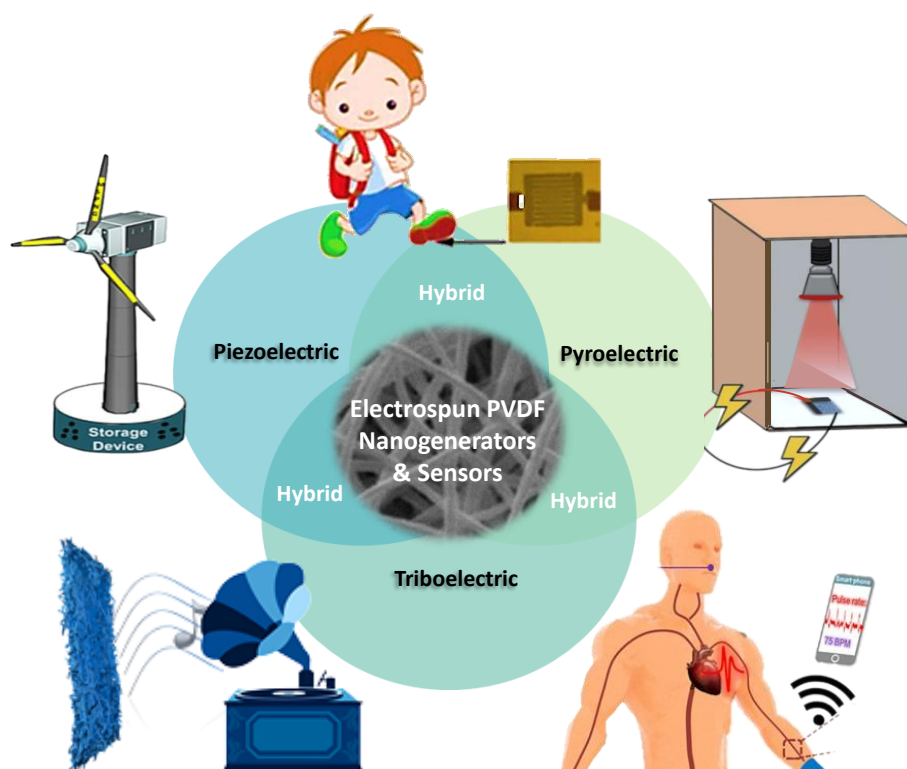
Sreelakshmi Moozhiiyil Purushothaman¹, Maité Fernandes Tronco¹, Bicy Kottathodi^{1,2}, Isabelle Royaud¹, Marc Ponçot¹, Nandakumar Kalarikkal², Sabu Thomas², Didier Rouxel^{1*}

¹Université de Lorraine, CNRS, IJL, F-54000, Nancy, France

²International and Interuniversity Centre for Nanoscience and Nanotechnology, Mahatma Gandhi University, Kerala, India

* corresponding author: Didier Rouxel didier.rouxel@univ-lorraine.fr

Graphical Abstract:



Abstract: Modern-day requirements for efficient, eco-friendly, and self-powered devices have resulted in a growing interest in piezoelectric polymers among the scientific community. Polyvinylidene fluoride (PVDF) is an excellent electroactive polymer that is flexible, with high mechanical strength, thermal stability, and biocompatibility. The relatively low cost and easiness to be fabricated into thin pliable films made PVDF one of the most studied polymers for the development of nanogenerators and wearable sensors. The piezoelectric properties and therefore the energy harvesting and sensing capabilities of PVDF are distinct characteristics of its electroactive polar phases, especially the β phase. Hence, several PVDF-based nanocomposites that could achieve a high β phase fraction have been widely explored. Electrospinning is one of the best methods for manufacturing such PVDF-based nanocomposite films. This article, therefore, highlights essential

information about different electrospinning parameters which help to enhance the β phase in PVDF. The review then progresses into the recent developments and technological advances of electrospun PVDF-based nanocomposite devices in energy harvesting and sensing applications. The piezo-, pyro-, and triboelectric properties of PVDF allow the fabrication of conventional and hybrid nanogenerators. The later can harvest energy simultaneously from multiple sources, sense various fluctuations in their surroundings, and transmit the acquired data immediately when integrated with Bluetooth or wireless devices. They are fine models of self-powered, portable, multifunctional, and sustainable engineering. Finally, a peek into the other possible applications of electrospun PVDF-nanocomposite fibers is also made. Overall, the review aims to illustrate the innovative research and developments of PVDF fiber-based devices and the relevance and prospects they hold as future green sources of energy.

Keywords: PVDF-Nanocomposites, Electrospinning, Piezoelectricity, Triboelectricity, Hybrid nanogenerators

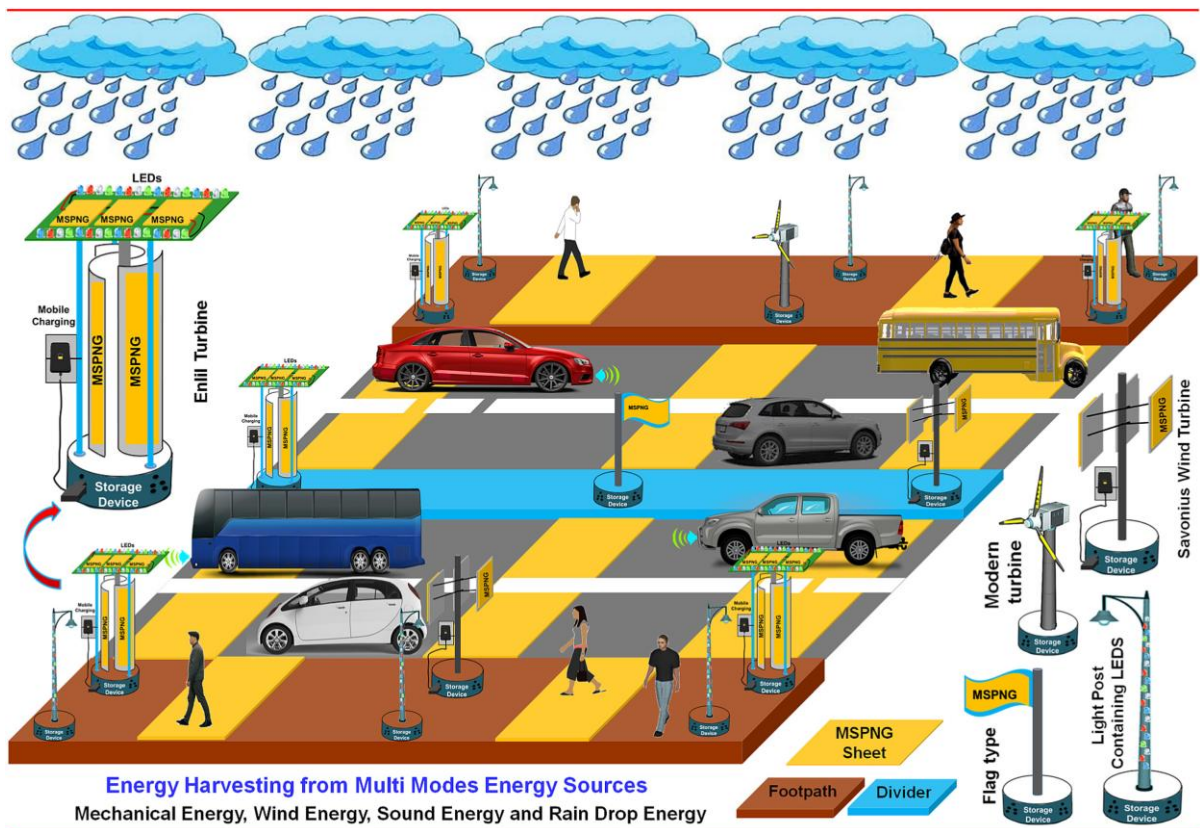
1. Introduction

Technological advances and rising global energy consumption have turned wireless and self-powered devices into one of the requirements of the 21st century. Compactness, flexibility, durability, portability, and the ability to be integrated with other devices are other features expected of such modern devices. A possible solution to satisfy all the aforementioned requirements is the use of electroactive materials. Hence, a wide variety of piezoelectric, pyroelectric, and triboelectric materials have been explored for the development of energy harvesters and self-powered sensors. The ability of these materials to electrically respond to the omnipresent energy sources of mechanical vibrations and heat makes them exceptionally suitable for sustainable energy harvesting.

Quartz is a well-known piezoelectric material and was one of the first to be identified [1]. Some of the later materials include zinc oxide (ZnO), barium titanate (BaTiO₃), and lead zirconate titanate (Pb(ZrTi)O₃) (PZT)[2–4]. These ceramic materials possess high piezoelectric coefficients and high electroactive potential but have poor flexibility and a high-cost preparation process. Their toxicity also questions their suitability as ideal clean and green sources of energy [5,6]. Hence, it became necessary to investigate another class of piezoelectric materials: polymers. Polymers are flexible, with enhanced mechanical strength, and are lightweight, affordable, and biocompatible [7–10]. Many piezoelectric polymers are available, whether synthetic such as polyvinylidene fluoride (PVDF), polyamides, and polyL-lactic acid (PLLA) [11,12], or natural like cellulose, keratin, collagen, or chitin [13]. Among these, PVDF is one of the most explored and efficient piezoelectric polymers, which also exhibits pyroelectric and triboelectric properties. The outstanding properties of this fluoropolymer lead to its frequent selection for the development of energy generators and sensors. This claim is statistically justified by the increasing number of publications on topics such as “PVDF”, “PVDF- Energy harvesting”, “PVDF-Electrospinning” and “PVDF-Electrospinning-Energy harvesting” (as obtained from the Web of Science core database of the Université de Lorraine, France).

This article provides a brief description of PVDF and explores a wide variety of PVDF-based nanocomposites. Because of the increasing use of electrospinning to manufacture PVDF

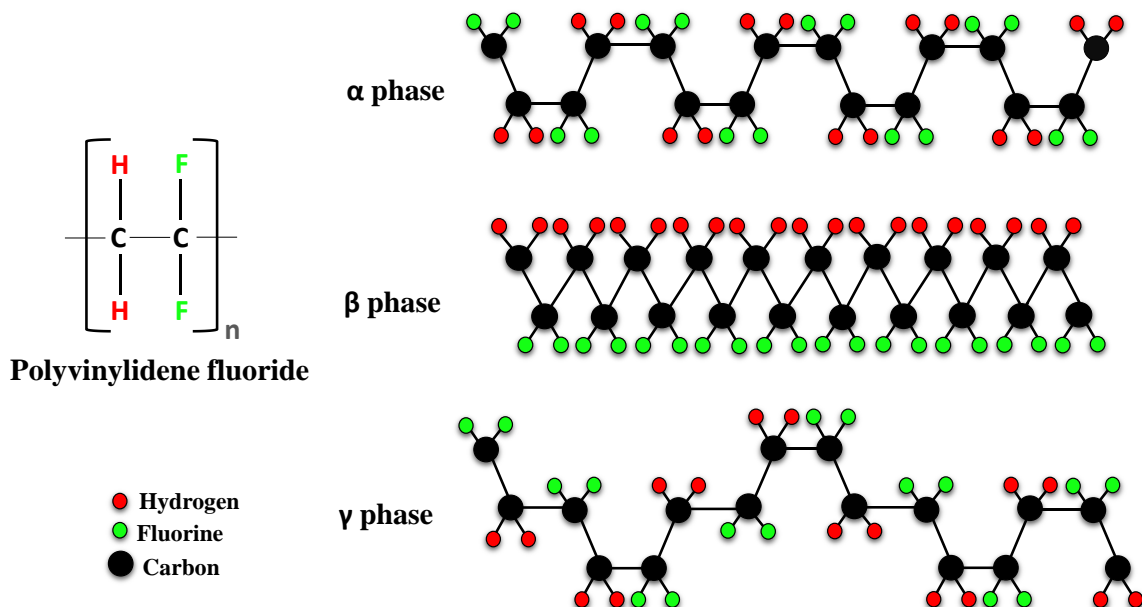
films, it also details the effect of various electrospinning parameters on PVDF. The review then focuses on the energy harvesting applications of electrospun PVDF and explains the recent trends and technological advances in the field of piezoelectric, pyroelectric, and triboelectric nanogenerators and sensors. Moreover, a new and emerging technology for energy harvesting, the hybrid nanogenerators, is also detailed. These devices can simultaneously harvest energy using the piezo, -pyro, and triboelectric properties of PVDF and sense various fluctuations in the surrounding environment. When integrated with wireless data-transmitting devices, they have the potential to become a true example of portable, multipurpose, multifunctional, and sustainable engineering. The inspiration behind this paper is to highlight the potential of electrospun PVDF films, with a focus on these devices, and inspire their integration as innovative sustainable sources of energy. To the best of our knowledge, there are no recent reviews that focus on all the above-mentioned types of nanogenerators together, and the wide variety of energy sources they could detect as sensors or use in the process of energy harvesting. In addition, a brief overview of other applications of such films is also presented. The current review is also significant as a good reference for the scientific community to look forward to the real-life applications and perhaps the commercialization of PVDF-based multifunctional devices as depicted in **Figure 1**.



“**Figure 1.** Schematic visualization of the futuristic possible applications of PVDF-based multi-modes single piezoelectric nanogenerator devices (MSPNG) (reproduced with permission from [14])”

1.1. Fundamentals of PVDF

PVDF ($-\text{CH}_2-\text{CF}_2-$)_n is a semicrystalline thermoplastic homopolymer [15,16]. It is a promising electroactive polymer with wide frequency responses, exceptional sensitivity, high piezoelectric coefficient, high dipole moment in the polar phases, and high thermal stability [17–25]. Depending on the different processing parameters and post-treatments, PVDF is found to exist in five different crystalline phases (α , β , γ , δ , and ϵ) [26]. The three principle phases are represented in **Figure 2**. In general, PVDF crystallizes in the non-polar α phase and is commonly obtained by crystallization from the melt. The polymer chains adopt a trans-gauche-trans-gauche (TGTG) conformation, which is the thermodynamically favorable form of PVDF due to the minimal steric strains [27–29]. Uni- or bi-axial stretching [30,31], poling under a high electric field [31,32], pressure quenching [33], or sample fabrication techniques such as electrospinning [34,35] or spin casting [36] align the polymer chains in the all-trans (TTTT) conformation called the β phase (also referred to as phase I) [29]. In this phase, the dipole moments of C–F and C–H bonds add up so that an effective dipole moment develops in the direction perpendicular to the carbon backbone. Hence, as the highly polar phase of PVDF, the β phase is the most widely studied [37–39]. A semipolar polymorph of PVDF known as the γ phase is obtained by annealing at high temperature and pressure, slow melting, and recrystallization from different solvents or using different surfactants. In the γ phase, the polymer chains take a TTTGTTTG or T3GT3G conformation [15,40]. Often, the β phase and γ phases are together called the electroactive phases of PVDF. The δ phase of PVDF is the polar analog of the α phase. The ϵ phase is the antipolar analog of the γ phase. The δ phase can be obtained through the transition of the α phase with apparently no change in the chain conformation, and by the application of electric fields near 1 MV/cm at room temperature. At high temperatures, the δ phase easily transforms into a mixture of polymorphs in which small amounts of the ϵ phase are obtained along with a higher amount of the γ phase. [26,41–43].



“Figure 2. Schematic representation of the α , β and γ phase of PVDF”

The content of the three principle crystalline phases in PVDF is commonly investigated using Fourier Transform Infrared Spectroscopy (FT-IR). From the FT-IR spectra, the α phase can be identified from the bands at 1423, 1383, 1214, 1146, 976, 854, 796, 764, 615, and 532 cm^{-1} [44–50]. The characteristic band of the β phase which is not composed of other crystal modifications occurs at 1275 cm^{-1} , and the bands at 510 and 841 cm^{-1} , though initially considered to be characteristic of the β phase, are characteristic of both the β and γ phases. The characteristic bands of the γ phase occur at 813 cm^{-1} , 833 cm^{-1} , and 1232 cm^{-1} [37,44,45,48,51–65]. Apart from identifying the presence of different crystalline phases from the band positions, the fraction of the electroactive (EA) phases and α phase can be estimated as follows:

$$F_{EA} = \left(\frac{A_{EA}}{\frac{K_{841}}{K_{763}} * A_{763} + A_{EA}} \right) * 100 \%$$

$$F(\alpha) = 1 - F_{EA}$$

where F represents the fraction of the corresponding phase; A_{EA} and A_{763} are the absorbance values at 840 and 763 cm^{-1} , respectively; K_{840} and K_{763} are the absorption coefficients at the respective wave numbers and are equal to 7.7×10^4 and $6.1 \times 10^4 \text{ cm}^2 \text{ mol}^{-1}$, respectively.

Furthermore, the individual fraction of β and γ can be estimated as follows:

$$F(\beta) = F_{EA} * \left(\frac{\Delta H'_\beta}{\Delta H'_\beta + \Delta H'_\gamma} \right)$$

$$F(\gamma) = F_{EA} * \left(\frac{\Delta H'_\gamma}{\Delta H'_\beta + \Delta H'_\gamma} \right)$$

where $\Delta H'_\beta$ and $\Delta H'_\gamma$ are the differences in optical density between the 1275 cm^{-1} peak and the nearest valley of 1260 cm^{-1} , and the 1234 cm^{-1} peak and the near valley of 1225 cm^{-1} , respectively [66].

X-ray diffraction (XRD) studies can also be used to distinguish the different phases in PVDF. XRD patterns show characteristic peaks of the α phase at 18.4° and 20.0° and two weak peaks at 26.6° and 35.9° corresponding to (020), (110), (021) and (200) reflections [43,66–69]. The peak at 20.6° due to the sum of the diffraction in the (110) and (200) planes and another one near 36.5° due to (020) reflections are the characteristic peaks of the β phase [61,66,69–73]. The characteristic peaks of the γ phase occur around 18.5° , 20.3° , and 39.0° because of the diffraction from the (020), (110/101), and (211) planes [66,67,70,74–76]. By curve deconvolution of the XRD spectra, the overall degree of crystallinity (χ_C), as well as crystallinity of β ($\chi_{C\beta}$) and γ ($\chi_{C\gamma}$) phases can be calculated using the following equations:

$$\chi_C = \frac{\sum A_{CR}}{\sum A_{CR} + \sum A_{amr}} * 100\%$$

$$\chi_{C\beta} = \chi_C * \frac{\sum A_\beta}{\sum A_\beta + \sum A_\gamma}$$

$$\chi_{c\gamma} = \chi_c * \frac{\sum A_\gamma}{\sum A_\beta + \sum A_\gamma}$$

where, $\sum A_{cr}$ and $\sum A_{amr}$ represent the summation of the total integral areas of crystalline diffraction peaks and amorphous halo, respectively; $\sum A_\beta$ and $\sum A_\gamma$ are the area under crystalline β - and γ - peaks, respectively [77].

The determination of the fraction of each crystalline phase is important as the electroactive response of PVDF is determined by the content of the electroactive polar phases, especially the β phase. This fraction can vary under the influence of the electric field, temperature, or mechanical stress [30,38,45,77,78]. Considering the electric properties of PVDF is helpful to further understand the reasons behind this. In PVDF each monomer unit has an electric dipole moment directed perpendicular to the carbon backbone. Each monomer unit has a dipole moment of 8.10^{-30} Cm in the β phase and 5.10^{-30} Cm in the α phase. However, as these monomer units crystallize in anti-parallel orientation, the net dipole moment becomes zero in the α phase [79–83]. Dipole moments of PVDF can be permanently aligned to acquire considerable remnant polarization by the application of a high electric field, with or without applying temperature. Though polarization can take place upon heating, thus allowing the chains to rotate more easily [84], the application of higher temperatures can cause depolarization of the PVDF samples. The thermal depolarization of PVDF was studied by Eberle and Eisenmenger using a mechanically stretched and poled PVDF film with a high fraction of β phase [85]. The β -PVDF which has high spontaneous polarization also exhibits the maximum ferroelectric response, highest remnant polarization, and coercive field [86–89]. In the study of Eberle and Eisenmenger, it was observed that with increased heating temperature, the remnant polarization of the PVDF film decreased slowly from $5.4\mu\text{C}/\text{cm}^2$ at 20°C and tended to zero at 180°C . Even after cooling down to 20°C , the values did not increase considerably except for an anomaly at 180°C . As the electroactive behavior of PVDF is associated with its absence of a center of symmetry, high dielectric constant, and also the polarization of the material, depolarization of the film will significantly lower all its electroactive properties [82,90–92].

Though well-known as a potential dielectric material, extensive studies on the electroactive behavior of PVDF leaped with the discovery of piezoelectricity in PVDF by Kawai in 1969 [93]. The value of piezoelectric coefficients, such as d_{33} and d_{31} are often used to evaluate the piezoelectric properties of PVDF. Typically, PVDF exhibits d_{31} values between 8 to 22 pC/N and d_{33} values between -24 to -34 pC/N. However, these values can be significantly tailored through the modification of the polymer processing conditions, heat treatments, poling under high electric field, nano-confinement, formation of blends, formation of nanocomposites by the addition of fillers, electrospinning and creation of porous structures [94–97]. The discovery and detailed studies on the piezoelectricity in PVDF later lead to the exploration of the pyroelectric properties of PVDF which are related to the ferroelectric phase content of PVDF. The pyroelectric coefficient (p) of PVDF is typically observed to be between 0.27×10^{-4} and 0.357×10^{-4} C /m² K. However, the pyroelectric properties are also tunable like the piezoelectric properties [98–100].

1.2. PVDF based nanocomposites

There are different manufacturing methods to modify the properties of PVDF like copolymerization, blending, and addition of nanofillers. Compared to copolymers and blends, PVDF-based nanocomposites allow them to obtain distinct physicochemical properties that

are otherwise difficult to tune. This is due to the higher surface-to-volume ratio and subsequent higher contact area of the fillers with the polymer matrix. The commonly used fillers can be classified as inorganic, organic, or bio-fillers, carbon-based fillers, and hybrid fillers. A few examples of inorganic fillers include metal nanoparticles like gold [55] or palladium [45], metal salts such as CaCl_2 , BaCl_2 [101], several ferrites such as ZnFe_2O_4 [102], CoFe_2O_4 [103], and carbon-based materials like carbon nanotubes, graphene or graphene oxide [77,104]. Examples of organic include nanocellulose, chitin, and chitosan [105–107], and hybrid fillers include organometallic compounds, combination of fillers like multi-walled carbon nanotubes (MWCNT)-Cloisite 30B hybrid nanoparticles and titanium dioxide (TiO_2) nanoparticles-graphene oxide (GO) [108–110].

The selection of the fillers is often made to improve (or alter) the properties of the matrix and is specific to the final application of the polymer nanocomposite. However, a few of the basic properties to be considered are the chemical composition, shape, size, and aspect ratio of the fillers [111–113]. The synergic effect of the nanofillers is generally due to the interaction of the electronegative fluorine atom with the electropositive metal atom in a metallic compound or the positive surface charge of the fillers. It sometimes can be due to the interaction of the electropositive hydrogen atom with the effective negative surface charge of the fillers. But in the case of fillers like nanocellulose, a hydrogen bond is formed between the fluorine atoms of PVDF and hydrogen atoms of the filler [45,114]. Karan *et al.* suggested that in the case of composite fillers such as aluminum oxides decorated reduced graphene oxide (AlO-rGO) sheets, β -phase nucleation can occur through stress-induced polarization, in addition to surface charge-induced polarization. Here, external mechanical forces build a potential in the AlO-rGO nanosheets which aligns the PVDF dipoles in the direction of the applied force [115]. Just like the filler composition, the morphology of the fillers can also affect PVDF-filler interaction. For example, Fu *et al.* demonstrated this dependence by studying PVDF- BaTiO_3 spherical nanoparticles (BTNPs) and PVDF- BaTiO_3 nanorods (BTNRs) composites [116]. The higher interfacial area of the BTNRs/PVDF composite compared to the BTNPs/PVDF nanocomposites was found to enhance the interface polarization in the first configuration. Mendes *et al.*, from studies on PVDF- BaTiO_3 composite films, concluded that smaller nanoparticles act as nucleating agents for the β phase of PVDF during polymer phase crystallization. Larger particles, due to the reduced relative interaction area for a given volume concentration, can cause defect formation [117]. Apart from the type of fillers used, the properties of the nanocomposite will also depend on its filler dispersion, lattice matching, processing conditions, and, importantly, the relative fraction of the fillers. Every researcher chooses the most adequate fraction of fillers by studying the different films they prepared based on prior assumptions. This can be clearly understood from every research article illustrating the wide variety of applications of PVDF-based nanocomposites.

Very often, the primary intention behind the addition of fillers in the PVDF matrix is to increase the fraction of β phase, and piezoelectric coefficients in the case of piezoelectric applications. Indeed, the presence of nanofillers was observed to reduce the nucleation energy barrier and thus enhance the crystallization rate and the degree of crystallinity of PVDF [94]. For example, Thakur *et al.* observed that, by introducing ZnO NPs into a PVDF matrix, the β -phase content increased up to 84% (0.85 vol% of ZnO) and the piezoelectric coefficient d_{33} increased to 50 pC/N from 22.3 pC/N at 50 Hz [118]. The addition of fillers to PVDF can

enhance its other properties as well, such as in the study of Elizalde *et al.* Here, they focused on altering the hydrophobicity and wettability of PVDF through the addition of chitosan. Similarly, Zhou focused on increasing the thermal conductivity of PVDF by adding core-shell-structured aluminum (Al) particles [119], while Ram *et al.* were working on both the thermal and electrical conductivity of PVDF-carbon black nanocomposite films [120]. The addition of such high electric conductivity fillers to PVDF increases the overall conductivity of PVDF-nanocomposite films, which also increases the d_{33} coefficient at lower concentrations of the fillers. It also leads to significant changes in the breakdown field, charge transport, charge distribution, and electric energy density of the material. In the case of highly conductive fillers, a drastic decrease in breakdown strength may occur due to high conductivity that limits the improvement of the piezoelectric performance of PVDF nanocomposites. The addition of fillers with high dielectric constants can significantly increase the dielectric permittivity of PVDF. However, on attaining the percolation threshold, the output of the piezoelectric devices is found to reduce drastically. The composites can also suffer from an abrupt variant in the dielectric loss. Sometimes, high filler loading might be necessary to achieve high dielectric permittivity, which weakens the processability, flexibility, and mechanical performance of the composites. Hence, there exists a certain threshold to provide an optimal balance [95,96,121–123]. Similar to increasing the conductivity of an insulator like PVDF, It is possible to impart other properties to the polymer nanocomposite that the polymer alone initially does not possess. For example, Durga Prasad, by the addition of ferromagnetic fillers like $ZnFe_2O_4$ and $CoFe_2O_4$ into ferroelectric PVDF, made multiferroic films [102], [103].

With time, the number of fillers used with PVDF has increased considerably and their effect on the properties of PVDF is becoming very specific. Thus, a list addressing every filler and its applications will be quite long. However, it was attempted to cover a majority of the recent ones in different sections of the review.

2. Manufacturing of PVDF films

With advances in the field of material manufacturing, a variety of techniques are used for the fabrication of PVDF films. Solvent casting [124][125] and spin coating [126][127] are some of the simplest techniques to obtain films, while melt spinning [128][129] and electrospinning are employed for fiber production. Hot-pressing and extrusion are also used for the production of PVDF films [39,130,131]. The latest addition to this list is an electric poling-assisted additive manufacturing (EPAM), which is a 3D printing process that incorporates electric poling, and allows simultaneous printing and poling of 3D free-form single structures [132,133].

Among them, one of the most promising techniques is electrospinning. It is used to produce highly oriented 2D nanofibrous films of PVDF with a high fraction of β phase without any post-treatment. The general trend observed within the literature about PVDF is the rapidly growing number of publications on electrospun PVDF films. This underlines that electrospinning is considered one of the best methods for manufacturing PVDF. Hence, this section proposes to discuss the preparation of electrospun PVDF nanofibers.

2.1. Electrospinning: basic principles and process

Electrospinning involves producing smooth and continuous fibers of different polymers with diameters down to the range of nanometers [134]. A viscoelastic jet derived from a polymer solution or melt is submitted through uniaxial stretching under the application of a high voltage. In general, an electrospinning setup consists of a high-voltage power supply, a spinneret, and a collector. When a high voltage is applied, the charge is induced at the surface of the polymer solution and as a result, a mutual charge repulsion opposing the cohesion and surface tension of the solution starts to develop. As the voltage increases, and because of the increasing charge repulsion, the solution droplets elongate into a conical shape called the Taylor cone. At a critical value of the voltage, the repulsive electric force overcomes the surface tension of the solution, and a charged jet of the polymer solution is ejected from the tip of the Taylor cone. As the jet extends, the solvent evaporates which results in its stretching and thinning.

The electrospinning process is influenced by a set of different parameters. These parameters are classified into three sets: the solution parameters, process parameters, and ambient parameters. The solution parameters include the type of material/polymer and solvents used, solution concentration, viscosity, conductivity, and surface tension. The process parameters include applied voltage, tip-to-collector distance (TCD), flow rate, spinneret choice, and the type of collector. Humidity and room temperature are the ambient parameters. Each of these parameters is chosen carefully to achieve efficient electrospinning [135–148].

2.2. Electrospinning of PVDF

To ensure the formation of PVDF fibers, optimization of the various sets of parameters plays an important and decisive role.

2.2.1. Effect of solvents and solution viscosity

The molecular weight, concentration of PVDF, and solvents used are the solution parameters that allow more tuning options over other parameters like viscosity, polarity, vapor pressure, and surface tension. An increase in the molecular weight of PVDF increases the viscosity of the solution. A more viscous solution will take longer to reach the collector and so the jet stretches more under the applied voltage and solvents evaporate better, enhancing the β phase content. Hence, higher molecular weight PVDF fibers generally have better piezoelectric and mechanical properties [149,150]. This was confirmed by the studies of Magniez *et al.* [151] and Zaarour *et al.* [152]. The weight percentage of PVDF also has a similar effect on the viscosity of the solution. With the increase in concentration, the uniformity and fraction of the β phase increase at first due to the improved stretching effects. If it increases beyond a critical limit, the solution becomes highly viscous and harder to stretch. As a result, the fraction of the β phase decreases [153]. Justifying this claim, Gade *et al.* reported that the β phase content decreased with an increase in concentration [154]. Baji also suggests that thinner fibers formed at lower concentrations will have higher β phase content [155].

In a similar study, Costa *et al.* suggested that adding a more volatile solvent (like acetone) to polar solvents like dimethylformamide (DMF) lowers the surface tension and increases the net evaporation rate of the solvents, thereby affecting the relative fraction of phases [156]. It also lowers the viscosity, α phase content, and formation of beads in PVDF fibers. However, too much acetone will speed up evaporation excessively and the solution may solidify at the tip of the needle [153,157,158]. Gee *et al.* studied the effects of different solvents on the electrospinning of PVDF. They used solvents like DMF, dimethyl sulfoxide (DMSO), and N-methyl-2-pyrrolidone (NMP) with a 6:4 volume ratio with acetone. They found DMF: acetone 6:4 v/v% to be the best combination to increase the fraction of β phase [159]. This solvent combination is often found in other works [108] but the ratio may vary from one to another. For example, Saha *et al.* suggested 7:3 [160] as the best ratio while 4:6 was preferred by Jiyong [161].

2.2.2. Effect of voltage

The applied voltage plays an irreplaceable role in altering the properties of PVDF fibers, especially the formation of the β phase. The fiber diameter is found to decrease and the fraction of β phase to increase with the increase of voltage. The excessive increase in voltage will result in the beading and eventually the breaking of the fibers [153,161,162]. This is clearly understood from the observation of Gade *et al.* [154]. A slightly different suggestion was put forward by Andrew and Clarke. They claim that the applied voltage has much less effect on the fraction of β phase for a less viscous solution and affects the solution with higher viscosity as mentioned above [163].

2.2.3. Effect of tip to collector distance (TCD)

The TCD affects the evaporation of the solvent and electric field intensity. As the TCD increases, the β phase content increases at first and then decreases, hence the most preferred TCD being between 10 to 20 cm [153,164]. Shao *et al.* reported that at a constant voltage, the average fiber diameter decreases with an increase in the TCD [165]. The studies of Motamedi *et al.* also support this observation [166]. Zaarour *et al.* reported that the pore size of porous fibers, groove size of grooved fibers, and roughness of rough fibers increased with an increase in the TCD [167].

2.2.4. Effect of flow rate

Finding the critical flow rate is necessary for the electrospinning of PVDF. Lower flow rates will cause a vacuum inside the needle, while at higher flow rates some polymer may deposit at the tip. A lower flow rate is preferred to ensure enough time to stretch and polarize the jet and the solvents to evaporate [153,164]. In general, the diameter of the PVDF fiber is found to increase with the increase in the flow rate [166,167]. On the contrary, Ghafari *et al.* did not find such sensitivity or change in fiber diameter with a change in flow rate [168]. Gade *et al.* observed that fiber diameter increased with flow rate, but β -phase content decreased from 92.5% at a flow rate of 2 ml/h to 85.5% at 8 ml/h [154]. Lei *et al.* reported the formation of the γ phase at a flow rate of 2000 μ L/h at 30°C, and the formation of the α phase at 50°C [169].

2.2.5. Effect of collector type

The fraction of the β phase was found to improve as a static collector was replaced with a rotating one due to the additional stretching force. Fu *et al.* observed that the fraction of β phase increased to 93.2% at a speed of 2000 rpm for the rotating drum [150]. Along with the increase in β phase content, a decrease in fiber diameter is also observed with an increase in collector speed. However, an increase beyond an optimum value will result in wider, non-uniform, or broken fibers [153,154,158,166]. Zaarour *et al.* reported that by increasing the rotation speed of the drum collector, the macropores of the fiber changed into elliptical shapes, grooves deepened, and roughness increased [167]. Thus, the collector speed has an intermediate optimum value which gives the best fibers.

2.2.6. Effect of temperature and humidity

The increase in the ambient temperature increases the solvent volatilization rate and reduces the surface tension and viscosity of the PVDF solution, thereby affecting the fiber morphology and fraction of β phase [153]. Huang *et al.* reported that with an increase in temperature, more uniform fibers with lesser beading were formed [170]. As the temperature increases, fiber diameter decreases but beading may occur. Mohamadi and Sanjani reported that with the temperature set to 40°C, the growth of the γ phase was seen. It was accounted for by the increase in thermal energy causing the rotation of the CF_2 group [171]. The relative humidity also affects solvent volatility and thus alters the surface morphology of the fibers. Szewczyk *et al.* observed that fibers spun at a relative humidity of 30% (PVDF-30) had a smooth surface and an average diameter of 0.92 μm while those spun at a relative humidity of 60% (PVDF-60) had a wrinkled surface and larger average diameter of 1.68 μm [172]. Zaarour *et al.* observed that smooth fibers were formed at 5% relative humidity, and macroporous, rough, and grooved fibers were produced at higher relative humidity [173]. Studies found that the relative humidity must not be increased beyond a critical value as this will inhibit the evaporation of solvents and hinder the electrospinning process [153,164,174].

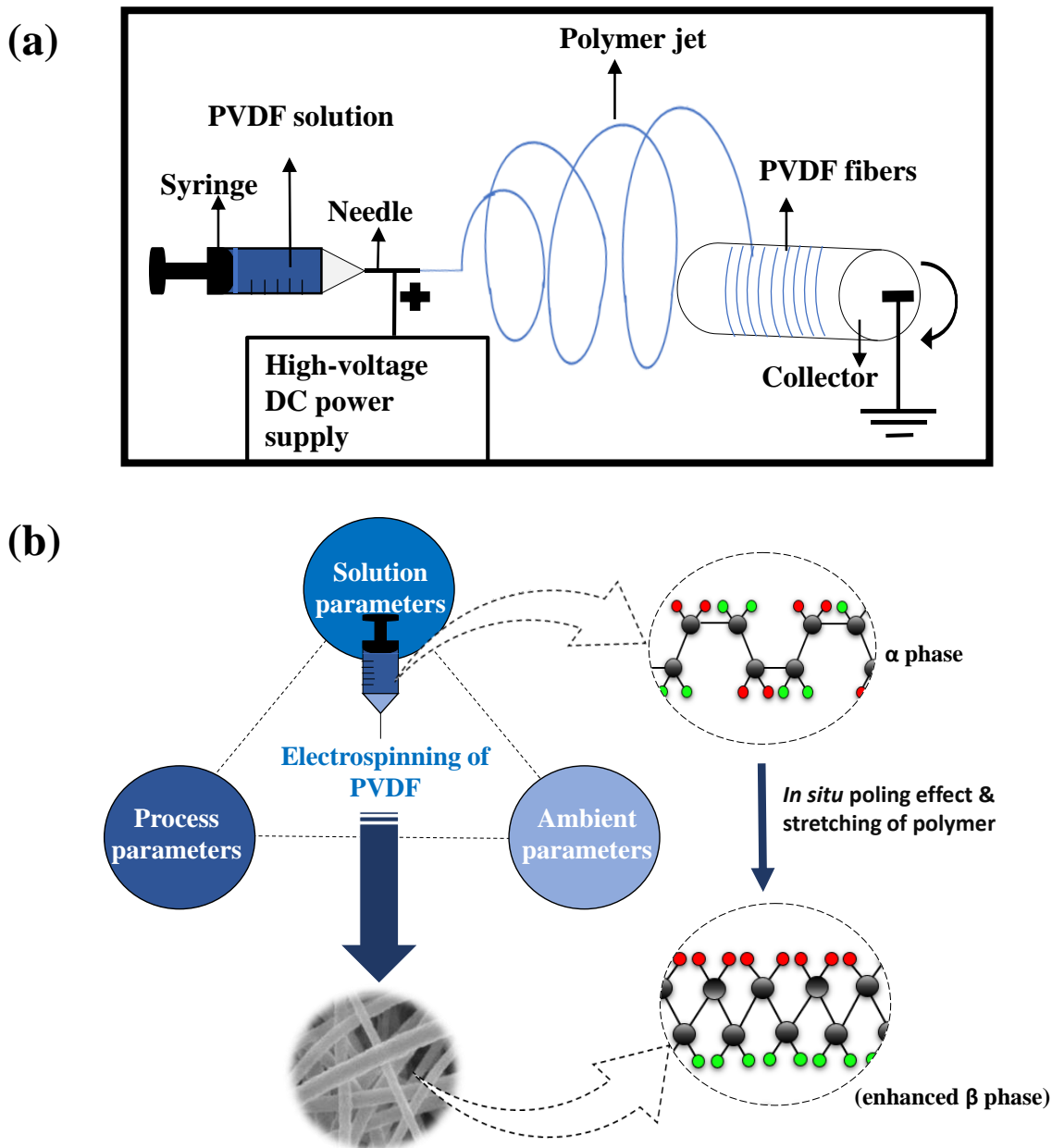
From the above discussions, the conclusion reached is that for every parameter there is an intermediate optimum value that gives the best fibers. Furthermore, as all of these parameters are somewhat interrelated and interdependent, varying one can vary the previously obtained optimum value of another parameter [174–176]. Once the optimum parameters have been found, electrospinning becomes a reliable way to produce PVDF fibers with a high electroactive phase fraction. Mechanical stretching and electrical poling are the most common methods to induce the β phase in PVDF. Electrospinning is the only technique that offers both of these methods within the process itself. The high voltage applied and the high drawing of the jet during electrospinning produce an *in situ* poling and stretching effect, and thereby induce preferred dipole orientation and all trans conformation in the electrospun PVDF fibers. The fraction of the β phase found in electrospun samples can be as high as 99% [177,178]. The electrospinning process of PVDF, the parameters which affect it, and the subsequent change in the crystalline phase are schematically shown in **Figure 3**. After acknowledging the advantages of PVDF for the manufacturing of electroactive PVDF nanofibers, the coming section of the review will present the recent developments and applications in which they can be of use.

3. Applications of electrospun PVDF- nanocomposites

The previous sections showed the interesting microcrystalline properties that can be achieved by PVDF fibers when the optimum electrospinning parameters are used. The next section will attempt to give an overview of the various application of such electrospun PVDF fibers.

3.1. Energy harvesting and sensing

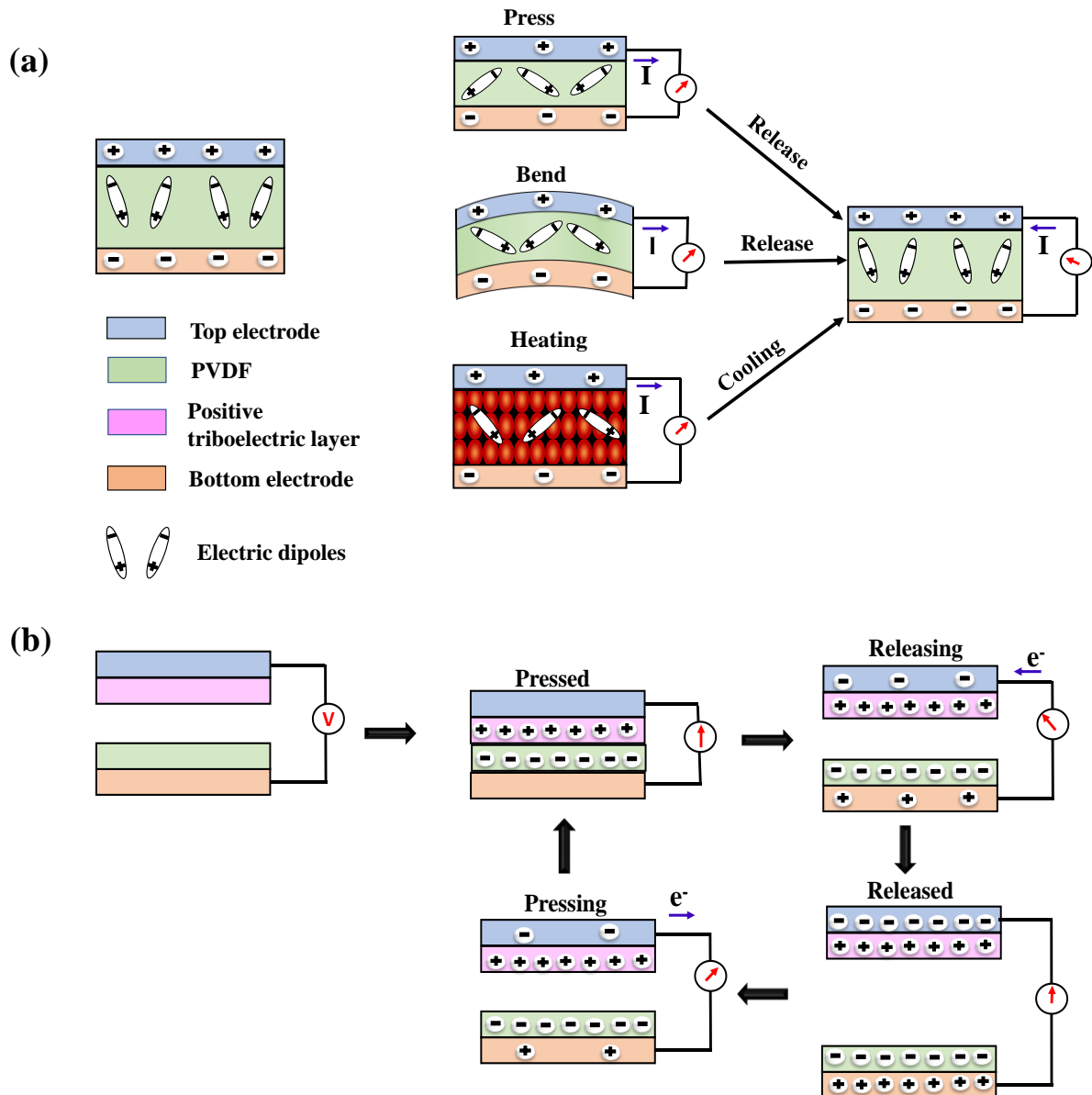
PVDF is an excellent electroactive material with high sensitivity, flexibility, biocompatibility, and non-toxicity. Compared to other manufacturing processes of PVDF, electrospun nanofibers are reported to possess the highest β phase content, high surface area, and surface charge production. Hence, they are one of the most ideal candidates to harness the otherwise lost mechanical and thermal energy. The interest shown by research for such materials is made apparent by the great efforts to develop PVDF-based novel energy harvesting devices or self-powered sensors. The different energy harvesting mechanisms in PVDF-based devices can be explained as follows:



“**Figure 3.** Schematic representation of (a) the process of electrospinning of PVDF, and (b) the parameters which affect it along with the subsequent change in crystalline phase”

under stress or other stimulations like change in temperature, deformation of the crystals, and rotation of dipoles occur within the crystalline phase of PVDF films. This forces a change in the dipole density of the film and causes the electric charges within the film to be out of equilibrium. Thus, the result is the variation of the electrostatic-induced charge density of the electrodes fixed on either side of the film, inducing a voltage and current flow in the external circuit. Once the stimulation is removed, the accumulated free charges flow back, resulting in a reverse electrical signal in the external circuit. When the external stimulation is completely removed, the device returns to its initial condition. The production of an electrical output by PVDF films in response to applied pressure forms the foundation of piezoelectric energy harvesting. Pyroelectric energy harvesting is based on the response of the PVDF films to

temperature [179–184]. Because of its unique electroactive properties, electrospun PVDF is an effective dielectric material for triboelectric energy harvesting as well [185]. In triboelectric energy generation, it is the charge transfer due to contact electrification and electrostatic induction that is responsible for the production of the electrical output. This electrostatic induction arises from the friction of two different layers with different electroaffinities, namely the positive triboelectric layer (losing electrons) and negative triboelectric layer (gaining electrons) which develop positive and negative charge respectively when subjected to pressure [185,186]. PVDF, especially in the β phase, can act as an excellent negative triboelectric layer that efficiently traps the electrons. This is made possible because of its high spontaneous polarization, high electronegativity, and high surface charge density. When the two triboelectric layers come in contact, they develop opposite charges and as they move away an electrical potential difference will begin to develop. This creates a flow of electrons from the electrode of the PVDF layer to the electrode of the positive triboelectric layer through an external circuit. As the separation between the layers increases, an electrostatic equilibrium is reached and the electron flow stops. When the two layers are again driven towards each other, the electrostatic equilibrium is again broken and the electrons flow back in the opposite direction, thus reducing the number of induced charges. Finally, all the induced charges are neutralized when the layers come in contact [187–189]. Interestingly, in PVDF-based devices, piezoelectric, pyroelectric, and triboelectric effects can act complementary to enhance the overall output performance and functionality of the device. This principle forms the basis of hybrid energy harvesting. For example, during the simultaneous application of pressure and heating, the piezoelectric output under the heated condition is observed to be higher due to thermal strain coupled with the piezoelectric effect. Similarly, the pyroelectric output improves upon increasing the stretching elongation of the device due to mechanical-strain-induced pyroelectric output [190]. Even when considering the application of external forces without heating, there still exists a complementary method to enhance the output of the devices through coupled mechanisms of piezoelectric and triboelectric energy harvesting. Indeed, when an external force is applied, the deformation of material can occur simultaneously with contact friction, thus allowing the complete exploitation of the applied mechanical energy. At first, when the triboelectric layers are brought toward each other, triboelectric charges develop due to interface friction. As the application of external force continues, a piezoelectric potential is also generated due to the deformation of the PVDF film. Then, there is a current flow in the circuit to balance the piezoelectric potential. As the external force is removed, the PVDF film recovers from compression and the piezoelectric potential disappears. With the triboelectric layers separating from each other, an internal triboelectric potential develops resulting in a current flow in the circuit [191]. **Figure 4** summarizes the principles of piezoelectric, pyroelectric, and triboelectric energy generation in PVDF-based devices. The following sections will discuss their architecture and applications.



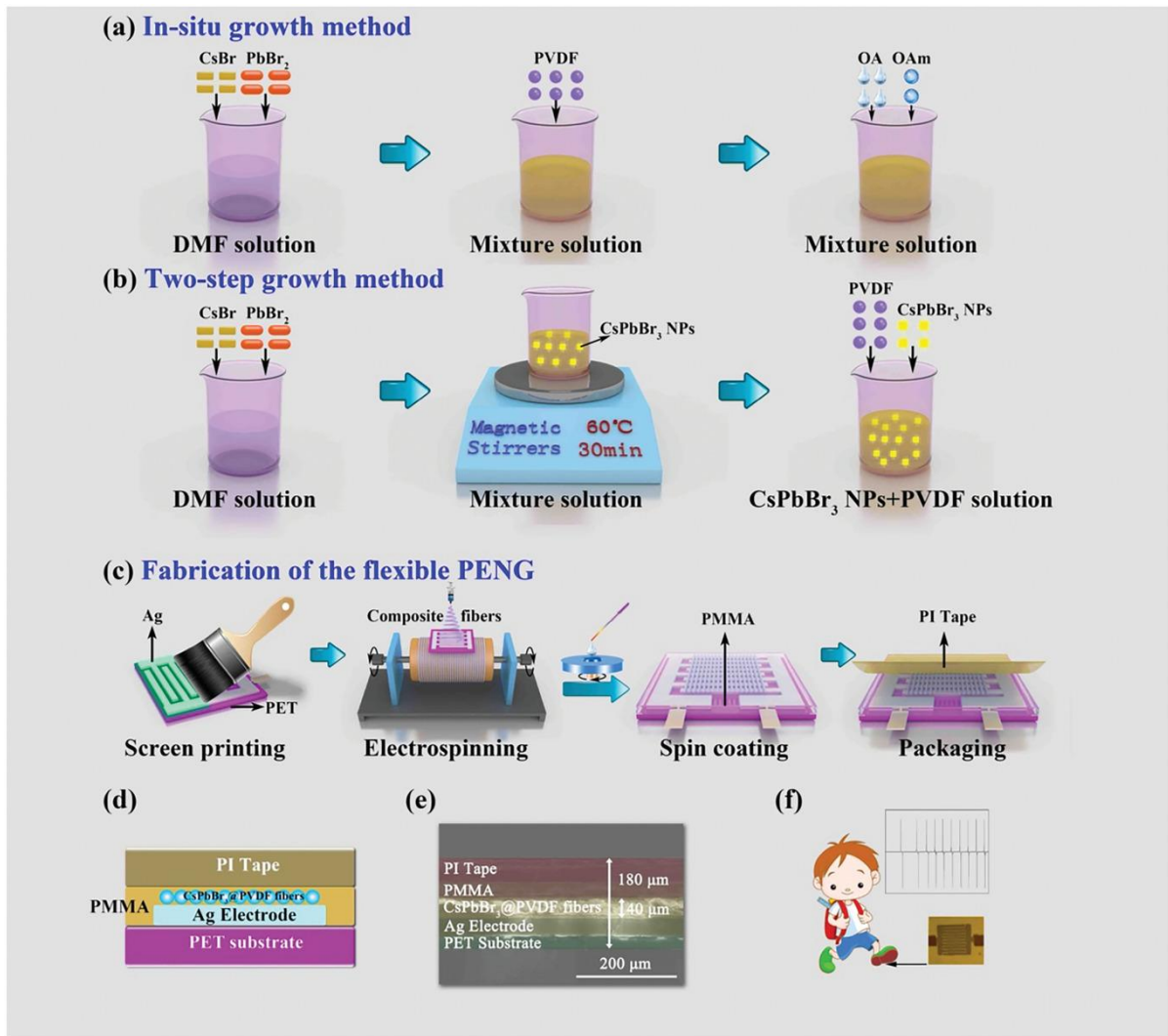
“Figure 4. Schematic representation of the principles of (a) piezoelectric, pyroelectric, and (b) triboelectric energy generation.”

3.1.1. Piezoelectric nanogenerators and sensors

The elemental structure of a piezoelectric nanogenerator (PENG) or sensor consists of four parts. The piezoelectric material is the active layer and is primarily responsible for the entire process of energy harvesting and sensing upon the application of pressure. The piezoelectric material is sandwiched between suitable electrodes connected to the external circuit. The entire PENG is wrapped in suitable materials like polydimethylsiloxane (PDMS) to protect it from damage from continuous use and exposure to different environments [192,193]. It is worth considering some of the recent PENGs, and innovations in their structure, output, and high-performance applications. The CsPbBr₃-PVDF PENG based on *in situ* growth of CsPbBr₃ nanocrystals in PVDF matrix fabricated by Chen *et al.* for mechanical

energy harvesting and motion sensing is a relevant example [194]. They used a one-step technique in which the solutions containing CsPbBr₃ precursors and PVDF was electrospun to produce the nanocomposite fibers. The PENG gave a maximum piezoelectric output voltage of 103 V and a current density of 170 μAcm^{-2} . The fabrication of the flexible PENG, its structure, cross-section, and energy harvesting during walking is schematically illustrated in **Figure 5**. Sengupta *et al.* developed another motion sensor and PENG using PVDF–polycarbazole nanofibers which were suitable for biosensing and bioactuation [195]. The PENG generated an open-circuit voltage (V_{oc}) of 2V under a pressure of 0.24 MPa and had a stable response in the frequency range of 1 to 7 Hz. In the study conducted by Amith *et al.*, the addition of Cloisite-30B nanoclay into PVDF was found to strengthen the β phase and piezoelectric response of electrospun PVDF fibers. In this study, the authors reported the PVDF/Cloisite-30B nanofiber composite to produce an output voltage of 4.74 V when actuated at 1500 rpm [196]. Ramasamy *et al.* presented a rare result in which oleylamine functionalized boron nitride nanosheets (OLABN) incorporated PVDF nanofibres with a high fraction of $\sim 92\%$ of γ -phase was used as the active material for energy harvesting and sensing [197]. The piezoelectric device developed from these fibers was able to detect a minimum force of 0.1 N and light up a 4V light-emitting diode (LED) upon finger tapping with the aid of a simple amplifier. A combination of ZnSnO₃–MoS₂ was used by Muduli *et al.* as fillers with PVDF to develop a PENG for biomechanical energy harvesting. Here, a 1 μF capacitor charged from the device was able to power a calculator with stability [198]. To explore the possibilities of another transition metal-based filler, Zhao *et al.* developed a highly sensitive pressure sensor based on flexible piezoelectric MXene/PVDF hybrid film [199]. They reported that with only 0.4 wt% MXene, the piezoelectric coefficient d_{33} of MXene/PVDF hybrid film reached values as high as 43 pC/N. The sensor gave a stable output for 10,000 s. A combination of BiCl₃ and ZnO was used by Zhang *et al.* as a filler to obtain PVDF/BiCl₃/ZnO composite fibers with a high β phase content of 92% [184]. The piezoelectric sensor developed from these fibers and simple aluminum foil electrodes gave a maximum V_{oc} of 3 V and 0.6 V for elbow and knee bending, and stretching between specific angles. This signals the applicability of the device as a wearable sensor for detecting vital signals such as breathing, heartbeats, and hand movements post-stroke or traumatic brain injury.

Shivalingappa *et al.* used silver nanoparticles as fillers with PVDF to fabricate a sensitive PENG [200], and Ongun *et al.* experimented with silver-doped zinc oxide nanoparticles [201]. The PENG of Shivalingappa *et al.* could trigger a burglar alarm when the pressure on the PENG was high enough to produce an output greater than 0.4 V. The device of Ongun's group had the potential to be used within flexible, portable electronic systems, and wearable gadgets. Similarly, Hasanzadeh *et al.* added ZnO nanoparticles along with graphene (graphene-ZnO nanocomposite) into PVDF fibers and found that an applied force of 1 N produced a peak-to-peak voltage (V_{pp}) of 840 mV. This was significantly higher than the outputs of the pristine PVDF and PVDF/ZnO nanofibers which were 640 mV and 710 mV respectively [202]. Another graphene-based filler incorporated PVDF nanofibres was developed using COOH-functionalized graphene nanosheet and talc nanosheet by Shetty *et al.* [203]. As they could obtain a power density of 1.72 $\mu\text{W/cm}^2$ when a pressure of 0.4 MPa was imparted, the authors suggested this material as a promising candidate for the fabrication of



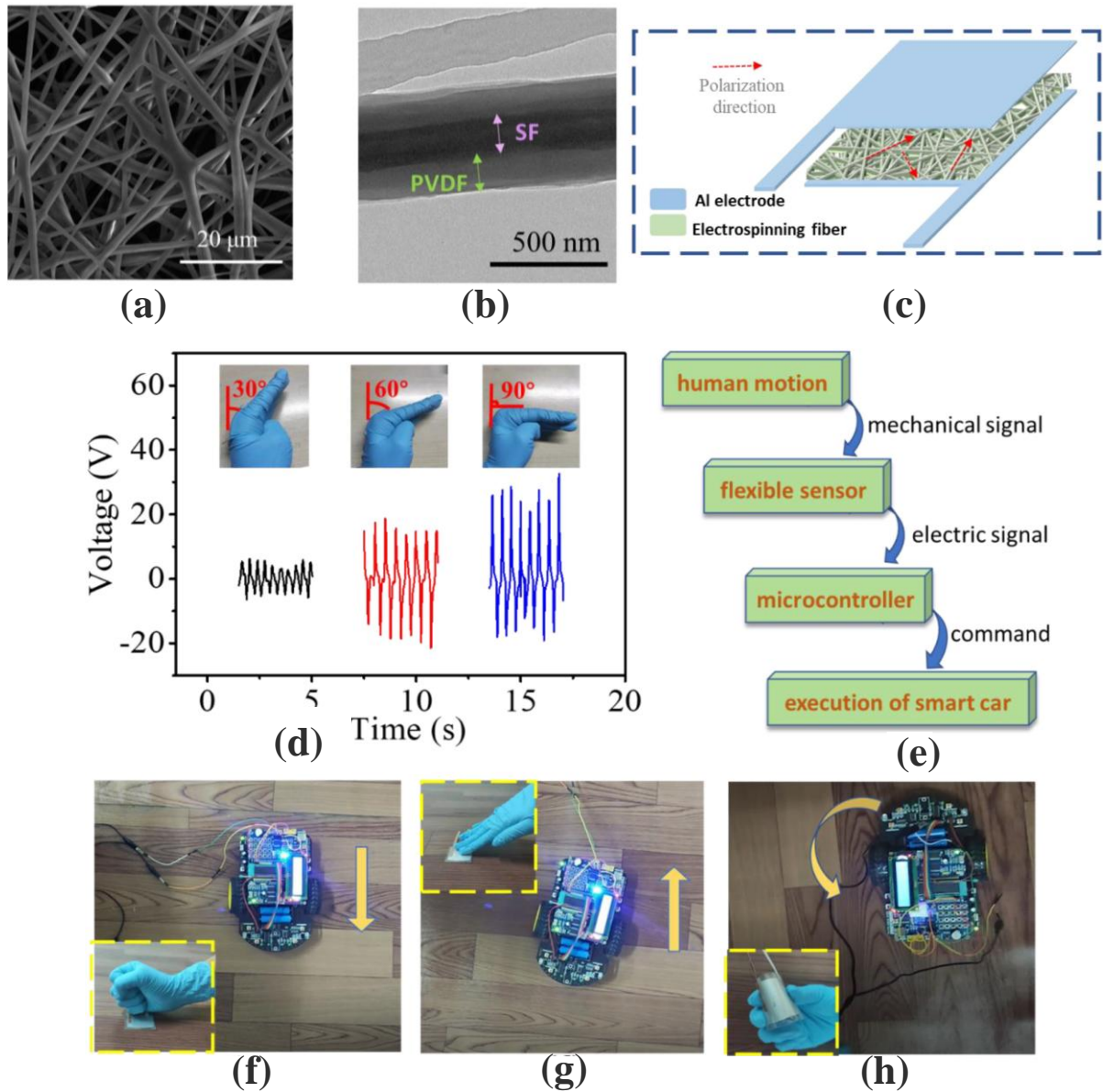
“Figure 5. a) Preparation of precursor solution of CsPbBr₃@PVDF for *in situ* growth method. b) Preparation of precursor solution of CsPbBr₃@PVDF for two- step growth method. c) Schematic diagram of the fabrication of the flexible PENG. d) Schematic diagram of the PENG structure. e) Cross section of the PENG based on in situ growth method. f) Display of energy collection during walking (reproduced with permission from [194]).”

portable and flexible electronic devices. Electrospun PVDF films with Y-doped ZnO fillers and a very high $F(\beta)$ of 98% were fabricated by Yi *et al.* thus combining the flexibility of PVDF and high piezoelectricity of Y-doped ZnO [204]. The PENG gave an output voltage of ~8 V under continuous punching for a trial lasting over 1100 s at 0.8 Hz. It could also charge a capacitor of 5 μ F to ~2.8 V or ~3.7 V in 50 s by walking or running.

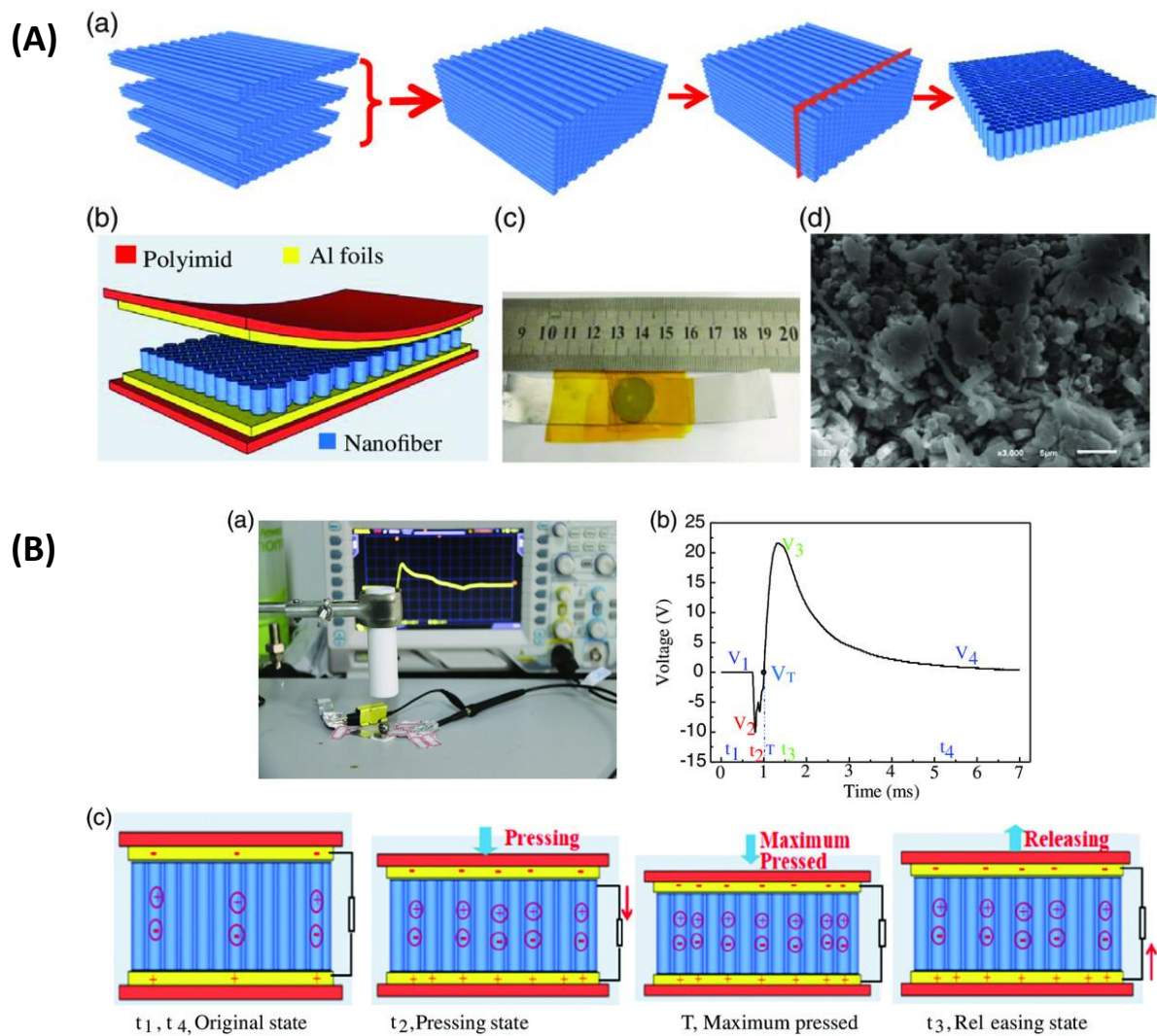
The possibility of using fillers derived from biological sources was explored by Ponnann *et al.* by using magnesiochromite nanocrystalline powder synthesized from egg shell membrane and incorporating it in PVDF nanofibers [205]. This PENG could provide stable output for over 750 cycles and could charge a 10 μ F capacitor within 643 s. Exploring the possibilities of different fillers, and using a different electrospinning technique was done by Wang *et al.*[206]. In Wang’s study, an all-organic and core-shell structured silk fibroin/PVDF nanofibers were fabricated using a coaxial electrospinning strategy. The ability of the device

to generate distinct output voltage for different movements of the human body was used for the development of a sensor in a human-machine interactive interface. This was demonstrated by making a smart car move forward, backward, and turn around by punching, tapping, and bending respectively (**Figure 6.**). A wearable piezoelectric device based on yarns and fabrics was woven by Xue *et al.* using a highly integrated PVDF/conductive nylon core-sheath structure [207]. In this study, a dense PVDF fibrous coating was electrospun on the outer surface of a conductive nylon yarn which functioned as one of the electrodes. The same nylon yarn was braided on top of the PVDF-coated nylon yarn via a 2D braiding technology to function as the second electrode. The output of the final piezoelectric yarn increased with the thickness of the PVDF layer. Bai *et al.* also used a distinct method by creating PVDF nanofiber array films via a combination of electrospinning and cutting methods [208]. The PVDF nanofiber films were stacked layer by layer along the same direction and compressed to get an oriented nanofiber bulk. It was then cut to obtain the PVDF nanofiber array film having dense vertical alignment as shown in **Figure 7.** From the power output of two such parallelly connected PENG, 12 LEDs could be lit without storage devices.

A bit different from the conventional fabrication methods, Du *et al.* used a laminating method to develop multilayered porous composite fibers-based piezoelectric nanogenerators [209]. The laminating process was beneficial as it increased the possibility of stressing every fiber by reducing the porosity of the fiber film. For this, they layered fiber membranes of PZT incorporated PVDF fibers along the same direction and compressed them together. The output of the PENG was found to increase with the increase in thickness, and an output voltage as high as 92 V was obtained from a 500 μm thick film. Another example of innovative design is the piezo-organic e-skin sensor (POESS) fabricated by Maity *et al.* through an all-organic strategy. Here, metal-free, highly-conductive, flexible, and biocompatible spongy electrodes were used instead of conventional electrodes [210]. Such an organic electrode-piezoelectric stack was developed by polymerization of aniline monomer by vapor phase polymerization using $\text{FeCl}_3 \cdot 6\text{H}_2\text{O}$ containing PVDF. The POESS was then attached to the human body for self-powered physiological signal monitoring such as wrist bending, neck stretching, throat movements, phonation recognition, and pulse measurement. An all-fiber piezoelectric nanogenerator (A-PNG) was designed by Mahanty *et al.* by using 0.5 wt% ZnO nanoparticles reinforced electrospun PVDF nanofibers as the active layer [211]. In this study, copper–nickel plate interlocked conducting micro-fiber-based polyester fabric was used as electrodes. Owing to its reliable piezoelectric response and skin conformable functionality, the A-PNG was attached to the throat, wrists, fingers, and knees for vocal cord movement monitoring, pulse monitoring, remote health care monitoring, sports activities, and related movements analysis respectively. The device was also used as a weight monitoring sensor which could give the weight of a person weighting between 45 and 80 kg. A core-shell type of PVDF yarn was developed by Li *et al.*, with a silver-plated nylon yarn as the core [212]. Li's group used TiO_2 as fillers and silver nanoparticles as an extra coating on top of the electrospun PVDF@ TiO_2 nanofibers. An extra layer of PVDF nanofibers was electrospun onto this yarn to fix the silver nanoparticles. Finally, a plain weave fabric was made with nanofiber yarns through a traditional textile weaving technique. Here, the core layer of silver-plated nylon yarn acted as the inner electrode and the other electrode was a metal electrode clip clamped to the outer surface of the PVDF nanofiber film. The sensor was fabricated by encapsulating this yarn in PDMS and had good response behavior which increased with the increase of effective contact area and applied weight.



“Figure 6. (a) SEM image and (b) TEM image of SF/PVDF nanofibers. (c) Schematic diagram of the structure of the piezoelectric device based on SF/PVDF nanofibers. (d) The sensor attached on the hand bending at various angles and the corresponding piezoelectric responses. (e) The interacting process between human motion and a smart toy car. The smart toy car moved towards different directions when (f) punching, (g) tapping, and (h) bending motion were applied on the SF/PVDF piezoelectric sensor (reproduced with permission from [206]).”



“Figure 7. (A) Processing and structure of PVDF nanofiber array film and nanogenerator. a) Schematic procedure of the preparation of the PVDF nanofiber array film. b,c) Schematic diagram and digital photograph of nanogenerator based on PVDF nanofiber array film. d) SEM image of PVDF nanofiber array film.

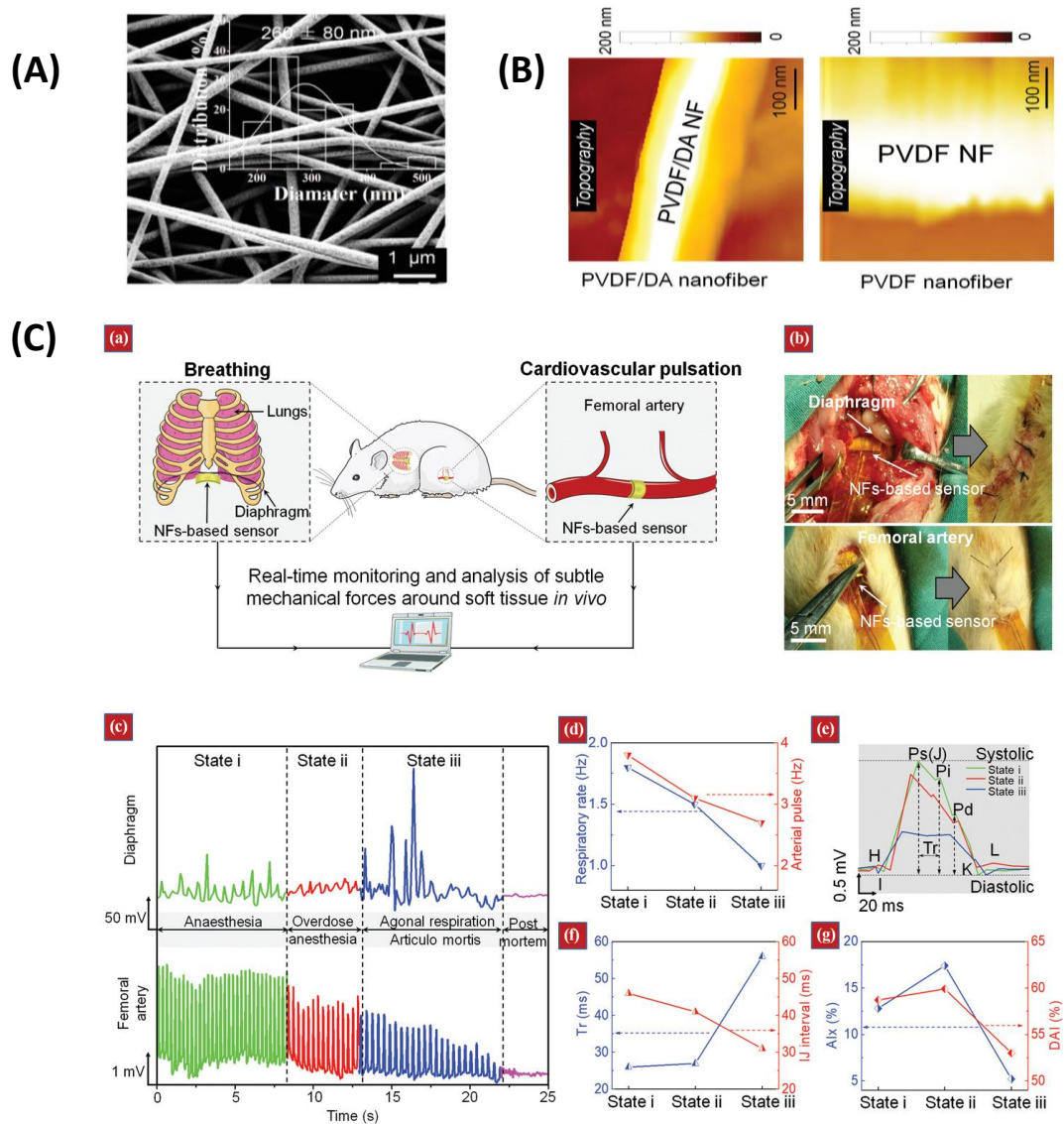
(B) a) Digital photograph of the test system. b,c) Output voltage curve features of the piezoelectric nanogenerator based on the nanofiber array film with a thickness of 2.3 mm and schematic diagram of working mechanism during one impact cycle, respectively (reproduced with permission from [208]).”

Similar to the advances made in manufacturing methods, researchers came up with advanced and novel applications for the different piezoelectric devices they fabricated. Yen *et al.* demonstrated that a dynamic soft sensing element made using $\text{AgNO}_3/\text{PVDF}$ composite fibers could be used for accurate diagnosis and treatment [213]. The device could detect the tremors produced in the biceps muscles and was beneficial in detecting muscle tremors after high-intensity training to obtain information regarding the changes in the symptoms of fasciculation. Furthermore, Li *et al.* fabricated a wearable and implantable biomedical sensor from electrospun core/shell PVDF/dopamine nanofibers [214]. The device was attached to the diaphragm and around the femoral artery of mice and could indicate the inhibition of respiration and loosening of the peripheral arterial walls under the effect of anesthesia by a

change in V_{pp} . Such a piezoelectric sensor offers great potential for the early assessment and prevention of cardiovascular diseases, respiratory disorders, and other pressure-related acute and chronic diseases. It could also be employed to harvest energy from biological deformations such as heartbeats and lung movements, and used to produce electrical stimulation for tissue repair and disease treatment (**Figure 8.**). A PVDF-based piezoelectric device was also used as a human-machine interface in Zhao's study [215]. They fabricated a matrix motion sensor by arranging several small motion sensors from PVDF/ZnO hybrid material. The individual ones were used to detect various movements like finger and foot pressing. With the one with a two-dimensionally arranged set of devices, an NAO robot could be moved and turned according to the walking directions of a person.

Sources other than motion or mechanical deformation can be used to initiate the piezoelectric response of the PENGs. Demirci *et al.* studied the piezoelectric and magnetoelectric energy harvesting capability of a device fabricated from PVDF/NiFe₂O₄ fibers [216]. The device was found to be able to harvest the magnetic fields from the coil of a kettle. It generated a maximum output voltage of 17.45 mV and electrical power of 0.40 μ W under a resistive load of 750 K Ω , at a low-level magnetic field frequency of 50 Hz. A novel PENG-sensor-photodetector was fabricated by Mondal *et al.* using a composite of all-inorganic cesium lead bromide (CsPbBr₃) perovskite rod and PVDF nanofiber [217]. The device is a potential vibration sensor for mobiles, air blower, and regular table fan with an output power of 4.24 mW and durability over 4 months. Similarly, Yang *et al.* used reduced graphene oxide incorporated PVDF fibers and developed a PENG for motion and air leakage detection that produced an output of 200 nA and 150 nA respectively [218]. A type of self-supporting smart air filter was developed by He *et al.* from electrospun PZT/PVDF nanofibers for the harvesting of wind energy along with air filtering [219]. The energy harvested was then used to inhibit bacterial growth. The energy harvester was designed to be a multifunctional device by sputtering a series of square gold particle layers over the fibers and using two metal meshes on either side as electrodes. The gold particle layer acted as a volatile organic compound sensing area in which resistance increases as cracks were formed. The formation of cracks is due to the swelling of the underlying PZT/PVDF fibers as they absorb ethanol vapors. The cracks were healed after the evaporation of ethanol and thus the conductivity of the sensing element was restored. Mousa *et al.* fabricated PVDF-cellulose nanocrystal membranes, that were used to make oil-wastewater separation and self-powered sensors [220]. With their higher water flux and oil rejection properties, they hold potential for future exploration, based on the energy harvesting from flowing droplets. Li *et al.* manufactured polyvinyl alcohol (PVA)-wrapped dopamine/polyvinylidene fluoride shell/core nanofibers and used them as a two-in-one humidity actuator-driven piezoelectric generator [221]. The ability of PVA to spontaneously form hydrogen bonds with water molecules under ambient humidity and anisotropic swelling allowed it to produce mechanical deformation within the PVDF fibers and thereby convert a change in humidity into electric power. Considering real-life applications, it was able to harvest energy from moisture changes in human breath, palm (based on its motion towards and away from the film) and also mental sweating. Thus, the device could be a candidate for human healthcare monitoring too. Another similar example is the study of Lu *et al.* [222]. They developed a PENG using 3D-Tb-modified (BaCa)(ZrTi)O₃ (BCZT)-PVDF core/shell nanofibrous membrane for microenergy harvesting from mechanical motion, acoustic waves and wind. The PENG could achieve 12-28 V as output voltage with wind speeds of 5 to 14 m/s. Hence, it holds the

potential to be used as a commercial digital temperature-humidity meter powered by wind energy.



“Figure 8. (A) SEM image of PVDF/DA nanofibers (NFs) showing their uniform sizes with average diameters of 260 ± 80 nm. (B) Surface topography of a single PVDF/DA NF and pure PVDF NF. (C) In vivo applications of PVDF/DA NF- based sensors. a) Schematic of the PVDF/DA NF- based sensor implantation for recording subtle mechanical pressure changes *in vivo*. b) Surgical images of the implanted PVDF/DA NF- based sensors attached on the diaphragm membrane in the abdominal cavity (top) and onto the femoral artery (bottom). c) Piezoelectric voltage signals induced by diaphragm motions and blood pulsing when the mouse was at different physiological states. State i: anaesthesia; state ii: overdose anaesthesia; state iii: continuous overdose anaesthesia (for diaphragm: agonal respiratory; for femoral artery: *articulo mortis*). d) Respiratory rate and arterial pulse of the mouse at different physiological states measured by a clinical vital signs monitor. e) Piezoelectric signals from femoral artery showing three typical BCG pulse waveforms of the Ps, Pi, and Pd. f) BCG values of IJ interval and Tr of a reflected wave from the hand periphery obtained from (e). g) Comparison of the femoral AIx and DAI among different physiological states, where AIx (%) was defined as $(Ps - Pi)/Ps$ and DAI was defined as Pd/Ps . (reproduced with permission from [214])”

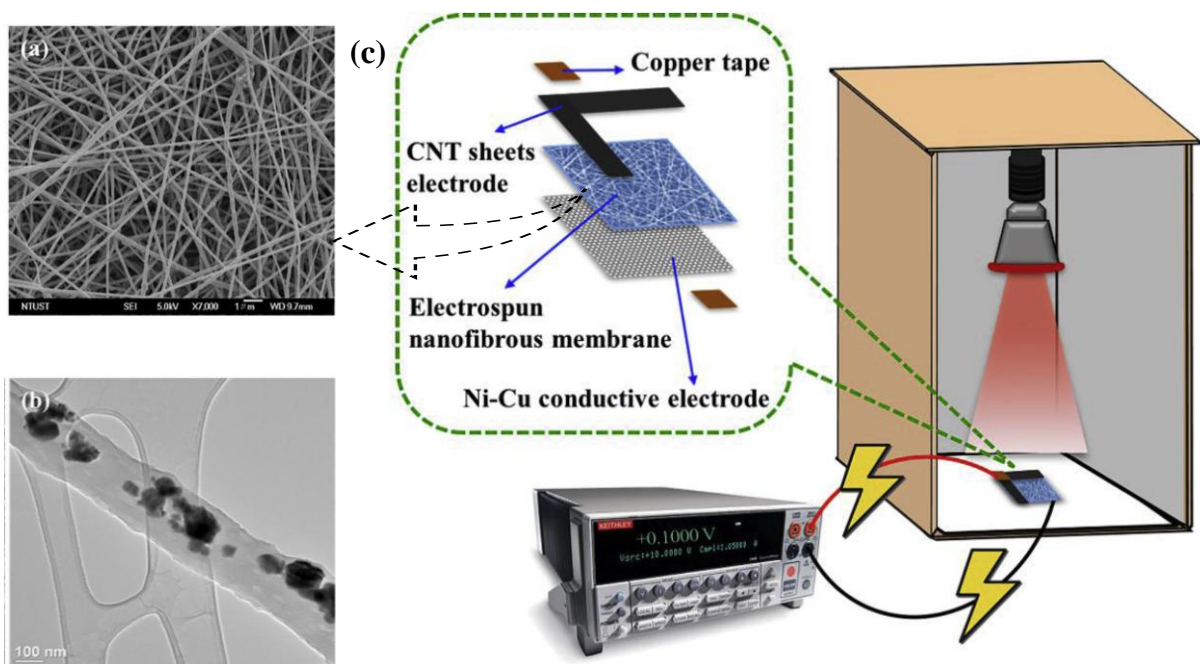
Acoustic waves are another interesting source for stimulating the piezoelectric effect in PVDF nanofibers. Mahanty *et al.* designed a highly sensitive all-fiber acousto- and piezoelectric nanogenerator (AAPNG) with $\text{MgCl}_2 \cdot 6\text{H}_2\text{O}$ added PVDF nanofibers [223]. The AAPNG is a highly sensitive device that generated an open circuit output voltage of 2 and 3 V at sound pressure levels (SPL) of 80 and 120 dB respectively. Because of its improved sensitivity to SPL, the AAPNG could be used as a noise detector and possibly as a self-powering microphone for sound recording. Another motion monitor and acoustic energy harvester with high-potential electronic skin applications were developed by Roy *et al.* [224]. They used naphthylamine bridging a [Cd(II)- μ -I4] two-dimensional metal-organic framework-reinforced PVDF composite nanofibers mat to fabricate this flexible and sensitive composite piezoelectric nanogenerator. When the composite fibers were used for acoustic energy harvesting, the architecture of the device became slightly different from the conventional way. In this case, the nanofiber mat was sandwiched in between two samples of indium tin oxide coated on a poly(ethylene terephthalate) (PET) sheet, with one circular hole of 1 cm diameter cut on each PET film. The hole allowed nanofibers to directly experience the sound vibrations. The as-prepared acoustic nanogenerator gave an open-circuit voltage of 6 V at a sound wave frequency of 120 Hz and 110 dB SPL. A piezoelectric acoustic detector with a frequency resolution better than 0.1 Hz was developed by Xu *et al.* [225]. For this PVDF membrane, a soft pad and a metal plate were put in sequence on a metal and pushed into the grooves of a metal template. The PVDF film was then peeled off to obtain a wave-shaped nanofiber membrane. The device thus produced clear-cut and comparatively higher responses to sounds of different frequencies and SPL. Based on the above results and the fact that every human being's voice has a unique characteristic frequency spectrum, the potential of the device to recognize individuals, words, musical notes or animal sounds were demonstrated by human trials and sounds from a computer played via a loudspeaker.

3.1.2. Pyroelectric nanogenerators and sensors

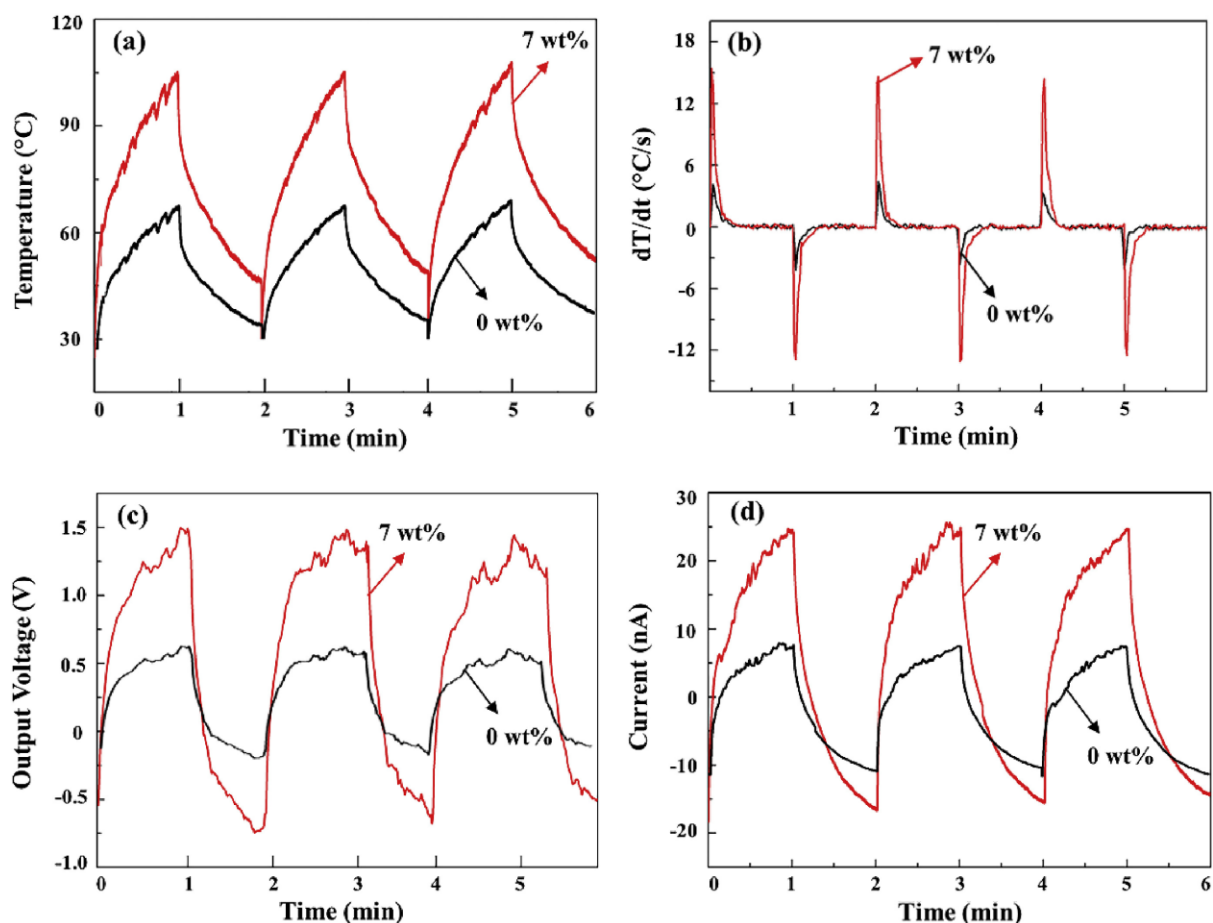
The structure of a pyroelectric nanogenerator based on PVDF films is similar to that of a PENG. In this case, the film with high β phase content is expected to possess a high pyroelectric coefficient as well so that it responds well to changes in temperature. The electrodes and protective coatings are chosen in such a way that along with performing their normal functions, they contribute to the process of heat transfer to the active layer [226,227]. In this section, the different structures and methods used by researchers to maximize the pyroelectric output and to widen the practical applications of the device will be explored.

Wu *et al.* developed an infrared-driven non-contact pyroelectric generator based on electrospun tungsten oxide incorporated PVDF nanofibrous membrane (PVDF/ $\text{WO}_{2.72}$) with improved Near Infrared (NIR) absorption and photothermal conversion ability [228]. They designed the generator using two types of electrodes to maximize the heat transfer and the pyroelectric output. Ni-Cu conductive fabric substrates were used as the bottom electrodes on which the PVDF nanofibers were directly electrospun. The top electrode was an L-shaped conductive carbon nanotube (CNT) sheet that partially covered the nanofibrous membrane, thus allowing maximum heat transfer (**Figure 9**). The as-prepared pyroelectric generator with 7 wt% $\text{WO}_{2.72}$ was subjected to NIR radiations, and the temperature rapidly increased to

107.1 °C after 60 s. Meanwhile, the maximum output voltage could reach 1.5 V and remained stable during multiple cycles (**Figure 10.**). The outputs suggested that the device could also be used as an efficient temperature sensor. Employing cesium tungsten bronze ($\text{Cs}_{0.33}\text{WO}_3$) incorporated screen-printed serpentine electrodes (SRE) and $\text{Cs}_{0.33}\text{WO}_3$ incorporated PVDF nanofibers Gokana *et al.* developed a potential pyroelectric nanogenerator to harvest solar energy [229]. Compromising between the heat transfer rate and resistance of the electrode, and considering the pyroelectric output of the devices made, the SRE which covers 54% of the PVDF film was found to be a suitable electrode. The pyroelectric nanogenerator made from this electrode and 7 wt% of $\text{Cs}_{0.33}\text{WO}_3$ added PVDF films could power a liquid crystal display (LCD) and four light-emitting diodes through capacitor charging. Along with demonstrating the pyroelectric application of PVDF, the study demonstrates how the engineering of electrode structure plays a crucial role in the final output.



“**Figure 9.** (a) SEM and (b) TEM images of electrospun PVDF/ $\text{WO}_{2.72}$ nanofibrous membranes, (c) Schematic illustrations of pyroelectric measurement (reproduced with permission from [228]).”



“Figure 10. (a) Temperature variation over time, (b) corresponding differential curve, (c) output voltage and (d) output current of $\text{WO}_{2.72}$ -free PVDF and 7 wt% PVDF/ $\text{WO}_{2.72}$ pyroelectric composites (reproduced with permission from [228]).”

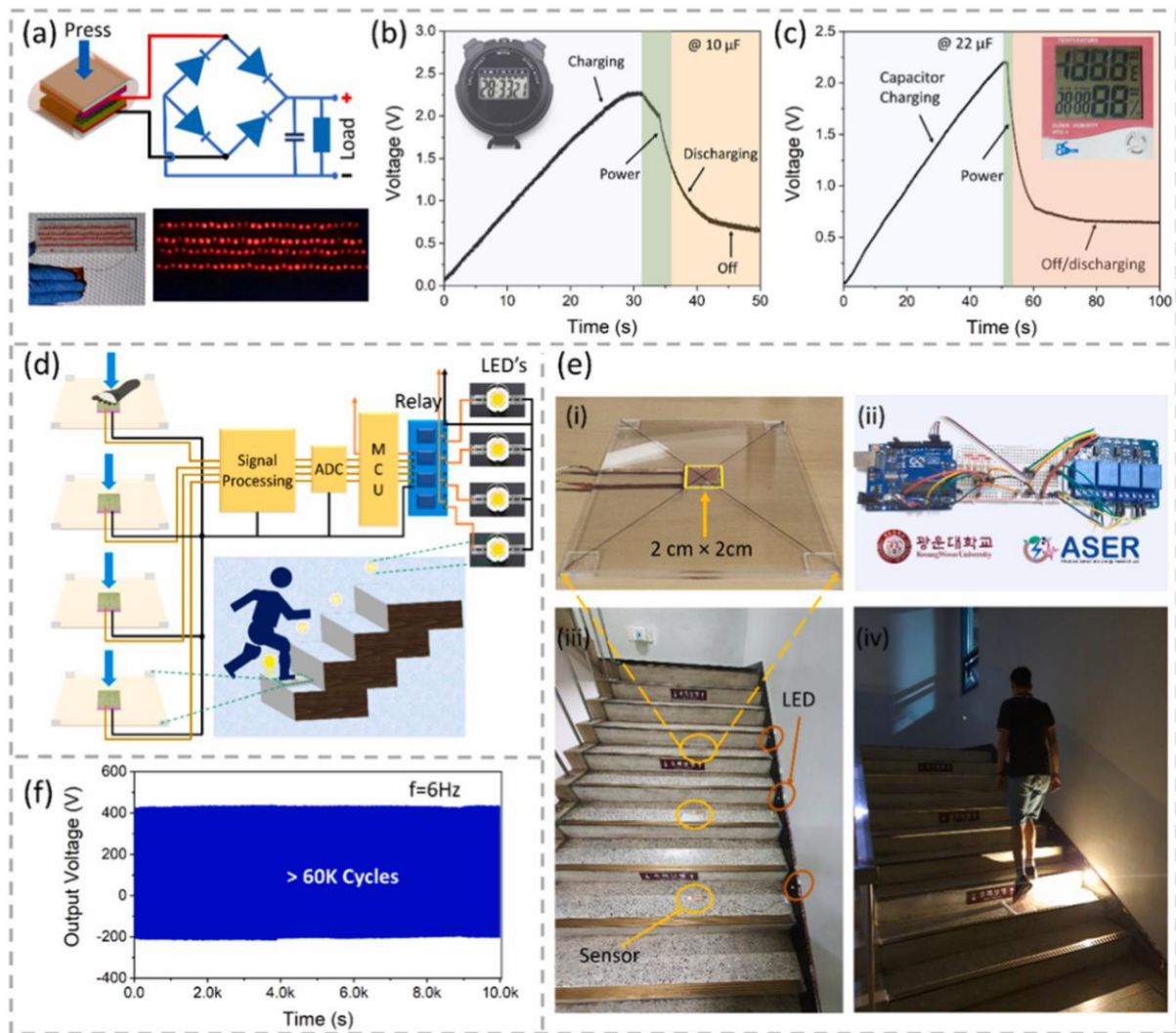
3.1.3. Triboelectric nanogenerators and sensors

Triboelectric nanogenerators (TENG) possess two active layers. As mentioned earlier, a PVDF nanofiber-based membrane acts as the triboelectric negative layer, and aluminum films, copper films, or nylon are commonly used as positive triboelectric layers. The separation between these active layers is maintained using spacers, binding yarns, or transition layers which are often made of polyimide (PI) films, Kapton films, etc. The electrodes and connection lead further to complete the TENG. There are four representative modes of operation of TENGs, among which the most common is the vertical separation mode. In this mode, the layer on which pressure is applied will come in contact with the other, and a transfer of charges occurs. As the pressure is released the layers attain the initial separation with the help of the spacers. In the lateral sliding mode, one triboelectric layer is made to slide over the other to produce charge separation. In the single-electrode mode charge transfer occurs as the surfaces of the triboelectric polymer fibers are brought to contact with the electrode. The fourth mode is the free-standing mode which is accomplished by arranging the triboelectric layers with electrodes attached to them underneath another frictional layer. The approaching and departing of the frictional layer from the electrodes

build an unbalanced charge distribution resulting in the flow of electrons between the electrodes [230–234]. As the performance of TENGs strongly depends on surface properties, their fabrication should focus on improving the effective contact area and minimizing the change in surface properties with time under friction exposure and environmental conditions. Accordingly, great efforts have been made to develop robust TENGs. In this section of the review, some of the recent attempts in the case of PVDF-based TENGs will be explored, and the development of highly durable TENGs will be discussed.

Bhatta *et al.* proposed the use of MXene ($\text{Ti}_3\text{C}_2\text{T}_x$) functionalized PVDF composite nanofiber as a negative triboelectric layer for triboelectric energy harvesting performance [235]. An electrospun Nylon 6/6 nanofibrous membrane acted as the positive triboelectric membrane. The fabricated TENG-energy storage device could successfully power 120 commercial LEDs under gentle tapping. It could charge a 10 μF capacitor up to 2.25 V within 31 s and a 22 μF capacitor up to 2.25 V within 50 seconds to turn on a sports watch for 5 seconds and operate a hygrometer sensor, respectively. This device was further used as a self-powered foot motion sensor, which automatically controls the lights on the steps as one moves over the stair (**Figure 11.**). Another PVDF-nylon TENG was developed by Sun *et al.* [236]. Herein they doped MoS_2/CNTs in PVDF to produce TENG that could give an open-circuit voltage reaching 300 V, and short-circuit current (I_{sc}) of $\sim 11.5 \mu\text{A}$ when the thickness of PVDF nanofibers was 0.08 mm and MoS_2/CNT concentration was 0.3 wt%. It gave a V_{pp} of ~ 50 V, 90 V, and 100 V when worn while walking, or running. Similar to the above, the large difference in triboelectric polarity of PVDF and nylon membranes encouraged Li *et al.* to structure a wearable, flexible, and lightweight TENG from these [237]. By attaching the TENG to various keys of a keyboard, an output voltage of 8 V is obtained while typing. Elbow bending produced 10 V.

Huang *et al.* developed an all-fiber-structured TENG as an energy harvester and self-powered human motion monitor [238]. Here, ethyl cellulose co-electrospun with polyamide 6 was used as the triboelectric positive material, and electrospun PVDF nanofibers with MXene sheet were used as the triboelectric negative material. This device could charge capacitors of varying capacitance and power 180 commercial LEDs. The motion monitoring ability of the TENG was confirmed from the output of the sensor detecting walking, hand clapping, and moving of arms. A TENG with ultrahigh outputs which reached 1502 V and 50.61 μA , was fabricated by Sun *et al.* [239]. For this, the friction layers were manufactured by growing triangular cone-structured polyaniline (PANI) nanofibers vertically on PI substrates and electrospinning PVDF on PI substrates. The micro/nanostructure obtained during electrospinning provided a rough surface which enhanced the generation of surface charges during the friction process. This TENG with stable output for over 50000 cycles and 12000 s at a frequency of 5Hz was later used to form self-powered electrostatic manipulation systems and to reciprocate the movement of macro-charged droplets. In a study conducted by Zhang *et al.*, an electrospun PVDF nanofibrous layer was put to aid the energy harvesting from a flexible triboelectric generator integrated with a high-efficiency energy storage unit [240]. This device gave a V_{oc} of 560 V and I_{sc} of 1.30 μA , respectively.



“Figure 11. Application and demonstrations of the TENG. (a) Schematic diagram of the TENG with rectifier circuit, photograph of more than 120 LEDs arranged in series connections, and photograph of the corresponding LEDs turned ON from the TENG upon simple hand tapping motion. (b) Charging and discharging characteristics curves of the capacitors utilized to operate a commercial sport watch (insert shows the turned ON condition hygrometer). (c) Charging and discharging characteristics curves of the capacitors utilized to operate a thermohygrometer sensor from the TENG under gentle hand tapping motion (insert shows the turned ON condition of thermohygrometer sensor) (d) Schematic illustration of the TENG utilized as a self-powered footstep motion sensor. (e) Photograph of (i) fabricated TENG utilized as self-powered foot motion sensor, (ii) sensor data processing and controlling circuitry, (iii) sensor and LED arrangements over the steps, and (iv), real-time step lights control application demonstration. (f) Durability test voltage waveform of TENG at 6 Hz input frequency. (reproduced with permission from [235]).”

Busolo *et al.* focused on improving the robustness of the TENG along with improving its energy harvesting potential [241]. For this, a conducting CNT yarn electrode was placed as a rotating collector which was coated with PVDF fibers by electrospinning. For the energy harvesting study, the as-prepared yarn was cyclically tapped against a Nylon 6 film sputter-coated with gold on its non-contact side to form the vertical-separation TENG. Under a constant tapping of 10 N force and 2 Hz frequency, a maximum root-mean-square (RMS)

power output of 72 nW at a 400M Ω resistance could be obtained. The ability of the triboelectric yarn (in single electrode mode) to generate voltage curves with distinct peaks, peak width, and peak amplitude portrays it as a wearable motion, haptic, and force sensor. Sun *et al.* developed a wearable, washable, and air-permeable TEN sensor which is also waterproof [242]. Electrospun PA66/MWCNT nanofiber film, conductive fabric electrode, and waterproof and breathable cotton fabric were sewn together to act as the triboelectric positive layer. Electrospun PVDF nanofiber film was sewn together to act as the waterproof, breathable fabric and the triboelectric negative layer. It could power 160 LEDs by itself and be combined with clothes to harvest the energy from hand, shoulder, or arm movement (49 V and 36 V, respectively). Tests revealed that the TENG has consistent output over 10000 cycles of pressure stimulation and 2–6 h of washing. By weaving Si_3N_4 doped PVDF and polyurethane nanofiber core-spun yarns into a double-layer fabric, Tao *et al.* developed a flexible, wearable, washable, and highly durable TENG [243]. Herein they used a four-needle conjugated electrospinning technique with copper fibers as the conductive core yarns. Later these yarns were woven into two plain fabrics using textile weaving technology and were sewn into a double-layer fabric by using nylon yarn. The output of the TENG depended on the fabric area and pressing frequency. The TENG was also successful in producing output signals with varying amplitudes and rates corresponding to the difference in the way of finger tapping. Thus, it was established that the TENG could clearly distinguish between various forces and frequencies and hence be used for human motion monitoring, intelligent textiles, etc. Adding to the list the highly durable TENGs, Cheng *et al.* developed a flexible, and self-healing ionic liquid elastomer-based triboelectric generator [244]. Herein, an electrospun PVDF/PU nanofibrous membrane was used as the triboelectric layer and was integrated on the CNTs-doped ionic liquid elastomer (ILC) electrodes by autonomous adhesion. This mechanical damage-resistance TENG with a stable output after five cutting-healing cycles is a promising wearable bioelectronic device for human healthcare detection and human-machine interaction.

In the framework of research during the Covid-19 pandemic, He *et al.* developed a respiration monitoring triboelectric nanogenerator (RM-TENG) The RM-TENG could be attached to a mask to be used as a convenient, smart, changeable, and self-powered mask filter [245]. It could successfully monitor respiratory parameters, such as respiratory rate (RR), inhalation time (t_{in}), exhalation time (t_{ex}), and their ratio ($\text{IER}=t_{in}/t_{ex}$) with good accuracy. Looking into the architecture of RM-TENG, polyacrylonitrile, and PVDF electrospun nanofiber mat functioned as the triboelectric layers, to which conductive aluminum fabrics (with and without holes) were attached as electrodes. A miniature printed circuit board was attached to collect and transmit the data. **Figure 12.** represents the signal wave forms and real-time RR and IER response of RM-TENG during walking and running when the mask was attached to RM-TENG. A novel approach in which a single self-powered device could simultaneously generate power from wave motion, sense, and wirelessly transmit wave information was put forward by Bhatta *et al.* [246]. The TENG had a composite nanofiber of 2D MXene/ PVDF and Nylon 6/6 as the triboelectric layers and a custom-fabricated ferromagnetic composite film of iron-silicon chromium (FeSiCr)/PDMS attached on top of it. A magnetic ball within an ellipsoid body of the device rotated distinctly according to different wave parameters which caused actuation in the TENG, therefore producing an output that was characteristic of the wave. An entire Bluetooth signal processing circuitry was powered from a capacitor (1 F, 5.5 V) charged for 124.5 min to 4.1

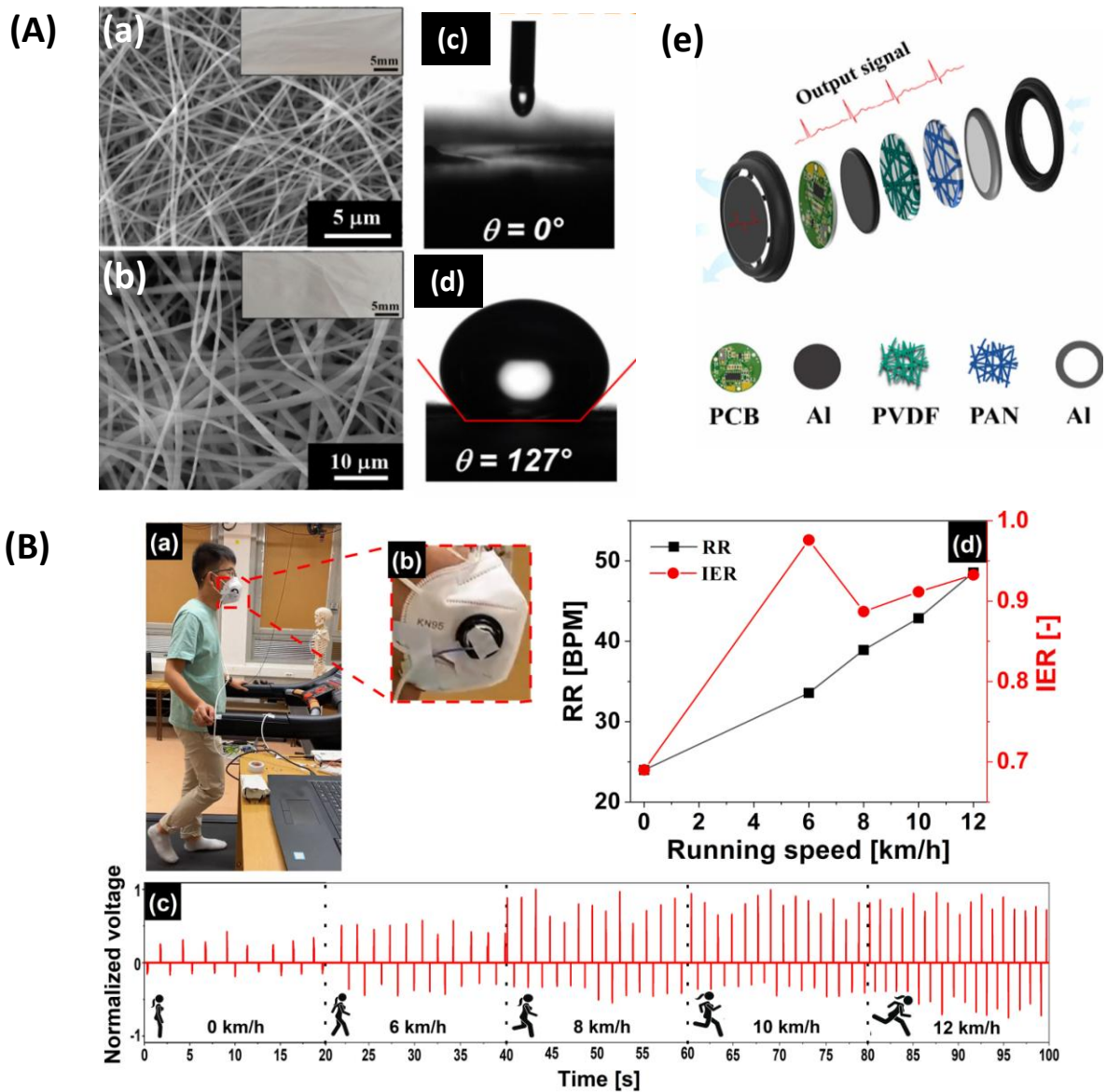
V using the device. Continuous data transmission was possible from the Bluetooth circuitry for 31.25 s and stopped as the capacitor voltage dropped below 3.75 V. Apart from using TENG as sensors, Yang *et al.* used electrospun nylon-PVDF nanofiber-based TENG for water/oil (W/O) emulsion separation [247]. In this case, the TENG was used to charge parallel electrodes to produce an asymmetric alternating voltage output of 2500 V for W/O emulsion separation. Under the action of electric field force the demulsification, coalescence, and sedimentation of droplets occurred and visible free water appeared at the bottom of the container. After 30 min of being subjected to the asymmetric AC electric field powered by TENG, the moisture content reduced from 5 wt% to 0.15 wt% in the W/O emulsion. The separation efficiency increased with an increase in the output voltage of the TENG and working time. Furthermore, a sandwich-like TENG was designed to harvest wind energy and demonstrate W/O emulsion separation from natural energy sources. In this case, PVDF nanofibers served as the flexible vibration layer, and nylon nanofibers as the bound layer, an output voltage of 1400 V was produced at a triggering frequency of 28 Hz driven by the wind with a speed of 8 m/s. This was then used to power four parallel electrodes which produced an asymmetric AC electric field. After 30 min of use, the device was able to lower the moisture content in a 500 ml W/O emulsion from 10 wt% to 0.18 wt%. This high efficiency, along with the low cost and safety of the TENG qualifies it for industrial wastewater treatment.

3.1.4. Hybrid nanogenerators and sensors

Hybrid nanogenerators are devices that combine piezoelectric, pyroelectric, or triboelectric mechanisms for efficient and advanced energy harvesting and sensing applications. They are manufactured to maximize the output from both mechanisms without one suppressing the other [191,248]. A few of the recent attempts at developing such novel devices, their structure, and fascinating real-time applications are discussed in this section.

Mahanty *et al.* developed an interesting all-fiber pyro- and piezoelectric nanogenerator (PPNG) healthcare monitor and sensor [249]. Herein, MWCNT-incorporated electrospun PVDF nanofibers were used by them as the active layer along with an interlocked conducting micro-fiber-based electrode to fabricate this device. This PPNG, with an ultra-fast response time of ~10 ms, also had a high electrical throughput and produced an output voltage of ~35 V under repeated finger tapping. The PPNG was even capable of harvesting large temperature fluctuations of ~14.30 K as well as sensing thermal fluctuations as low as ~5.4 K. The device also exhibited different and characteristic responses for different biomechanical signals such as wrist and palm movements, pulse rate, or vocal cord vibrations. Thus, the PPNG could be used as a biomedical sensor capable of monitoring body temperature as well as body movements. This possibility was further demonstrated by integrating the PPNG with a Bluetooth module or Wi-Fi module connected to smartphones, for wireless healthcare monitoring. With a slightly more complex architecture, Wang *et al.* fabricated an all-in-one electronic skin textile for both temperature and pressure sensing [250]. The temperature sensing layer was made up of flexible thermal-resistance carbon nanofibers with localized graphitic structures while PVDF/ZnO nanofibrous membrane acted as the pressure sensing layer. The change in resistance as the temperature changes allowed the e-skin to detect temperature accurately. Practical pressure sensing applications were

demonstrated by sensitive weight identification, finger touch pressing, and human carotid pulse capture. Expiratory air temperature monitoring



“Figure 12. (A) SEM image of PAN-NFM (insert is the photograph of the PAN-NFM); (b) SEM image of PVDF-NFM (insert is the photograph of the PVDF-NFM); (c) Water contact angle on flat PAN-NFM; (d) Water contact angle on flat PVDF-NFM. (e) Schematic illustration of the RM-TENG. (B) (a) Photo of the subject walking on the treadmill with a mask attached to the RM-TENG. (b) The enlarged mask attached to the RM-TENG. (c) The signal waveforms recorded by the RM-TENG after the subject walked/ran on the treadmill at various speeds. (d) The real-time RR and IER obtained from the RM-TENG after the subject walked/ran on the treadmill at various speeds (only 20 s of data recording for each test is displayed for the clear peaks and frequencies). (reproduced with permission from [245]).”

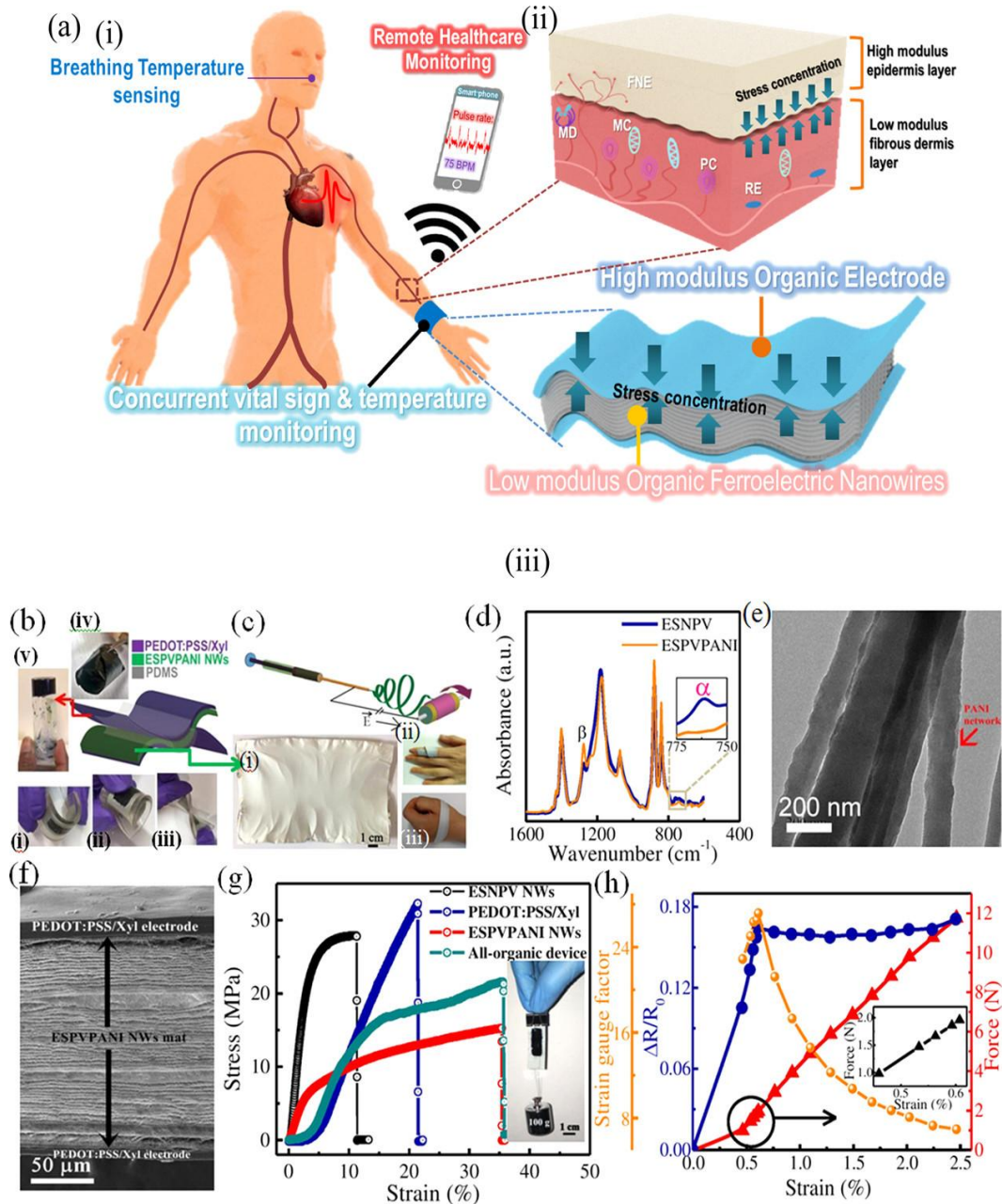
depicted the potential of the e-skin in real-time temperature sensing. The sensor units could also be arranged as e-skin sensor arrays that can distinguish the contour of physical objects. It

was finally able to track the real-time touch movements visually which could operate small robots, artificial prosthetics, etc.

Similarly, Ghosh *et al.* developed an all-organic stretchable energy harvester with electrodes made of a xylitol-added poly(3,4-ethylenedioxythiophene): poly(4-styrenesulfonate) film [190]. PANI-reinforced PVDF nanofibers were the piezo and pyro-active material and PDMS coating acted as the protective layer. The device produced maximum pyro- and piezoelectric power outputs of $3 \mu\text{W}/\text{m}^2$ and $31 \mu\text{W}/\text{cm}^2$ respectively under periodic thermal and mechanical oscillations. It was also attached to a philtrum to demonstrate its breath-sensing functionality and a peak-to-peak voltage of $\sim 555 \text{ mV}$ was obtained corresponding to the temperature fluctuation from 298 to 304 K during inhalation and exhalation. By producing a positive pyroelectric output peak as a hot object approached, and a negative pyroelectric output as it moved away (vice versa in the case of a cold object), the device demonstrated its purpose as a temperature sensor. It was also integrated into a smartphone to warrant the applicability of this sensor towards wireless human-machine interfacing point-of-care diagnostic devices (**Figure 13**). Xia *et al.* developed a flexible, multi-site tactile and thermal sensor (MTTS) using PVDF nanofibers as the active material, etched copper wire polyimide film as the top electrode, and aluminum electrode array as the bottom one [251]. By arranging several of these sensors into a 2-D array the group successfully employed it for spatial mapping and recording of the 2-D motion trajectory of an object. The output voltage and current from each sensor of the array were recorded as the mapping of the external pressure and thermal stimulus from the object. The piezoelectric and pyroelectric components were extracted from the composite output through the mapping relationship between the signals. The simultaneous pressure and temperature mapping of the human palm and foot were performed using the device and the results showed very few errors from the actual pressure and temperature. The study demonstrated that integration of the MTTS with a wireless sensing system can have extraordinary potential in human behavior detection, disability aids, thermoelectric distribution detection, etc. In addition to the nucleation of the β phase, Li *et al.* explored the possibility of enhancing the piezoelectric and triboelectric effects in PVDF fibers through the addition of fillers [252]. In the study, by simply adding carbon-coated zinc oxide (ZnO@C) nanoparticles, they demonstrated that the piezoelectricity improved due to the nucleation of the β phase and the triboelectricity improved due to the shift in surface potential. The device made from 5% ZnO@C/PVDF nanofibers showed a very high output voltage of 37 V and 39 V as PENG and TENG respectively. It was then put to test as a motion sensor and was successful in producing characteristic outputs for different arm movements and also detecting even slight vibrations, with an output voltage of 0.1 V.

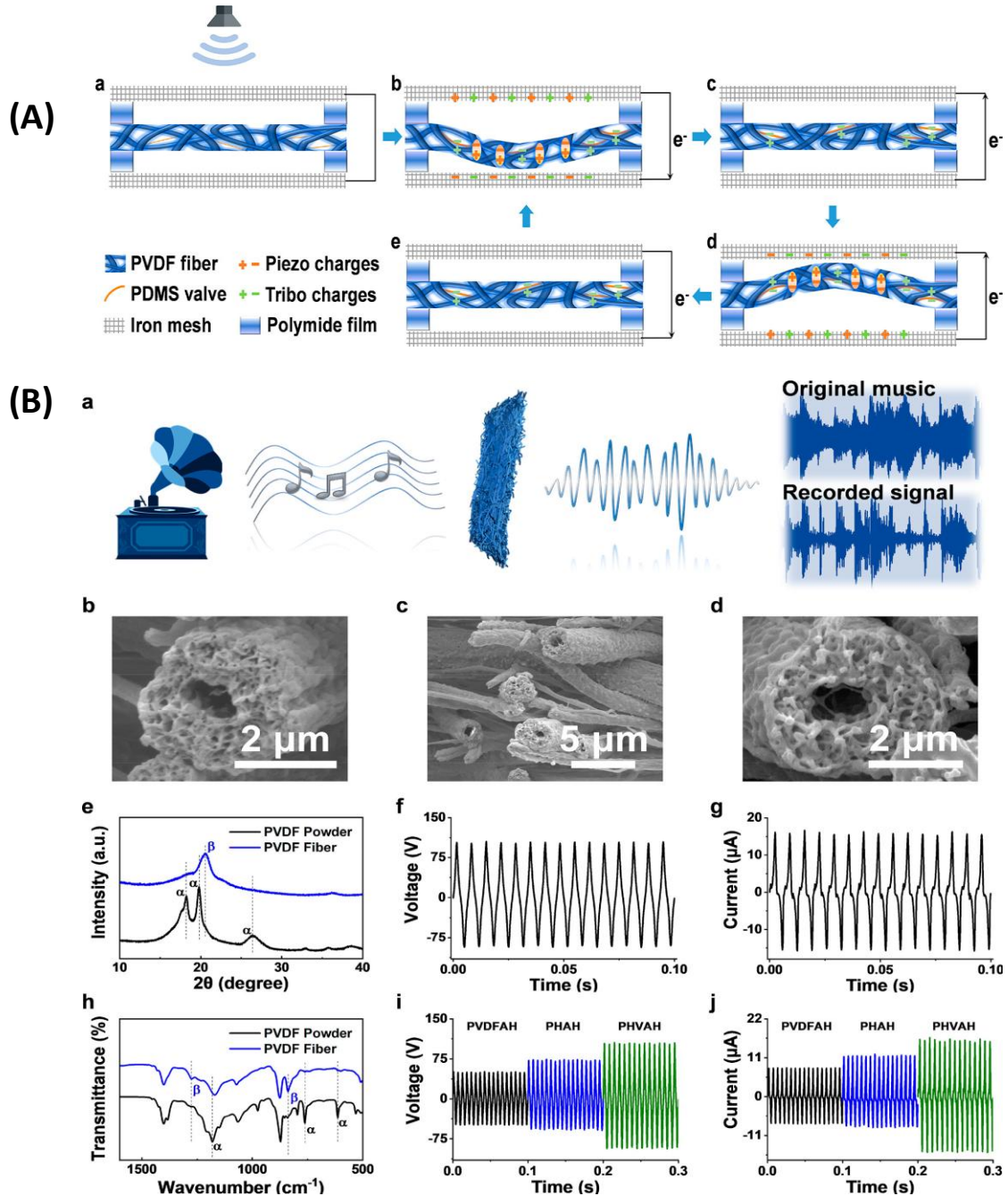
A piezo-tribo hybrid nanogenerator for efficient acoustic harvesting was fabricated by Yu *et al.* from nanoporous PVDF hollow fiber and PDMS valve (PHVAH) [253]. The hollow PVDF fibrous membrane was obtained by removing the polyethylene glycol (PEG) in the PVDF/PEG fiber prepared by coaxial electrospinning. Then, by immersing this membrane in the diluted PDMS, the PDMS valve structure which can mimic the eardrum could be formed between the hollow fibers. To facilitate the direct contact of sound waves with the fibers, iron meshes were placed on both sides of the membranes as electrodes. As the membrane deformed due to sound waves a piezoelectric output was generated along with a triboelectric output due to the rubbing of the PVDF hollow fibers with the PDMS valves and iron meshes

(Figure 14.). The optimum output of the acoustic harvester from the combined piezo and triboelectric effects was equal to 105.5 V under the sound stimulation of 117.6 dB and 150 Hz. PHVAH showed high sensitivity, wide frequency response (70 to 1500 Hz), stability, and flexibility and thus, could be used for real-time detection of sound changes and further harvesting of acoustic energy. In the study of Niu *et al.* on nylon-6/PVDF single-layer nanofibers, the device was



“Figure 13. a) Schematics of (i) wireless arterial pulse monitoring, (ii) epidermal–dermal layer of the human skin, and (iii) developed all-organic epidermal sensor. (b) Three-dimensional (3-D) design and optical images of the all-organic nanoharvester possessing bending (i), folding (ii), and twisting (iii) abilities and composed of (iv) flexible PEDOT:PSS/Xyl electrode manufactured from (v) the PEDOT:PSS/Xyl gel. (c) Schematic of electrospinning used for fabrication of (i) ESPVPANI nanowire mat possessing (ii) excellent flexibility and (iii) conformability to human skin, (d) Fourier transform infrared (FT-IR) spectra, (e) high-resolution transmission electron microscopy (HR-TEM) image, (f) cross-sectional field emission scanning electron microscopy (FE-SEM) image of the all-

organic nanoharvester, (g) stress–strain curves, where the inset shows an optical image of the all-organic nanoharvester (without poly(dimethylsiloxane) (PDMS) encapsulation) loaded with a tensile force based on a hanging mass of 100 g, and (h) resistance change and corresponding strain gauge factor of the PEDOT:PSS/Xyl electrode under a range of compressive forces and strains. The inset shows the force versus strain graph up to 0.6% strain. (reproduced with permission from [190]).”



“**Figure 14.** (A) Structure illustration and mechanism diagram of PHVAH driven by sound: (a) Initial equilibrium state. (b) PVDF hollow fiber and polydimethylsiloxane valve (PHV) membrane deformed by sound waves. (c) Membrane recovers from the deformation. (d) PHV membrane deformed by sound waves in the opposite direction. (e) Membrane recovers from the deformation again. (B) (a) Schematic diagram of the realization from sound to electricity with the fabricated PHVAH. (b) Morphology of single PVDF hollow fiber (PH) fiber. (c) Morphology of PH fibers. (d) Morphology of PVDF fiber with PDMS valves. (e) X-ray diffraction (XRD) pictures of PVDF powder and PVDF fiber prepared by coaxial electrospinning. (f) Optimal output voltage of PHVAH under a sound

stimulus of 117.6 dB and 150 Hz. (g) Optimal output current of PHVAH under a sound stimulus of 117.6 dB and 150 Hz. (h) Fourier-transform infrared spectra (FTIR) images of PVDF powder and PVDF fiber. (i) Output voltages of PVDF acoustic harvester (AH), PHAH, and PHVAH under a sound stimulus of 117.6 dB and 150 Hz. (j) Output currents of PVDFAH, PHAH, and PHVAH under a sound stimulus of 117.6 dB and 150 Hz. (reproduced with permission from [253]).”

fabricated so that it behaves like an assembly of many small PENGs and TENGs [254]. Here, the small number of nylon-6 nanofibers incorporated into the PVDF fibrous matrix by co-electrospinning acted as a dopant to form macro dipoles. This improved the charge transport from the dielectric layer to the external electrodes and also caused an endogenous triboelectric effect with PVDF nanofibers. The device was completed with the addition of stainless-steel mesh electrodes and produced a peak voltage output of 201.4 V under a sound wave of frequency 230 Hz, 118 dB SPL. The practical application of the device was put to test by using it to charge batteries and capacitors, light LEDs, and power an electronic watch, and an electric torch. The charge of capacitors when the device was kept in a noisy workshop with a hammer sounds further justified its applicability.

Based on the above-mentioned research works it is clearly understood that electrospun PVDF films are high potential candidates for different types of nanogenerators and sensors. The study also reveals different types of fillers which contribute to the electroactive response of PVDF, the architecture, and a wide variety of non-conventional energy generation techniques.

3.2. Other Applications

The applications of PVDF or electrospun PVDF nanofibers are not limited to energy harvesting. Over time, both PVDF and electrospun PVDF nanofibers created their own space in several fields from material science to biology and medicine. Along with the intensive study on the polymer, great efforts are being taken to develop novel devices from it for various applications.

Because of the biocompatibility, non-degradable nature, and low fiber diameter of electrospun PVDF nanofibers, Klapstova *et al* used it as glaucoma drainage implants by mixing it with polyethyleneoxide (PEO) [255]. Meanwhile, Agueda *et al.* used PVDF nanofibers for renal tissue regeneration [256]. Along with biocompatibility, minimal cellular and tissue response, and chemical inertness, the possibility of producing uniform fibers with larger pore sizes was the reason for them to choose PVDF nanofibers. By soaking PVDF nanofibers in benzocaine and its complex with β -cyclodextrin (benzocaine- β -cyclodextrin or BNC: β -CD) Rajamohan *et al.* developed a drug delivery system of BNC and BNC: β -CD [257] (**Figure 15 (a)**).

PVDF nanofibers are also extensively used for the fabrication of different filters. Because of their filtration efficiency, small pore size, and large surface-to-volume ratio, Victor *et al.* used PVDF-titanium nanotube fibers to develop an antibacterial filter media [258]. In the future, this filter could be used for filtration of other microbes, facemasks, and industrial-scale air filters. Wang *et al.* also used electrospun PVDF membrane to produce air filters that out-performed commercial masks by capturing up to 99.9% of coronavirus

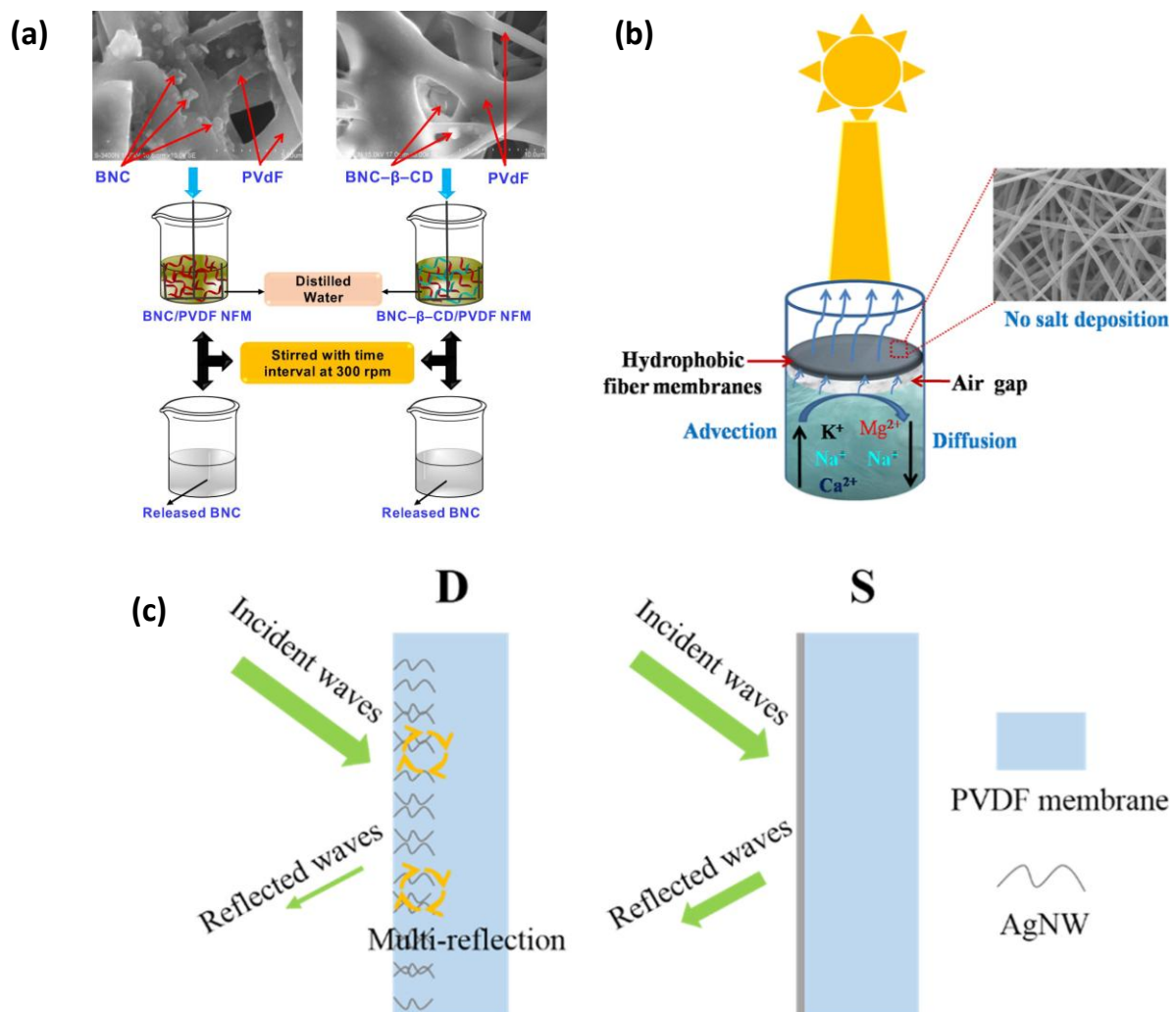
aerosols [259]. Pascariu *et al.* demonstrated that electrospun PVDF fibers with lanthanide (Ln) doped ZnO nanoparticles (Ln=Sm, La, Er) as fillers could be developed into membranes for adsorption and photocatalytic degradation of dyes and organic pollutants [260]. When put to test for the degradation of methylene blue (MB) and rhodamine B (RhB) the PVDF/ZnO:La membrane showed color removal efficiency of 96.33 % and 93.36 % respectively. By using ultrathin PVDF fibers with high surface area, smaller pores, and rough surface, Yang *et al.* developed a high-efficiency coalescence membrane [261]. The membrane, with poor oleophilicity under water, efficiently separated different types of emulsions which indicated its applicability to clean different oil wastewaters. A multi-functional fiber membrane for sewage treatment and desalination was developed by Tessema *et al.* from cesium tungsten oxide/graphitic carbon nitride ($\text{Cs}_{0.32}\text{WO}_3@g\text{-C}_3\text{N}_4$) hybrids doped PVDF nanofibers [262]. The multifunctionality of the membrane could be attributed to the hydrophobicity of PVDF. Organic dyes like 4-nitro phenol and tetracycline were also efficiently removed by the membrane making it a suitable candidate for practical waste water treatment in the future (**Figure 15 (b).**).

Electrospun PVDF fibers, because of their electrochemical stability, mechanical strength, and flexibility can be used for battery applications [263]. A self-standing electrolyte membrane was created by Makhlooghiazad *et al.* from triisobutyl(methyl)phosphonium bis(fluorosulfonyl)imide ([P1i444][FSI]) OIPC mixed with 20 mol% of NaFSI or NaTFSI and combined with electrospun PVDF membranes. The PVDF nanofibers, along with providing structural support, interacted with NaTFSI-doped electrolytes and thus made them more conductive and superior to several other fiber-based electrolytes in Na metal batteries. Similarly, Barbosa *et al.* used electrospun PVDF fibers as separators for lithium-ion batteries [264]. In this case, the ionic conductivity of the PVDF fibers was enhanced by the addition of ionic liquids sharing the same anion, but different cations. By improving the electrical conductivity of PVDF nanofibers, it became suitable for electromagnetic interference (EMI) shielding. Qian *et al.* used electrospun porous PVDF nanofibers and developed an efficient lightweight EMI shielding membrane by dip-coating silver nanowires (AgNWs) onto it [265]. The AgNWs reached well into the pores of the PVDF fibers and increased the electrical conductivity of the fibers by forming 3D AgNW networks. This also resulted in the multiple reflections of the EM wave (**Figure 15 (c).**). Ann Rose *et al.* also used electrospun PVDF fibers for EMI shielding [266]. Here they added graphene as the filler to improve electrical conductivity and by increasing its concentration, the EMI shielding property increased. Thus, PVDF can play an important role in reducing the growing radiation pollution as well.

4. Conclusions

PVDF is an excellent electroactive polymer, and one of the most studied polymers for the development of nanogenerators, wearable sensors, and many other applications. The elemental information about PVDF, and a wide variety of PVDF-based nanocomposites were discussed in the review. The process of electrospinning, its interest in film production, and the advantages of electrospun PVDF fibers were also explained. Following this, the review details how the different electrospinning parameters help to enhance the β phase, and thereby enhance the piezo-, pyro- and triboelectric performances of PVDF. The review then

progresses into the recent developments of PVDF fiber-based devices in energy harvesting and sensing applications. This section highlighted the advances made to harvest the otherwise wasted mechanical and thermal energy. The innovations brought in the fabrication of different types of nanogenerators and their significance in real life as a renewable and green source of energy are discussed. Along with the conventional nanogenerators, the technological advances of hybrid nanogenerators are explored. These types of devices which could simultaneously harvest energy from multiple sources, sense various fluctuations in the surrounding environment, and also be integrated with wireless data transmitting devices are a true example of portable, multipurpose, and sustainable engineering. This review aims to highlight the potential of electrospun PVDF films to develop such functional devices and inspire their use as innovative sustainable sources of energy in the near future. Finally, a peek into the other possible applications of electrospun PVDF nanofibers like tissue regeneration, drug delivery, filtration, or EMI shielding is made to depict other possible uses of the material. Overall, the review is hoped to serve as a useful reference for the scientific community and to look forward to the possible commercialization of PVDF-based multifunctional devices.



“Figure 15. (a) Schematic procedure for drug release from PVDF nanofibrous membranes (reproduced with permission from [257]), (b) Schematic illustration of salt resistance hydrophobic

CS_xWO₃@g-C₃N₄/PVDF fiber membranes (reproduced with permission from [262]), Schematic electromagnetic interference shielding mechanisms for the dip-coated and spray-coated PVDF/AgNW hybrid membranes (reproduced with permission from [265]).”

Acknowledgments

The authors of the work would like to thank Indo-French Centre for the Promotion of Advanced Research/Centre Franco-Indien pour la Promotion de la Recherche Avancée (IFCPAR/CEFIPRA), French National Centre for Scientific Research (Centre national de la recherche scientifique, CNRS) and Lorraine University of Excellence for the support.

REFERENCES

1. Curie, J.; Curie, P. Développement Par Compression de l'électricité Polaire Dans Les Cristaux Hémihédres à Faces Inclinaées. *Bulletin de Minéralogie* **1880**, 90–93.
2. Momeni, K.; Odegard, G.M.; Yassar, R.S. Nanocomposite Electrical Generator Based on Piezoelectric Zinc Oxide Nanowires. *Journal of Applied Physics* **2010**, *108*, 114303.
3. Koka, A.; Zhou, Z.; Tang, H.; Sodano, H.A. Controlled Synthesis of Ultra-Long Vertically Aligned BaTiO₃ Nanowire Arrays for Sensing and Energy Harvesting Applications. *Nanotechnology* **2014**, *25*, 375603.
4. Smith, G.L.; Pulskamp, J.S.; Sanchez, L.M.; Potrepka, D.M.; Proie, R.M.; Ivanov, T.G.; Rudy, R.Q.; Nothwang, W.D.; Bedair, S.S.; Meyer, C.D. PZT-Based Piezoelectric MEMS Technology. *Journal of the American Ceramic Society* **2012**, *95*, 1777–1792.
5. Kordlar, A.G.; Koohsorkhi, J.; Nejad, E.T. Barium Titanate Nanorods on Micro-Machined Silicon Substrate for Performance Enhancement of Piezoelectric Nanogenerators (NGs). *Solid-State Electronics* **2021**, *186*, 108168, doi:10.1016/j.sse.2021.108168.
6. Kang, M.-G.; Jung, W.-S.; Kang, C.-Y.; Yoon, S.-J. Recent Progress on PZT Based Piezoelectric Energy Harvesting Technologies. In Proceedings of the Actuators; MDPI, 2016; Vol. 5, p. 5.
7. Kaczmarek, H.; Królikowski, B.; Klimiec, E.; Chylińska, M.; Bajer, D. Advances in the Study of Piezoelectric Polymers. *Russian Chemical Reviews* **2019**, *88*, 749.
8. Sadasivuni, K.K.; Cabibihan, J.-J.; Ponnamma, D.; Al-Maadeed, M.A.S.A.; Kim, J. *Biopolymer Composites in Electronics*; Elsevier, 2016; ISBN 978-0-08-100974-1.
9. Tandon, B.; Magaz, A.; Balint, R.; Blaker, J.J.; Cartmell, S.H. Electroactive Biomaterials: Vehicles for Controlled Delivery of Therapeutic Agents for Drug Delivery and Tissue Regeneration. *Advanced Drug Delivery Reviews* **2018**, *129*, 148–168, doi:10.1016/j.addr.2017.12.012.
10. Usher, T.D.; Cousins, K.R.; Zhang, R.; Ducharme, S. The Promise of Piezoelectric Polymers. *Polymer International* **2018**, *67*, 790–798, doi:10.1002/pi.5584.
11. Smith, M.; Kar-Narayan, S. Piezoelectric Polymers: Theory, Challenges and Opportunities. *International Materials Reviews* **2021**, *0*, 1–24, doi:10.1080/09506608.2021.1915935.
12. Lee, S.J.; Arun, A.P.; Kim, K.J. Piezoelectric Properties of Electrospun Poly(l-Lactic Acid) Nanofiber Web. *Materials Letters* **2015**, *148*, 58–62, doi:10.1016/j.matlet.2015.02.038.
13. Fukada, E. Piezoelectricity of Biopolymers. *Biorheology* **1995**, *32*, 593–609, doi:10.1016/0006-355X(95)00039-C.

14. Karan, S.K.; Maiti, S.; Agrawal, A.K.; Das, A.K.; Maitra, A.; Paria, S.; Bera, A.; Bera, R.; Halder, L.; Mishra, A.K.; et al. Designing High Energy Conversion Efficient Bio-Inspired Vitamin Assisted Single-Structured Based Self-Powered Piezoelectric/Wind/Acoustic Multi-Energy Harvester with Remarkable Power Density. *Nano Energy* **2019**, *59*, 169–183, doi:10.1016/j.nanoen.2019.02.031.
15. Lovinger, A.J. Poly(Vinylidene Fluoride). *Developments in Crystalline Polymers—1* **1982**, 195–273, doi:10.1007/978-94-009-7343-5_5.
16. Nandi, A.K.; Mandelkern, L. The Influence of Chain Structure on the Equilibrium Melting Temperature of Poly(Vinylidene Fluoride). *Journal of Polymer Science Part B: Polymer Physics* **1991**, *29*, 1287–1297, doi:10.1002/POLB.1991.090291012.
17. Joseph, J.; Kumar, M.; Tripathy, S.; Kumar, G.D.V.S.; Singh, S.G.; Vaniari, S.R.K. A Highly Flexible Tactile Sensor with Self-Poled Electrospun PVDF Nanofiber. In Proceedings of the 2018 IEEE SENSORS; October 2018; pp. 1–4.
18. Xin, Y.; Guo, C.; Qi, X.; Tian, H.; Li, X.; Dai, Q.; Wang, S.; Wang, C. Wearable and Unconstrained Systems Based on PVDF Sensors in Physiological Signals Monitoring: A Brief Review. *Ferroelectrics* **2016**, *500*, 291–300, doi:10.1080/00150193.2016.1230440.
19. Xin, Y.; Sun, H.; Tian, H.; Guo, C.; Li, X.; Wang, S.; Wang, C. The Use of Polyvinylidene Fluoride (PVDF) Films as Sensors for Vibration Measurement: A Brief Review. *Ferroelectrics* **2016**, *502*, 28–42, doi:10.1080/00150193.2016.1232582.
20. Wang, X.; Sun, F.; Yin, G.; Wang, Y.; Liu, B.; Dong, M. Tactile-Sensing Based on Flexible PVDF Nanofibers via Electrospinning: A Review. *Sensors (Switzerland)* **2018**, *18*, doi:10.3390/s18020330.
21. Saxena, P.; Shukla, P. A Comprehensive Review on Fundamental Properties and Applications of Poly(Vinylidene Fluoride) (PVDF). *Adv Compos Hybrid Mater* **2021**, *4*, 8–26, doi:10.1007/s42114-021-00217-0.
22. He, Z.; Rault, F.; Lewandowski, M.; Mohsenzadeh, E.; Salaün, F. Electrospun PVDF Nanofibers for Piezoelectric Applications: A Review of the Influence of Electrospinning Parameters on the β Phase and Crystallinity Enhancement. *Polymers* **2021**, *13*, 1–23, doi:10.3390/polym13020174.
23. Xin, Y.; Zhu, J.; Sun, H.; Xu, Y.; Liu, T.; Qian, C. A Brief Review on Piezoelectric PVDF Nanofibers Prepared by Electrospinning. *Ferroelectrics* **2018**, *526*, 140–151, doi:10.1080/00150193.2018.1456304.
24. Kang, G. dong; Cao, Y. ming Application and Modification of Poly(Vinylidene Fluoride) (PVDF) Membranes - A Review. *Journal of Membrane Science* **2014**, *463*, 145–165, doi:10.1016/j.memsci.2014.03.055.
25. Lang, S.; Muensit, N. Review of Some Lesser-Known Applications of Piezoelectric and Pyroelectric Polymers. *Applied Physics A: Materials Science and Processing* **2006**, *85*, 125–134, doi:10.1007/s00339-006-3688-8.
26. Lovinger, A.J. Annealing of Poly(Vinylidene Fluoride) and Formation of a Fifth Phase. *Macromolecules* **1982**, *15*, 40–44, doi:10.1021/ma00229a008.
27. Doll, W.W.; Lando, J.B. Polymorphism of Poly(Vinylidene Fluoride). III. The Crystal Structure of Phase II. *Journal of Macromolecular Science, Part B* **1970**, *4*, 309–329, doi:10.1080/00222347008212505.
28. Bachmann, A.; Lando, J.B. A Reexamination of the Crystal Structure of Phase II of Poly(Vinylidene Fluoride). *Macromolecules* **1981**, *14*, 40–46.
29. Lovinger, A.J.; Laboratories, H.; Hill, M. Crystallization and Morphology of Melt-Solidified Poly (Vinylidene Fluoride). **1980**, *18*, 793–809.
30. Li, L.; Zhang, M.; Rong, M.; Ruan, W. Studies on the Transformation Process of PVDF from α to β Phase by Stretching. *RSC Advances* **2013**, *4*, 3938–3943, doi:10.1039/C3RA45134H.

31. Sencadas, V.; Lanceros-Mendéz, S.; Gregorio Filho, R.; Chinaglia, D.L.; Pouzada, A.S. Influence of the Processing Conditions and Corona Poling on the Morphology of β -PVDF. *Proceedings - International Symposium on Electrets* **2005**, *2005*, 161–164, doi:10.1109/ISE.2005.1612345.
32. Ye, Y.; Jiang, Y.; Wu, Z.; Zeng, H.; Yang, Y.; Li, W. Characterization and Ferroelectric Properties of Electric Poled PVDF Films.
33. Scheinbeim, J.; Nakafuku, C.; Newman, B.A.; Pae, K.D. High-pressure Crystallization of Poly(Vinylidene Fluoride). *Journal of Applied Physics* **2008**, *50*, 4399, doi:10.1063/1.326429.
34. Lim, J.Y.; Kim, S.; Seo, Y. Enhancement of β -Phase in PVDF by Electrospinning. *AIP Conference Proceedings* **2015**, *1664*, 070006, doi:10.1063/1.4918441.
35. Wang, Y.R.; Zheng, J.M.; Ren, G.Y.; Zhang, P.H.; Xu, C. A Flexible Piezoelectric Force Sensor Based on PVDF Fabrics. *Smart Materials and Structures* **2011**, *20*, 045009, doi:10.1088/0964-1726/20/4/045009.
36. Kang, S.J.; Park, Y.J.; Sung, J.; Jo, P.S.; Park, C.; Kim, K.J.; Cho, B.O. Spin Cast Ferroelectric Beta Poly(Vinylidene Fluoride) Thin Films via Rapid Thermal Annealing. *Applied Physics Letters* **2008**, *92*, 012921, doi:10.1063/1.2830701.
37. Hasegawa, R.; Takahashi, Y.; Chatani, Y.; Adokoro, H.T. Crystal Structures of Three Crystalline Forms of Poly(Vinylidene Fluoride). *Polymer Journal* **1972**, *3:5*, 600–610, doi:10.1295/polymj.3.600.
38. Biswas, A.; Henkel, K.; Schmeißer, D.; Mandal, D. Comparison of the Thermal Stability of the α , β and γ Phases in Poly(Vinylidene Fluoride) Based on in Situ Thermal Fourier Transform Infrared Spectroscopy. *Phase Transitions* **2017**, *90*, 1205–1213, doi:10.1080/01411594.2017.1337902.
39. Muduli, S.P.; Parida, S.; Rout, S.K.; Rajput, S.; Kar, M. Effect of Hot Press Temperature on β -Phase, Dielectric and Ferroelectric Properties of Solvent Casted Poly(Vinylidene Fluoride) Films. *Materials Research Express* **2019**, *6*, 095306, doi:10.1088/2053-1591/AB2D85.
40. Prest, W.M.; Luca, D.J. The Formation of the γ Phase from the α and β Polymorphs of Polyvinylidene Fluoride. *Journal of Applied Physics* **2008**, *49*, 5042, doi:10.1063/1.324439.
41. He, F.; Fan, J.; Lau, S. Thermal, Mechanical, and Dielectric Properties of Graphite Reinforced Poly(Vinylidene Fluoride) Composites. *Polymer Testing* **2008**, *27*, 964–970, doi:10.1016/J.POLYMERTESTING.2008.08.010.
42. Samadi, A.; Hosseini, S.M.; Mohseni, M. Investigation of the Electromagnetic Microwaves Absorption and Piezoelectric Properties of Electrospun Fe₃O₄-GO/PVDF Hybrid Nanocomposites. *Organic Electronics* **2018**, *59*, 149–155, doi:10.1016/J.ORGEL.2018.04.037.
43. Davis, G.T.; McKinney, J.E.; Broadhurst, M.G.; Roth, S.C. Electric-field-induced Phase Changes in Poly(Vinylidene Fluoride). *Journal of Applied Physics* **2008**, *49*, 4998, doi:10.1063/1.324446.
44. Biswas, A.; Henkel, K.; Schmeißer, D.; Mandal, D. Comparison of the Thermal Stability of the α , β and γ Phases in Poly(Vinylidene Fluoride) Based on in Situ Thermal Fourier Transform Infrared Spectroscopy. <http://dx.doi.org/10.1080/01411594.2017.1337902> **2017**, *90*, 1205–1213, doi:10.1080/01411594.2017.1337902.
45. Mandal, D.; Kim, K.J.; Lee, J.S. Simple Synthesis of Palladium Nanoparticles, β -Phase Formation, and the Control of Chain and Dipole Orientations in Palladium-Doped Poly(Vinylidene Fluoride) Thin Films. *Langmuir* **2012**, *28*, 10310–10317, doi:10.1021/LA300983X/SUPPL_FILE/LA300983X_SI_001.PDF.
46. Ramasundaram, S.; Yoon, S.; Kim, K.; Park, C. Preferential Formation of Electroactive Crystalline Phases in Poly(Vinylidene Fluoride)/Organically Modified Silicate Nanocomposites. *Journal of Polymer Science Part B* **2008**, doi:10.1002/POLB.21550.
47. Enomoto, S.; Kawai, Y.; Sugita, M. Infrared Spectrum of Poly(Vinylidene Fluoride). *Journal of Polymer Science Part A-2: Polymer Physics* **1968**, *6*, 861–869, doi:10.1002/POL.1968.160060506.

48. Hasegawa, R.; Kobayashi, M.; Tadokoro, H. Molecular Conformation and Packing of Poly(Vinylidene Fluoride). Stability of Three Crystalline Forms and the Effect of High Pressure. *Polymer Journal* 1972 3:5 **1972**, 3, 591–599, doi:10.1295/polymj.3.591.
49. Hussein, A.A. Preparation and Characterization of Electrical, Morphological and Topographic Properties for Advanced Conductive PMMA/PVDF/PANI Ternary Blend for Low Percolation Threshold Devices. *International Journal of Nanoelectronics and Materials* **2019**, 12.
50. Bormashenko, Y.; Pogreb, R.; Stanevsky, O.; Bormashenko, E. Vibrational Spectrum of PVDF and Its Interpretation. *Polymer Testing* **2004**, 23, 791–796, doi:10.1016/J.POLYMERTESTING.2004.04.001.
51. Martins, P.; Lopes, A.C.; Lanceros-Mendez, S. Electroactive Phases of Poly(Vinylidene Fluoride): Determination, Processing and Applications. *Progress in Polymer Science* **2014**, 39, 683–706, doi:10.1016/J.PROGPOLYMSCI.2013.07.006.
52. Garain, S.; Jana, S.; Sinha, T.K.; Mandal, D. Design of in Situ Poled Ce³⁺-Doped Electrospun PVDF/Graphene Composite Nanofibers for Fabrication of Nanopressure Sensor and Ultrasensitive Acoustic Nanogenerator. *ACS Applied Materials and Interfaces* **2016**, 8, 4532–4540, doi:10.1021/ACSAMI.5B11356/SUPPL_FILE/AM5B11356_SI_003.AVI.
53. Jana, S.; Garain, S.; Sen, S.; Mandal, D. The Influence of Hydrogen Bonding on the Dielectric Constant and the Piezoelectric Energy Harvesting Performance of Hydrated Metal Salt Mediated PVDF Films. *Physical Chemistry Chemical Physics* **2015**, 17, 17429–17436, doi:10.1039/C5CP01820J.
54. Maity, K.; Mahanty, B.; Sinha, T.K.; Garain, S.; Biswas, A.; Ghosh, S.K.; Manna, S.; Ray, S.K.; Mandal, D. Two-Dimensional Piezoelectric MoS₂-Modulated Nanogenerator and Nanosensor Made of Poly(Vinylidene Fluoride) Nanofiber Webs for Self-Powered Electronics and Robotics. *Energy Technology* **2017**, 5, 234–243, doi:10.1002/ENTE.201600419.
55. Mandal, D.; Henkel, K.; Schmeißer, D. The Electroactive β -Phase Formation in Poly(Vinylidene Fluoride) by Gold Nanoparticles Doping. *Materials Letters* **2012**, 73, 123–125, doi:10.1016/j.matlet.2011.11.117.
56. Salimi, A.; Yousefi, A.A. FTIR Studies of β -Phase Crystal Formation in Stretched PVDF Films. *Polymer Testing* **2003**, 22, 699–704, doi:10.1016/S0142-9418(03)00003-5.
57. Barrau, S.; Ferri, A.; Da Costa, A.; Defebvin, J.; Leroy, S.; Desfeux, R.; Lefebvre, J.M. Nanoscale Investigations of α - And γ -Crystal Phases in PVDF-Based Nanocomposites. *ACS Applied Materials and Interfaces* **2018**, 10, 13092–13099, doi:10.1021/acsami.8b02172.
58. Bormashenko, Y.; Pogreb, R.; Stanevsky, O.; Bormashenko, E. Vibrational Spectrum of PVDF and Its Interpretation. *Polymer Testing* **2004**, 23, 791–796, doi:10.1016/J.POLYMERTESTING.2004.04.001.
59. Yang, D.; Chen, Y. β -Phase Formation of Poly(Vinylidene Fluoride) from the Melt Induced by Quenching. *Journal of Materials Science Letters* 1987 6:5 **1987**, 6, 599–603, doi:10.1007/BF01739296.
60. Zheng, J.; He, A.; Li, J.; Han, C.C. Polymorphism Control of Poly(Vinylidene Fluoride) through Electrospinning. *Macromolecular Rapid Communications* **2007**, 28, 2159–2162, doi:10.1002/MARC.200700544.
61. Yee, W.A.; Kotaki, M.; Liu, Y.; Lu, X. Morphology, Polymorphism Behavior and Molecular Orientation of Electrospun Poly(Vinylidene Fluoride) Fibers. *Polymer* **2007**, 48, 512–521, doi:10.1016/J.POLYMER.2006.11.036.
62. Buckley, J.; Cebe, P.; Cherdack, D.; Crawford, J.; Ince, B.S.; Jenkins, M.; Pan, J.; Reveley, M.; Washington, N.; Wolchover, N. Nanocomposites of Poly(Vinylidene Fluoride) with Organically Modified Silicate. *Polymer* **2006**, 47, 2411–2422, doi:10.1016/J.POLYMER.2006.02.012.
63. Manna, S.; Batabyal, S.K.; Nandi, A.K. Preparation and Characterization of Silver–Poly(Vinylidene Fluoride) Nanocomposites: Formation of Piezoelectric Polymorph of Poly(Vinylidene Fluoride). *Journal of Physical Chemistry B* **2006**, 110, 12318–12326, doi:10.1021/JP061445Y.

64. Mandal, D.; Henkel, K.; Schmeisser, D. Comment on "Preparation and Characterization of Silver-Poly(Vinylidene Fluoride) Nanocomposites: Formation of Piezoelectric Polymorph of Poly(Vinylidene Fluoride)." *Journal of Physical Chemistry B* **2011**, *115*, 10567–10569, doi:10.1021/JP201335J/SUPPL_FILE/JP201335J_SI_001.PDF.
65. Karan, S.K.; Mandal, D.; Khatua, B.B. Self-Powered Flexible Fe-Doped RGO/PVDF Nanocomposite: An Excellent Material for a Piezoelectric Energy Harvester. *Nanoscale* **2015**, *7*, 10655–10666, doi:10.1039/C5NR02067K.
66. Cai, X.; Lei, T.; Sun, D.; Lin, L. A Critical Analysis of the α , β and γ Phases in Poly(Vinylidene Fluoride) Using FTIR. *RSC Advances* **2017**, *7*, 15382–15389, doi:10.1039/c7ra01267e.
67. Shaik, H.; Rachith, S.N.; Rudresh, K.J.; Sheik, A.S.; Thulasi Raman, K.H.; Kondaiah, P.; Mohan Rao, G. Towards β -Phase Formation Probability in Spin Coated PVDF Thin Films. *J Polym Res* **2017**, *24*, 35, doi:10.1007/s10965-017-1191-x.
68. Dhatarwal, P.; Sengwa, R.J. Polymer Compositional Ratio-Dependent Morphology, Crystallinity, Dielectric Dispersion, Structural Dynamics, and Electrical Conductivity of PVDF/PEO Blend Films. *Macromol. Res.* **2019**, *27*, 1009–1023, doi:10.1007/s13233-019-7142-0.
69. Song, Y.M.; Zhao, Z.D.; Yu, W.X.; Li, B.; Chen, X.F. Morphological Structures of Poly(Vinylidene Fluoride)/Montmorillonite Nanocomposites. *Science in China, Series B: Chemistry* **2007**, *50*, 790–796, doi:10.1007/s11426-007-0079-8.
70. Nishiyama, T.; Sumihara, T.; Sasaki, Y.; Sato, E.; Yamato, M.; Horibe, H. Crystalline Structure Control of Poly(Vinylidene Fluoride) Films with the Antisolvent Addition Method. *Polym J* **2016**, *48*, 1035–1038, doi:10.1038/pj.2016.62.
71. Du, C.; Zhu, B.-K.; Xu, Y.-Y. Effects of Stretching on Crystalline Phase Structure and Morphology of Hard Elastic PVDF Fibers. *Journal of Applied Polymer Science* **2007**, *104*, 2254–2259, doi:10.1002/app.25635.
72. Lei, T.; Cai, X.; Wang, X.; Yu, L.; Hu, X.; Zheng, G.; Lv, W.; Wang, L.; Wu, D.; Sun, D.; et al. Spectroscopic Evidence for a High Fraction of Ferroelectric Phase Induced in Electrospun Polyvinylidene Fluoride Fibers. *RSC Adv.* **2013**, *3*, 24952–24958, doi:10.1039/C3RA42622J.
73. Dutta, B.; Kar, E.; Bose, N.; Mukherjee, S. Significant Enhancement of the Electroactive β -Phase of PVDF by Incorporating Hydrothermally Synthesized Copper Oxide Nanoparticles. *RSC Adv.* **2015**, *5*, 105422–105434, doi:10.1039/C5RA21903E.
74. Horibe, H.; Hosokawa, Y.; Oshiro, H.; Sasaki, Y.; Takahashi, S.; Kono, A.; Nishiyama, T.; Danno, T. Effect of Heat-Treatment Temperature after Polymer Melt and Blending Ratio on the Crystalline Structure of PVDF in a PVDF/PMMA Blend. *Polym J* **2013**, *45*, 1195–1201, doi:10.1038/pj.2013.53.
75. Horibe, H.; Sasaki, Y.; Oshiro, H.; Hosokawa, Y.; Kono, A.; Takahashi, S.; Nishiyama, T. Quantification of the Solvent Evaporation Rate during the Production of Three PVDF Crystalline Structure Types by Solvent Casting. *Polym J* **2014**, *46*, 104–110, doi:10.1038/pj.2013.75.
76. Kim, H.; Fernando, T.; Li, M.; Lin, Y.; Tseng, T.-L.B. Fabrication and Characterization of 3D Printed BaTiO₃/PVDF Nanocomposites. *Journal of Composite Materials* **2018**, *52*, 197–206, doi:10.1177/0021998317704709.
77. Roy, K.; Ghosh, S.K.; Sultana, A.; Garain, S.; Xie, M.; Bowen, C.R.; Henkel, K.; Schmeißer, D.; Mandal, D. A Self-Powered Wearable Pressure Sensor and Pyroelectric Breathing Sensor Based on GO Interfaced PVDF Nanofibers. *ACS Applied Nano Materials* **2019**, *2*, 2013–2025, doi:10.1021/acsanm.9b00033.
78. Maity, K.; Garain, S.; Henkel, K.; Schmeißer, D.; Mandal, D. Self-Powered Human-Health Monitoring through Aligned PVDF Nanofibers Interfaced Skin-Interactive Piezoelectric Sensor. *ACS Applied Polymer Materials* **2020**, *2*, 862–878, doi:10.1021/acsapm.9b00846.
79. Broadhurst, M.G.; Davis, G.T. Physical Basis for Piezoelectricity in PVDF. *Ferroelectrics* **1984**, *60*, 3–13, doi:10.1080/00150198408017504.

80. Nakhmanson, S.M.; Nardelli, M.B.; Bernholc, J. Collective Polarization Effects in β - Polyvinylidene Fluoride and Its Copolymers with Tri- and Tetrafluoroethylene. *Phys. Rev. B* **2005**, *72*, 115210, doi:10.1103/PhysRevB.72.115210.
81. Abdalla, S.; Obaid, A.; Al-Marzouki, F.M. Preparation and Characterization of Poly(Vinylidene Fluoride): A High Dielectric Performance Nano-Composite for Electrical Storage. *Results in Physics* **2016**, *6*, 617–626, doi:10.1016/j.rinp.2016.09.003.
82. Broadhurst, M.G.; Davis, G.T.; McKinney, J.E.; Collins, R.E. Piezoelectricity and Pyroelectricity in Polyvinylidene Fluoride—A Model. *Journal of Applied Physics* **1978**, *49*, 4992–4997, doi:10.1063/1.324445.
83. Kepler, R.G. Piezoelectricity, Pyroelectricity, and Ferroelectricity in Organic Materials. *Annu. Rev. Phys. Chem.* **1978**, *29*, 497–518, doi:10.1146/annurev.pc.29.100178.002433.
84. Bamji, S.S.; Kao, K.J.; Perlman, M.M. Piezoelectricity and Pyroelectricity of Polyvinylidene Fluoride Corona-Poled at Elevated Temperature. *Journal of Polymer Science: Polymer Physics Edition* **1980**, *18*, 1945–1954, doi:10.1002/pol.1980.180180907.
85. Eberle, G.; Eisenmenger, W. Thermal Depolarization of PVDF.
86. da Silva, A.B.; Wisniewski, C.; Esteves, J.V.A.; Gregorio, R. Effect of Drawing on the Dielectric Properties and Polarization of Pressed Solution Cast β -PVDF Films. *J Mater Sci* **2010**, *45*, 4206–4215, doi:10.1007/s10853-010-4515-3.
87. Kaur, S.; Kumar, A.; Sharma, A.L.; Singh, D.P. Influence of Annealing on Dielectric and Polarization Behavior of PVDF Thick Films. *J Mater Sci: Mater Electron* **2017**, *28*, 8391–8396, doi:10.1007/s10854-017-6556-8.
88. Electric Energy Storage Properties of Poly(Vinylidene Fluoride). *Appl. Phys. Lett.* **2010**, *96*, 192905, doi:10.1063/1.3428656.
89. Li, J.; Meng, Q.; Li, W.; Zhang, Z. Influence of Crystalline Properties on the Dielectric and Energy Storage Properties of Poly(Vinylidene Fluoride). *J. Appl. Polym. Sci.* **2011**, *122*, 1659–1668, doi:10.1002/app.34020.
90. Bergman, J.G.; McFee, J.H.; Crane, G.R. Pyroelectricity and Optical Second Harmonic Generation in Polyvinylidene Fluoride Films. *Appl. Phys. Lett.* **1971**, *18*, 203–205, doi:10.1063/1.1653624.
91. Fukada, E.; Furukawa, T. Piezoelectricity and Ferroelectricity in Polyvinylidene Fluoride. *Ultrasonics* **1981**, *19*, 31–39, doi:10.1016/0041-624X(81)90030-5.
92. Pfister, G.; Abkowitz, M.; Crystal, R.G. Pyroelectricity in Polyvinylidene Fluoride. *Journal of Applied Physics* **1973**, *44*, 2064–2071, doi:10.1063/1.1662513.
93. Kawai, H. The Piezoelectricity of Poly (Vinylidene Fluoride). *Japanese Journal of Applied Physics* **1969**, *8*, 975–976, doi:10.1143/jjap.8.975.
94. Wan, C.; Bowen, C.R. Multiscale-Structuring of Polyvinylidene Fluoride for Energy Harvesting: The Impact of Molecular-, Micro- and Macro-Structure. *J. Mater. Chem. A* **2017**, *5*, 3091–3128, doi:10.1039/C6TA09590A.
95. Surmenev, R.A.; Orlova, T.; Chernozem, R.V.; Ivanova, A.A.; Bartasyte, A.; Mathur, S.; Surmeneva, M.A. Hybrid Lead-Free Polymer-Based Nanocomposites with Improved Piezoelectric Response for Biomedical Energy-Harvesting Applications: A Review. *Nano Energy* **2019**, *62*, 475–506, doi:10.1016/j.nanoen.2019.04.090.
96. Surmenev, R.A.; Chernozem, R.V.; Pariy, I.O.; Surmeneva, M.A. A Review on Piezo- and Pyroelectric Responses of Flexible Nano- and Micropatterned Polymer Surfaces for Biomedical Sensing and Energy Harvesting Applications. *Nano Energy* **2021**, *79*, 105442, doi:10.1016/j.nanoen.2020.105442.
97. Yousry, Y.M.; Yao, K.; Chen, S.; Liew, W.H.; Ramakrishna, S. Mechanisms for Enhancing Polarization Orientation and Piezoelectric Parameters of PVDF Nanofibers. *Advanced Electronic Materials* **2018**, *4*, 1700562, doi:10.1002/aelm.201700562.
98. Whatmore, R.W. Pyroelectric Devices and Materials. *Reports on Progress in Physics* **1999**, *49*, 1335, doi:10.1088/0034-4885/49/12/002.

99. DeRossi, D.; DeReggi, A.S.; Broadhurst, M.G.; Roth, S.C.; Davis, G.T. Method of Evaluating the Thermal Stability of the Pyroelectric Properties of Polyvinylidene Fluoride: Effects of Poling Temperature and Field. *Journal of Applied Physics* **1982**, *53*, 6520–6525, doi:10.1063/1.330078.
100. Li, H.Z.; Li, W.Z.; Yang, Y.J.; Tai, H.L.; Du, X.S.; Gao, R.Y.; Li, S.Y. Pyroelectric Performances of 1-3 Ferroelectric Composites Based on Barium Titanate Nanowires/Polyvinylidene Fluoride. *Ceramics International* **2018**, *44*, 19254–19261, doi:10.1016/j.ceramint.2018.07.150.
101. Prasad, G.; Sathiyathan, P.; Prabu, A.A.; Kim, K.J. Piezoelectric Characteristics of Electrospun PVDF as a Function of Phase-Separation Temperature and Metal Salt Content. *Macromolecular Research* **2017**, *25*, 981–988, doi:10.1007/s13233-017-5127-4.
102. Durga Prasad, P.; Hemalatha, J. Dielectric and Energy Storage Density Studies in Electrospun Fiber Mats of Polyvinylidene Fluoride (PVDF)/Zinc Ferrite (ZnFe₂O₄) Multiferroic Composite. *Physica B: Condensed Matter* **2019**, *573*, 1–6, doi:10.1016/j.physb.2019.08.023.
103. Dorneanu, P.P.; Cojocaru, C.; Olaru, N.; Samoila, P.; Airinei, A.; Sacarescu, L. Electrospun PVDF Fibers and a Novel PVDF/CoFe₂O₄ Fibrous Composite as Nanostructured Sorbent Materials for Oil Spill Cleanup. *Applied Surface Science* **2017**, *424*, 389–396, doi:10.1016/j.apsusc.2017.01.177.
104. Sultana, S.M.N.; Pawar, S.P.; Kamkar, M.; Sundararaj, U. Tailoring MWCNT Dispersion, Blend Morphology and EMI Shielding Properties by Sequential Mixing Strategy in Immiscible PS/PVDF Blends. *Journal of Elec Materi* **2020**, *49*, 1588–1600, doi:10.1007/s11664-019-07371-8.
105. Lee, J.E.; Shin, Y.E.; Lee, G.H.; Kim, J.; Ko, H.; Chae, H.G. Polyvinylidene Fluoride (PVDF)/Cellulose Nanocrystal (CNC) Nanocomposite Fiber and Triboelectric Textile Sensors. *Composites Part B: Engineering* **2021**, *223*, 109098, doi:10.1016/j.compositesb.2021.109098.
106. Gopi, S.; Balakrishnan, P.; Pius, A.; Thomas, S. Chitin Nanowhisker (ChNW)-Functionalized Electrospun PVDF Membrane for Enhanced Removal of Indigo Carmine. *Carbohydrate Polymers* **2017**, *165*, 115–122, doi:10.1016/j.carbpol.2017.02.046.
107. Boributh, S.; Chanachai, A.; Jiratananon, R. Modification of PVDF Membrane by Chitosan Solution for Reducing Protein Fouling. *2009*, *342*, 97–104, doi:10.1016/j.memsci.2009.06.022.
108. Roy, K.; Jana, S.; Mallick, Z.; Ghosh, S.K.; Dutta, B.; Sarkar, S.; Sinha, C.; Mandal, D. Two-Dimensional MOF Modulated Fiber Nanogenerator for Effective Acoustoelectric Conversion and Human Motion Detection. *Langmuir* **2021**, *37*, 7107–7117, doi:10.1021/acs.langmuir.1c00700.
109. Hosseini, S.M.; Yousefi, A.A. Piezoelectric Sensor Based on Electrospun PVDF-MWCNT-Cloisite 30B Hybrid Nanocomposites. *Organic Electronics* **2017**, *50*, 121–129, doi:10.1016/j.orgel.2017.07.035.
110. Deshmukh, K.; Ahamed, M.B.; Deshmukh, R.R.; Pasha, S.K.K.; Sadasivuni, K.K.; Ponnamma, D.; AlMaadeed, M.A.-A. Striking Multiple Synergies in Novel Three-Phase Fluoropolymer Nanocomposites by Combining Titanium Dioxide and Graphene Oxide as Hybrid Fillers. *J Mater Sci: Mater Electron* **2017**, *28*, 559–575, doi:10.1007/s10854-016-5559-1.
111. Agboola, O.; Fayomi, O.S.I.; Ayodeji, A.; Ayeni, A.O.; Alagbe, E.E.; Sanni, S.E.; Okoro, E.E.; Moropeng, L.; Sadiku, R.; Kupolati, K.W.; et al. A Review on Polymer Nanocomposites and Their Effective Applications in Membranes and Adsorbents for Water Treatment and Gas Separation. *Membranes (Basel)* **2021**, *11*, 139, doi:10.3390/membranes11020139.
112. Thomas, S.; Stephen, R.; Bandyopadhyay, S.; Thomas, S. Polymer Nanocomposites: Preparation, Properties and Applications. *Rubber Fibers Plastics International* **2007**, *2*, 49–56.
113. Puggal, S.; Dhall, N.; Singh, N.; Litt, M. A Review on Polymer Nanocomposites: Synthesis, Characterization and Mechanical Prop. *Indian Journal of Science and Technology* **2016**, *9*, doi:10.17485/ijst/2016/v9i4/81100.
114. Ram, F.; Ambone, T.; Sharma, A.; Murugesan, R.; Kajale, D.; Borkar, V.; Ali, S.F.; Balu, P.K.; Kumaraswamy, G.; Shanmuganathan, K. Fluorinated Nanocellulose-Reinforced All-Organic

- Flexible Ferroelectric Nanocomposites for Energy Generation. *Journal of Physical Chemistry C* **2018**, *122*, 16540–16549, doi:10.1021/acs.jpcc.8b03470.
115. Karan, S.K.; Bera, R.; Paria, S.; Das, A.K.; Maiti, S.; Maitra, A.; Khatua, B.B. An Approach to Design Highly Durable Piezoelectric Nanogenerator Based on Self-Poled PVDF/AlO-RGO Flexible Nanocomposite with High Power Density and Energy Conversion Efficiency. *Advanced Energy Materials* **2016**, *6*, 1601016, doi:10.1002/aenm.201601016.
 116. Fu, J.; Hou, Y.; Zheng, M.; Zhu, M. Comparative Study of Dielectric Properties of the PVDF Composites Filled with Spherical and Rod-like BaTiO₃ Derived by Molten Salt Synthesis Method. *J Mater Sci* **2018**, *53*, 7233–7248, doi:10.1007/s10853-018-2114-x.
 117. Mendes, S.F.; Costa, C.M.; Caparros, C.; Sencadas, V.; Lanceros-Méndez, S. Effect of Filler Size and Concentration on the Structure and Properties of Poly(Vinylidene Fluoride)/BaTiO₃ Nanocomposites. *J Mater Sci* **2012**, *47*, 1378–1388, doi:10.1007/s10853-011-5916-7.
 118. Thakur, P.; Kool, A.; Hoque, N.A.; Bagchi, B.; Khatun, F.; Biswas, P.; Brahma, D.; Roy, S.; Banerjee, S.; Das, S. Superior Performances of in Situ Synthesized ZnO/PVDF Thin Film Based Self-Poled Piezoelectric Nanogenerator and Self-Charged Photo-Power Bank with High Durability. *Nano Energy* **2018**, *44*, 456–467, doi:10.1016/j.nanoen.2017.11.065.
 119. Zhou, W.; Zuo, J.; Ren, W. Thermal Conductivity and Dielectric Properties of Al/PVDF Composites. *Composites Part A: Applied Science and Manufacturing* **2012**, *43*, 658–664, doi:10.1016/j.compositesa.2011.11.024.
 120. Ram, R.; Soni, V.; Khastgir, D. Electrical and Thermal Conductivity of Polyvinylidene Fluoride (PVDF) – Conducting Carbon Black (CCB) Composites: Validation of Various Theoretical Models. *Composites Part B: Engineering* **2020**, *185*, 107748, doi:10.1016/j.compositesb.2020.107748.
 121. Dielectric Properties and Thermal Conductivity of PVDF Reinforced with Three Types of Zn Particles - ScienceDirect Available online: <https://www.sciencedirect.com/science/article/abs/pii/S1359835X15003139?via%3Dihub> (accessed on 24 May 2023).
 122. Pusty, M.; Shirage, P.M. Insights and Perspectives on Graphene-PVDF Based Nanocomposite Materials for Harvesting Mechanical Energy. *Journal of Alloys and Compounds* **2022**, *904*, 164060, doi:10.1016/j.jallcom.2022.164060.
 123. Yang, W.; Yu, S.; Sun, R.; Du, R. Nano- and Microsize Effect of CCTO Fillers on the Dielectric Behavior of CCTO/PVDF Composites. *Acta Materialia* **2011**, *59*, 5593–5602, doi:10.1016/j.actamat.2011.05.034.
 124. Biswas, A.; Henkel, K.; Schmeißer, D.; Mandal, D. Comparison of the Thermal Stability of the α , β and γ Phases in Poly(Vinylidene Fluoride) Based on in Situ Thermal Fourier Transform Infrared Spectroscopy. <http://dx.doi.org/10.1080/01411594.2017.1337902> **2017**, *90*, 1205–1213, doi:10.1080/01411594.2017.1337902.
 125. Salimi, A.; Yousefi, A.A. Conformational Changes and Phase Transformation Mechanisms in PVDF Solution-Cast Films. *Journal of Polymer Science Part B: Polymer Physics* **2004**, *42*, 3487–3495, doi:10.1002/polb.20223.
 126. Nishiyama, T.; Sumihara, T.; Sato, E.; Horibe, H. Effect of Solvents on the Crystal Formation of Poly(Vinylidene Fluoride) Film Prepared by a Spin-Coating Process. *Polym J* **2017**, *49*, 319–325, doi:10.1038/pj.2016.116.
 127. Dhevi, D.M.; Prabu, A.A.; Pathak, M.; Kim, K.J. Spin-Coating Temperature Induced Changes in Ferroelectric Crystallinity in Polyvinylidene Fluoride Ultrathin Films. *Advanced Materials Research* **2012**, *584*, 197–200, doi:10.4028/www.scientific.net/AMR.584.197.
 128. Wang, Y.; Cakmak, M.; White, J.L. Structure Development in Melt Spinning Poly(Vinylidene Fluoride) Fibers and Tapes. *Journal of Applied Polymer Science* **1985**, *30*, 2615–2632, doi:10.1002/app.1985.070300625.
 129. Samon, J.M.; Schultz, J.M.; Hsiao, B.S.; Seifert, S.; Stribeck, N.; Gurke, I.; Saw, C. Structure Development during the Melt Spinning of Polyethylene and Poly(Vinylidene Fluoride) Fibers

- by in Situ Synchrotron Small- and Wide-Angle X-Ray Scattering Techniques. *Macromolecules* **1999**, *32*, 8121–8132, doi:10.1021/ma9906332.
130. Huang, Z.-X.; Wang, M.-M.; Feng, Y.-H.; Qu, J.-P. β -Phase Formation of Polyvinylidene Fluoride via Hot Pressing under Cyclic Pulsating Pressure. *Macromolecules* **2020**, *53*, 8494–8501, doi:10.1021/acs.macromol.0c01609.
 131. Liu, Z.; Li, S.; Zhu, J.; Mi, L.; Zheng, G. Fabrication of β -Phase-Enriched PVDF Sheets for Self-Powered Piezoelectric Sensing. *ACS Appl. Mater. Interfaces* **2022**, *14*, 11854–11863, doi:10.1021/acsami.2c01611.
 132. Kim, H.; Torres, F.; Villagran, D.; Stewart, C.; Lin, Y.; Tseng, T.-L.B. 3D Printing of BaTiO₃/PVDF Composites with Electric In Situ Poling for Pressure Sensor Applications. *Macromolecular Materials and Engineering* **2017**, *302*, 1700229, doi:10.1002/mame.201700229.
 133. Bodkhe, S.; Rajesh, P.S.M.; Gosselin, F.P.; Therriault, D. Simultaneous 3D Printing and Poling of PVDF and Its Nanocomposites. *ACS Appl. Energy Mater.* **2018**, *1*, 2474–2482, doi:10.1021/acsaem.7b00337.
 134. Bhardwaj, N.; Kundu, S.C. Electrospinning: A Fascinating Fiber Fabrication Technique. *Biotechnology Advances* **2010**, *28*, 325–347, doi:10.1016/j.biotechadv.2010.01.004.
 135. Bera, B. Literature Review on Electrospinning Process (A Fascinating Fiber Fabrication Technique). **2016**, *2*, 14.
 136. Doshi, J.; Reneker, D.H. Electrospinning Process and Applications of Electrospun Fibers. *Journal of Electrostatics* **1995**, *35*, 151–160, doi:10.1016/0304-3886(95)00041-8.
 137. Unnithan, A.R.; Arathyram, R.S.; Kim, C.S. Electrospinning of Polymers for Tissue Engineering. In *Nanotechnology Applications for Tissue Engineering*; Elsevier, 2015; pp. 45–55 ISBN 978-0-323-32889-0.
 138. Robb, B.; Lennox, B. 3 - The Electrospinning Process, Conditions and Control. In *Electrospinning for Tissue Regeneration*; Bosworth, L.A., Downes, S., Eds.; Woodhead Publishing Series in Biomaterials; Woodhead Publishing, 2011; pp. 51–66 ISBN 978-1-84569-741-9.
 139. Li, Z.; Wang, C. Effects of Working Parameters on Electrospinning. In *One-Dimensional nanostructures: Electrospinning Technique and Unique Nanofibers*; Li, Z., Wang, C., Eds.; SpringerBriefs in Materials; Springer: Berlin, Heidelberg, 2013; pp. 15–28 ISBN 978-3-642-36427-3.
 140. Cramariuc, B.; Cramariuc, R.; Scarlet, R.; Manea, L.R.; Lupu, I.G.; Cramariuc, O. Fiber Diameter in Electrospinning Process. *Journal of Electrostatics* **2013**, *71*, 189–198, doi:10.1016/j.elstat.2012.12.018.
 141. Wang, C.; Cheng, Y.-W.; Hsu, C.-H.; Chien, H.-S.; Tsou, S.-Y. How to Manipulate the Electrospinning Jet with Controlled Properties to Obtain Uniform Fibers with the Smallest Diameter?—A Brief Discussion of Solution Electrospinning Process. *J Polym Res* **2011**, *18*, 111–123, doi:10.1007/s10965-010-9397-1.
 142. Casper, C.L.; Stephens, J.S.; Tassi, N.G.; Chase, D.B.; Rabolt, J.F. Controlling Surface Morphology of Electrospun Polystyrene Fibers: Effect of Humidity and Molecular Weight in the Electrospinning Process. *Macromolecules* **2004**, *37*, 573–578, doi:10.1021/ma0351975.
 143. Samatham, R.; Kim, K.J. Electric Current as a Control Variable in the Electrospinning Process. *Polymer Engineering & Science* **2006**, *46*, 954–959, doi:10.1002/pen.20565.
 144. Yarin, A.L.; Koombhongse, S.; Reneker, D.H. Taylor Cone and Jetting from Liquid Droplets in Electrospinning of Nanofibers. *Journal of Applied Physics* **2001**, *90*, 4836–4846, doi:10.1063/1.1408260.
 145. Moghe, A.K.; Gupta, B.S. Co-axial Electrospinning for Nanofiber Structures: Preparation and Applications. *Polymer Reviews* **2008**, *48*, 353–377, doi:10.1080/15583720802022257.
 146. Varesano, A.; Carletto, R.A.; Mazzuchetti, G. Experimental Investigations on the Multi-Jet Electrospinning Process. *Journal of Materials Processing Technology* **2009**, *209*, 5178–5185, doi:10.1016/j.jmatprotec.2009.03.003.

147. Simonet, M.; Schneider, O.D.; Neuenschwander, P.; Stark, W.J. Ultraporous 3D Polymer Meshes by Low-Temperature Electrospinning: Use of Ice Crystals as a Removable Void Template. *Polymer Engineering & Science* **2007**, *47*, 2020–2026, doi:10.1002/pen.20914.
148. Givens, S.R.; Gardner, K.H.; Rabolt, J.F.; Chase, D.B. High-Temperature Electrospinning of Polyethylene Microfibers from Solution. *Macromolecules* **2007**, *40*, 608–610, doi:10.1021/ma062398a.
149. Han, G.; Su, Y.; Feng, Y.; Lu, N. Approaches for Increasing the β -Phase Concentration of Electrospun Polyvinylidene Fluoride (PVDF) Nanofibers. *ES Materials & Manufacturing* **2019**, *Volume 6*, 75–80.
150. Fu, R.; Chen, S.; Lin, Y.; He, Y.; Gu, d Y. Preparation and Piezoelectric Investigation of Electrospun Polyvinylidene Fluoride Fibrous Membrane. *Journal of Nanoscience and Nanotechnology* **2016**, *16*, 12337–12343, doi:10.1166/jnn.2016.13750.
151. Magniez, K.; De Lavigne, C.; Fox, B.L. The Effects of Molecular Weight and Polymorphism on the Fracture and Thermo-Mechanical Properties of a Carbon-Fibre Composite Modified by Electrospun Poly (Vinylidene Fluoride) Membranes. *Polymer* **2010**, *51*, 2585–2596, doi:10.1016/j.polymer.2010.04.021.
152. Zaarour, B.; Zhu, L.; Jin, X. Controlling the Surface Structure, Mechanical Properties, Crystallinity, and Piezoelectric Properties of Electrospun PVDF Nanofibers by Maneuvering Molecular Weight. *Soft Materials* **2019**, *17*, 181–189, doi:10.1080/1539445X.2019.1582542.
153. He, Z.; Rault, F.; Lewandowski, M.; Mohsenzadeh, E.; Salaün, F. Electrospun PVDF Nanofibers for Piezoelectric Applications: A Review of the Influence of Electrospinning Parameters on the β Phase and Crystallinity Enhancement. *Polymers* **2021**, *13*, 1–23, doi:10.3390/polym13020174.
154. Gade, H.; Nikam, S.; Chase, G.G.; Reneker, D.H. Effect of Electrospinning Conditions on β -Phase and Surface Charge Potential of PVDF Fibers. *Polymer* **2021**, *228*, 123902, doi:10.1016/j.polymer.2021.123902.
155. Baji, A.; Mai, Y.-W.; Li, Q.; Liu, Y. Electrospinning Induced Ferroelectricity in Poly(Vinylidene Fluoride) Fibers. *Nanoscale* **2011**, *3*, 3068–3071, doi:10.1039/C1NR10467E.
156. Costa, L.M.M.; Bretas, R.E.S.; Gregorio, R. Effect of Solution Concentration on the Electrospinning/Electrospray Transition and on the Crystalline Phase of PVDF. *Materials Sciences and Applications* **2010**, *01*, 247–252, doi:10.4236/msa.2010.14036.
157. Zheng, J.; He, A.; Li, J.; Han, C.C. Polymorphism Control of Poly(Vinylidene Fluoride) through Electrospinning. *Macromolecular Rapid Communications* **2007**, *28*, 2159–2162, doi:10.1002/MARC.200700544.
158. Singh, R.K.; Lye, S.W.; Miao, J. Holistic Investigation of the Electrospinning Parameters for High Percentage of β -Phase in PVDF Nanofibers. *Polymer* **2021**, *214*, 123366, doi:10.1016/j.polymer.2020.123366.
159. Gee, S.; Johnson, B.; Smith, A.L. Optimizing Electrospinning Parameters for Piezoelectric PVDF Nanofiber Membranes. *Journal of Membrane Science* **2018**, *563*, 804–812, doi:10.1016/j.memsci.2018.06.050.
160. Saha, S.; Yauvana, V.; Chakraborty, S.; Sanyal, D. Synthesis and Characterization of Polyvinylidene-Fluoride (PVDF) Nanofiber for Application as Piezoelectric Force Sensor. *Materials Today: Proceedings* **2019**, *18*, 1450–1458, doi:10.1016/j.matpr.2019.06.613.
161. Jiyong, H.; Yinda, Z.; Hele, Z.; Yuanyuan, G.; Xudong, Y. Mixed Effect of Main Electrospinning Parameters on the β -Phase Crystallinity of Electrospun PVDF Nanofibers. *Smart Mater. Struct.* **2017**, *26*, 085019, doi:10.1088/1361-665X/aa7245.
162. Ghafari, E.; Lu, N. Self-Polarized Electrospun Polyvinylidene Fluoride (PVDF) Nanofiber for Sensing Applications. *Composites Part B: Engineering* **2019**, *160*, 1–9, doi:10.1016/j.compositesb.2018.10.011.
163. Andrew, J.S.; Clarke, D.R. Effect of Electrospinning on the Ferroelectric Phase Content of Polyvinylidene Difluoride Fibers. *Langmuir* **2008**, *24*, 670–672, doi:10.1021/la7035407.

164. Kalimuldina, G.; Turdakyn, N.; Abay, I.; Medeubayev, A.; Nurpeissova, A.; Adair, D.; Bakenov, Z. A Review of Piezoelectric PVDF Film by Electrospinning and Its Applications. *Sensors* **2020**, *20*, 5214, doi:10.3390/s20185214.
165. Shao, H.; Fang, J.; Wang, H.; Lin, T. Effect of Electrospinning Parameters and Polymer Concentrations on Mechanical-to-Electrical Energy Conversion of Randomly-Oriented Electrospun Poly(Vinylidene Fluoride) Nanofiber Mats. *RSC Adv.* **2015**, *5*, 14345–14350, doi:10.1039/C4RA16360E.
166. Motamedi, A.S.; Mirzadeh, H.; Hajiesmaeilbaigi, F.; Bagheri-Khoulenjani, S.; Shokrgozar, M. Effect of Electrospinning Parameters on Morphological Properties of PVDF Nanofibrous Scaffolds. *Prog Biomater* **2017**, *6*, 113–123, doi:10.1007/s40204-017-0071-0.
167. Zaarour, B.; Zhu, L.; Jin, X. Maneuvering the Secondary Surface Morphology of Electrospun Poly (Vinylidene Fluoride) Nanofibers by Controlling the Processing Parameters. *Mater. Res. Express* **2019**, *7*, 015008, doi:10.1088/2053-1591/ab582d.
168. Ghafari, E.; Jiang, X.; Lu, N. Surface Morphology and Beta-Phase Formation of Single Polyvinylidene Fluoride (PVDF) Composite Nanofibers. *Adv Compos Hybrid Mater* **2018**, *1*, 332–340, doi:10.1007/s42114-017-0016-z.
169. Lei, T.; Zhu, P.; Cai, X.; Yang, L.; Yang, F. Electrospinning of PVDF Nanofibrous Membranes with Controllable Crystalline Phases. *Appl. Phys. A* **2015**, *120*, 5–10, doi:10.1007/s00339-015-9197-x.
170. Huang, F.; Wei, Q.; Wang, J.; Cai, Y.; Huang, Y. Effect of Temperature on Structure, Morphology and Crystallinity of PVDF Nanofibers via Electrospinning. *e-Polymers* **2008**, *8*, doi:10.1515/epoly.2008.8.1.1758.
171. Mohamadi, S.; Sharifi-Sanjani, N. Crystallization of PVDF in Graphene-Filled Electrospun PVDF/PMMA Nanofibers Processed at Three Different Conditions. *Fibers and Polymers* **2016**, *17*, 582–592.
172. Szewczyk, P.K.; Ura, D.P.; Stachewicz, U. Humidity Controlled Mechanical Properties of Electrospun Polyvinylidene Fluoride (PVDF) Fibers. *Fibers* **2020**, *8*, 65, doi:10.3390/fib810065.
173. Zaarour, B.; Zhu, L.; Huang, C.; Jin, X. Controlling the Secondary Surface Morphology of Electrospun PVDF Nanofibers by Regulating the Solvent and Relative Humidity. *Nanoscale Res Lett* **2018**, *13*, 285, doi:10.1186/s11671-018-2705-0.
174. Cozza, E.S.; Monticelli, O.; Marsano, E.; Cebe, P. On the Electrospinning of PVDF: Influence of the Experimental Conditions on the Nanofiber Properties. *Polymer International* **2013**, *62*, 41–48, doi:10.1002/pi.4314.
175. Xin, Y.; Zhu, J.; Sun, H.; Xu, Y.; Liu, T.; Qian, C. A Brief Review on Piezoelectric PVDF Nanofibers Prepared by Electrospinning. *Ferroelectrics* **2018**, *526*, 140–151, doi:10.1080/00150193.2018.1456304.
176. Hwang, K.; Kwon, B.; Byun, H. Preparation of PVdF Nanofiber Membranes by Electrospinning and Their Use as Secondary Battery Separators. *Journal of Membrane Science* **2011**, *378*, 111–116, doi:10.1016/j.memsci.2011.06.005.
177. Lei, T.; Yu, L.; Zheng, G.; Wang, L.; Wu, D.; Sun, D. Electrospinning-Induced Preferred Dipole Orientation in PVDF Fibers. *J Mater Sci* **2015**, *50*, 4342–4347, doi:10.1007/s10853-015-8986-0.
178. Mokhtari, F.; Latifi, M.; Shamshirsaz, M. Electrospinning/Electrospray of Polyvinylidene Fluoride (PVDF): Piezoelectric Nanofibers. *The Journal of The Textile Institute* **2015**, 1–19, doi:10.1080/00405000.2015.1083300.
179. Holmes-Siedle, A.G.; Wilson, P.D.; Verrall, A.P. PVdF: An Electronically-Active Polymer for Industry. *Materials & Design* **1983**, *4*, 910–918, doi:10.1016/0261-3069(84)90003-7.
180. Ueberschlag, P. PVDF Piezoelectric Polymer. *Sensor Review* **2001**, *21*, 118–126, doi:10.1108/02602280110388315.

181. Wang, S.; Bai, Y.; Zhang, T. Chapter 1 - Materials, Systems, and Devices for Wearable Bioelectronics. In *Wearable Bioelectronics*; Parlak, O., Salleo, A., Turner, A., Eds.; Materials Today; Elsevier, 2020; pp. 1–48 ISBN 978-0-08-102407-2.
182. Lang, S.B. IX. Literature Guide to Pyroelectricity 1978-1979. *Ferroelectrics* **1980**, *23*, 133–160, doi:10.1080/00150198008018796.
183. Zhao, J.; Li, F.; Wang, Z.; Dong, P.; Xia, G.; Wang, K. Flexible PVDF Nanogenerator-Driven Motion Sensors for Human Body Motion Energy Tracking and Monitoring. *J Mater Sci: Mater Electron* **2021**, *32*, 14715–14727, doi:10.1007/s10854-021-06027-w.
184. Zhang, D.; Zhang, X.; Li, X.; Wang, H.; Sang, X.; Zhu, G. Enhanced Piezoelectric Performance of PVDF / BiCl₃ / ZnO Nanofiber-Based Piezoelectric Nanogenerator. *European Polymer Journal* **2022**, *166*, 110956–110956, doi:10.1016/j.eurpolymj.2021.110956.
185. Shaikh, M.O.; Huang, Y.-B.; Wang, C.-C.; Chuang, C.-H. Wearable Woven Triboelectric Nanogenerator Utilizing Electrospun PVDF Nanofibers for Mechanical Energy Harvesting. *Micromachines* **2019**, *10*, 438, doi:10.3390/mi10070438.
186. Baytekin, H.T.; Patashinski, A.Z.; Branicki, M.; Baytekin, B.; Soh, S.; Grzybowski, B.A. The Mosaic of Surface Charge in Contact Electrification. *Science* **2011**, *333*, 308–312, doi:10.1126/science.1201512.
187. Cheon, S.; Kang, H.; Kim, H.; Son, Y.; Lee, J.Y.; Shin, H.-J.; Kim, S.-W.; Cho, J.H. High-Performance Triboelectric Nanogenerators Based on Electrospun Polyvinylidene Fluoride–Silver Nanowire Composite Nanofibers. *Advanced Functional Materials* **2018**, *28*, 1703778, doi:10.1002/adfm.201703778.
188. Huang, T.; Wang, C.; Yu, H.; Wang, H.; Zhang, Q.; Zhu, M. Human Walking-Driven Wearable All-Fiber Triboelectric Nanogenerator Containing Electrospun Polyvinylidene Fluoride Piezoelectric Nanofibers. *Nano Energy* **2015**, *14*, 226–235, doi:10.1016/j.nanoen.2015.01.038.
189. Zheng, Y.; Cheng, L.; Yuan, M.; Wang, Z.; Zhang, L.; Qin, Y.; Jing, T. An Electrospun Nanowire-Based Triboelectric Nanogenerator and Its Application in a Fully Self-Powered UV Detector. *Nanoscale* **2014**, *6*, 7842–7846, doi:10.1039/C4NR01934B.
190. Ghosh, S.K.; Sinha, T.K.; Xie, M.; Bowen, C.R.; Garain, S.; Mahanty, B.; Roy, K.; Henkel, K.; Schmeißer, D.; Kim, J.K.; et al. Temperature-Pressure Hybrid Sensing All-Organic Stretchable Energy Harvester. *ACS Applied Electronic Materials* **2021**, *3*, 248–259, doi:10.1021/acsaelm.0c00816.
191. Guo, Y.; Zhang, X.-S.; Wang, Y.; Gong, W.; Zhang, Q.; Wang, H.; Brugger, J. All-Fiber Hybrid Piezoelectric-Enhanced Triboelectric Nanogenerator for Wearable Gesture Monitoring. *Nano Energy* **2018**, *48*, 152–160, doi:10.1016/j.nanoen.2018.03.033.
192. Ghosh, S.K.; Mandal, D. Synergistically Enhanced Piezoelectric Output in Highly Aligned 1D Polymer Nanofibers Integrated All-Fiber Nanogenerator for Wearable Nano-Tactile Sensor. *Nano Energy* **2018**, *53*, 245–257, doi:10.1016/j.nanoen.2018.08.036.
193. Maity, K.; Mandal, D. All-Organic High-Performance Piezoelectric Nanogenerator with Multilayer Assembled Electrospun Nanofiber Mats for Self-Powered Multifunctional Sensors. *ACS Appl. Mater. Interfaces* **2018**, *10*, 18257–18269, doi:10.1021/acsaami.8b01862.
194. Chen, H.; Zhou, L.; Fang, Z.; Wang, S.; Yang, T.; Zhu, L.; Hou, X.; Wang, H.; Wang, Z.L. Piezoelectric Nanogenerator Based on In Situ Growth All-Inorganic CsPbBr₃ Perovskite Nanocrystals in PVDF Fibers with Long-Term Stability. *Advanced Functional Materials* **2021**, *31*, 1–12, doi:10.1002/adfm.202011073.
195. Sengupta, A.; Das, S.; Dasgupta, S.; Sengupta, P.; Datta, P. Flexible Nanogenerator from Electrospun PVDF-Polycarbazole Nanofiber Membranes for Human Motion Energy-Harvesting Device Applications. *ACS Biomaterials Science and Engineering* **2021**, *7*, 1673–1685, doi:10.1021/acsbmaterials.0c01730.
196. Amith, V.; Sridhar, R.; Gangadhar, A.; Vishnumurthy, K.A. Design and Synthesis of PVDF-Cloisite-30B Nanocomposite Fibers for Energy Harvesting Applications. *Surfaces and Interfaces* **2021**, *22*, 100869, doi:10.1016/j.surfin.2020.100869.

197. Sekkarapatti Ramasamy, M.; Rahaman, A.; Kim, B. Influence of Oleylamine–Functionalized Boron Nitride Nanosheets on the Crystalline Phases, Mechanical and Piezoelectric Properties of Electrospun PVDF Nanofibers. *Composites Science and Technology* **2021**, *203*, 108570, doi:10.1016/j.compscitech.2020.108570.
198. Muduli, S.P.; Veeralingam, S.; Badhulika, S. Interface Induced High-Performance Piezoelectric Nanogenerator Based on a Electrospun Three-Phase Composite Nano Fiber for Wearable Applications. **2021**, doi:10.1021/acsam.1c02371.
199. Zhao, Q.; Yang, L.; Ma, Y.; Huang, H.; He, H.; Ji, H.; Wang, Z.; Qiu, J. Highly Sensitive, Reliable and Flexible Pressure Sensor Based on Piezoelectric PVDF Hybrid Film Using MXene Nanosheet Reinforcement. *Journal of Alloys and Compounds* **2021**, *886*, 161069, doi:10.1016/j.jallcom.2021.161069.
200. Shivalingappa, R.T.; Narayana, H.; Narasimha, R.; Purushothaman, P.; Badiger, P.; Savarn, S.; Majumdar, U.; Angadi, G. Development of Poly (Vinylidene Fluoride)/ Silver Nanoparticle Electrospun Nanofiber Mats for Energy Harvesting. **2021**, doi:10.1177/09673911211042005.
201. Zeyrek Ongun, M.; Oguzlar, S.; Kartal, U.; Yurddaskal, M.; Cihanbegendi, O. Energy Harvesting Nanogenerators: Electrospun β -PVDF Nanofibers Accompanying ZnO NPs and ZnO@Ag NPs. *Solid State Sciences* **2021**, *122*, 106772, doi:10.1016/j.solidstatesciences.2021.106772.
202. Hasanzadeh, M.; Ghahhari, M.R.; Bidoki, S.M. Enhanced Piezoelectric Performance of PVDF-Based Electrospun Nanofibers by Utilizing in Situ Synthesized Graphene-ZnO Nanocomposites. *Journal of Materials Science: Materials in Electronics* **2021**, doi:10.1007/s10854-021-06132-w.
203. Shetty, S.; Shanmugaraj, A.M.; Anandhan, S. Physico-Chemical and Piezoelectric Characterization of Electroactive Nanofabrics Based on Functionalized Graphene/Talc Nanolayers/PVDF for Energy Harvesting. *J Polym Res* **2021**, *28*, 419, doi:10.1007/s10965-021-02786-6.
204. Yi, J.; Song, Y.; Cao, Z.; Li, C.; Xiong, C. Gram-Scale Y-Doped ZnO and PVDF Electrospun Film for Piezoelectric Nanogenerators. *Composites Science and Technology* **2021**, *215*, 109011, doi:10.1016/j.compscitech.2021.109011.
205. Ponnar, S.; Schmidt, T.W.; Li, T.; Gunasekaran, H.B.; Ke, X.; Huang, Y.; Mubarak, S.; Anand Prabu, A.; Weng, Z.; Wu, L. Electrospun Polyvinylidene Fluoride-Magnesiocromite Nanofiber-Based Piezoelectric Nanogenerator for Energy Harvesting Applications. *ACS Applied Polymer Materials* **2021**, *3*, 4879–4888, doi:10.1021/acsapm.1c00627.
206. Wang, S.; Shi, K.; Chai, B.; Qiao, S.; Huang, Z.; Jiang, P.; Huang, X. Core-Shell Structured Silk Fibroin/PVDF Piezoelectric Nanofibers for Energy Harvesting and Self-Powered Sensing. *Nano Materials Science* **2021**, doi:10.1016/j.nanoms.2021.07.008.
207. Xue, L.; Fan, W.; Yu, Y.; Dong, K.; Liu, C.; Sun, Y.; Zhang, C.; Chen, W.; Lei, R.; Rong, K.; et al. A Novel Strategy to Fabricate Core-Sheath Structure Piezoelectric Yarns for Wearable Energy Harvesters. *Adv. Fiber Mater.* **2021**, *3*, 239–250, doi:10.1007/s42765-021-00081-z.
208. Bai, Z.; Song, Y.; Peng, J.; Chen, D.; Zhou, Y.; Tao, Y.; Gu, S.; Xu, J.; Deng, Z.; Yin, X.; et al. Poly (Vinylidene Fluoride) Nanofiber Array Films with High Strength for Effective Impact Energy Harvesting. **2021**, *2100345*, 1–8, doi:10.1002/ente.202100345.
209. Du, X.; Zhou, Z.; Zhang, Z.; Yao, L.; Zhang, Q.; Yang, H. Porous, Multi-Layered Piezoelectric Composites Based on Highly Oriented PZT/PVDF Electrospinning Fibers for High-Performance Piezoelectric Nanogenerators. *J Adv Ceram* **2022**, *11*, 331–344, doi:10.1007/s40145-021-0537-3.
210. Maity, K.; Garain, S.; Henkel, K.; Schmeißer, D.; Mandal, D. Self-Powered Human-Health Monitoring through Aligned PVDF Nanofibers Interfaced Skin-Interactive Piezoelectric Sensor. *ACS Applied Polymer Materials* **2020**, *2*, 862–878, doi:10.1021/acsapm.9b00846.
211. Mahanty, B.; Ghosh, S.K.; Jana, S.; Mallick, Z.; Sarkar, S.; Mandal, D. ZnO Nanoparticle Confined Stress Amplified All-Fiber Piezoelectric Nanogenerator for Self-Powered Healthcare Monitoring. *Sustainable Energy Fuels* **2021**, *5*, 4389–4400, doi:10.1039/D1SE00444A.

212. Peng, X.L.M.W.H.; Zhang, X.; Ting, Y.; Li, W.T.; Lou, C.; Lin, J. Hierarchically Structured Polyvinylidene Fluoride Core-Shell Composite Yarn Based on Electrospinning Coating Method to Improve Piezoelectricity. **2022**, 1–11, doi:10.1002/pat.5613.
213. Yen, C.-K.; Dutt, K.; Yao, Y.-S.; Wu, W.-J.; Shiue, Y.-L.; Pan, C.-T.; Chen, C.-W.; Chen, W.-F. Development of Flexible Biceps Tremors Sensing Chip of PVDF Fibers with Nano-Silver Particles by Near-Field Electrospinning. *Polymers* **2022**, *14*, 331, doi:10.3390/polym14020331.
214. Li, T.; Qu, M.; Carlos, C.; Gu, L.; Jin, F.; Yuan, T.; Wu, X.; Xiao, J.; Wang, T.; Dong, W.; et al. High-Performance Poly(Vinylidene Difluoride)/Dopamine Core/Shell Piezoelectric Nanofiber and Its Application for Biomedical Sensors. *Advanced Materials* **2021**, *33*, 2006093, doi:10.1002/adma.202006093.
215. Zhao, J.; Li, F.; Wang, Z.; Dong, P.; Xia, G.; Wang, K. Flexible PVDF Nanogenerator-Driven Motion Sensors for Human Body Motion Energy Tracking and Monitoring. *J Mater Sci: Mater Electron* **2021**, *32*, 14715–14727, doi:10.1007/s10854-021-06027-w.
216. Demirci, D.; Koç, M.; Aktürk, S. Piezoelectric and Magnetoelectric Properties of PVDF / NiFe₂O₄ Based Electrospun Nanofibers for Flexible Piezoelectric Nanogenerators. **2022**, *36*, 143–159, doi:10.1016/j.cap.2022.01.013.
217. Mondal, S.; Paul, T.; Maiti, S.; Das, B.K.; Chattopadhyay, K.K. Human Motion Interactive Mechanical Energy Harvester Based on All Inorganic Perovskite-PVDF. *Nano Energy* **2020**, *74*, 104870–104870, doi:10.1016/j.nanoen.2020.104870.
218. Yang, J.; Zhang, Y.; Li, Y.; Wang, Z.; Wang, W.; An, Q.; Tong, W. Piezoelectric Nanogenerators Based on Graphene Oxide/PVDF Electrospun Nanofiber with Enhanced Performances by In-Situ Reduction. *Materials Today Communications* **2021**, *26*, doi:10.1016/j.mtcomm.2020.101629.
219. He, W.; Guo, Y.; Zhao, Y.B.; Jiang, F.; Schmitt, J.; Yue, Y.; Liu, J.; Cao, J.; Wang, J. Self-Supporting Smart Air Filters Based on PZT/PVDF Electrospun Nanofiber Composite Membrane. *Chemical Engineering Journal* **2021**, *423*, 130247, doi:10.1016/j.cej.2021.130247.
220. Mousa, H.M.; Fahmy, H.S.; Abouzeid, R.; Abdel-Jaber, G.T.; Ali, W.Y. Polyvinylidene Fluoride-Cellulose Nanocrystals Hybrid Nanofiber Membrane for Energy Harvesting and Oil-Water Separation Applications. *Materials Letters* **2022**, *306*, 130965, doi:10.1016/j.matlet.2021.130965.
221. Li, T.; Jin, F.; Qu, M.; Yang, F.; Zhang, J.; Yuan, T.; Dong, W.; Zheng, J.; Wang, T.; Feng, Z.-Q. Power Generation from Moisture Fluctuations Using Polyvinyl Alcohol-Wrapped Dopamine/Polyvinylidene Difluoride Nanofibers. *Small* **2021**, *17*, 2102550, doi:10.1002/smll.202102550.
222. Lu, H.; Zhang, J.; Yang, L.; Zhang, Y.; Wu, Y.; Zheng, H. Enhanced Output Performance of Piezoelectric Nanogenerators by Tb-Modified (BaCa)(ZrTi)O₃ and 3D Core/Shell Structure Design with PVDF Composite Spinning for Microenergy Harvesting. *ACS Appl. Mater. Interfaces* **2022**, *14*, 12243–12256, doi:10.1021/acsami.1c23946.
223. Mahanty, B.; Ghosh, S.K.; Jana, S.; Roy, K.; Sarkar, S.; Mandal, D. All-Fiber Acousto-Electric Energy Harvester from Magnesium Salt-Modulated PVDF Nanofiber. *Sustainable Energy and Fuels* **2021**, *5*, 1003–1013, doi:10.1039/d0se01185a.
224. Roy, K.; Jana, S.; Mallick, Z.; Ghosh, S.K.; Dutta, B.; Sarkar, S.; Sinha, C.; Mandal, D. Two-Dimensional MOF Modulated Fiber Nanogenerator for Effective Acoustoelectric Conversion and Human Motion Detection. *Langmuir* **2021**, *37*, 7107–7117, doi:10.1021/acs.langmuir.1c00700.
225. Xu, F.; Yang, J.; Dong, R.; Jiang, H.; Wang, C.; Liu, W.; Jiang, Z. Wave - Shaped Piezoelectric Nanofiber Membrane Nanogenerator for Acoustic Detection and Recognition. *Advanced Fiber Materials* **2021**, *3*, 368–380, doi:10.1007/s42765-021-00095-7.
226. Li, H.; Koh, C.S.L.; Lee, Y.H.; Zhang, Y.; Phan-Quang, G.C.; Zhu, C.; Liu, Z.; Chen, Z.; Sim, H.Y.F.; Lay, C.L.; et al. A Wearable Solar-Thermal-Pyroelectric Harvester: Achieving High Power

- Output Using Modified RGO-PEI and Polarized PVDF. *Nano Energy* **2020**, *73*, 104723, doi:10.1016/j.nanoen.2020.104723.
227. Leng, Q.; Chen, L.; Guo, H.; Liu, J.; Liu, G.; Hu, C.; Xi, Y. Harvesting Heat Energy from Hot/Cold Water with a Pyroelectric Generator. *J. Mater. Chem. A* **2014**, *2*, 11940–11947, doi:10.1039/C4TA01782J.
 228. Wu, C.M.; Chou, M.H.; Chala, T.F.; Shimamura, Y.; Ichi Murakami, R. Infrared-Driven Poly(Vinylidene Difluoride)/Tungsten Oxide Pyroelectric Generator for Non-Contact Energy Harvesting. *Composites Science and Technology* **2019**, *178*, 26–32, doi:10.1016/j.compscitech.2019.05.004.
 229. Gokana, M.R.; Wu, C.-M.; Matora, K.G.; Qi, J.Y.; Yen, W.-T. Effects of Patterned Electrode on near Infrared Light-Triggered Cesium Tungsten Bronze/Poly(Vinylidene)Fluoride Nanocomposite-Based Pyroelectric Nanogenerator for Energy Harvesting. *Journal of Power Sources* **2022**, *536*, 231524, doi:10.1016/j.jpowsour.2022.231524.
 230. Lee, J.P.; Lee, J.W.; Baik, J.M. The Progress of PVDF as a Functional Material for Triboelectric Nanogenerators and Self-Powered Sensors. *Micromachines* **2018**, *9*, 532, doi:10.3390/mi9100532.
 231. Shaikh, M.O.; Huang, Y.-B.; Wang, C.-C.; Chuang, C.-H. Wearable Woven Triboelectric Nanogenerator Utilizing Electrospun PVDF Nanofibers for Mechanical Energy Harvesting. *Micromachines* **2019**, *10*, 438, doi:10.3390/mi10070438.
 232. Cheon, S.; Kang, H.; Kim, H.; Son, Y.; Lee, J.Y.; Shin, H.-J.; Kim, S.-W.; Cho, J.H. High-Performance Triboelectric Nanogenerators Based on Electrospun Polyvinylidene Fluoride–Silver Nanowire Composite Nanofibers. *Advanced Functional Materials* **2018**, *28*, 1703778, doi:10.1002/adfm.201703778.
 233. Zheng, Y.; Cheng, L.; Yuan, M.; Wang, Z.; Zhang, L.; Qin, Y.; Jing, T. An Electrospun Nanowire-Based Triboelectric Nanogenerator and Its Application in a Fully Self-Powered UV Detector. *Nanoscale* **2014**, *6*, 7842–7846, doi:10.1039/C4NR01934B.
 234. Chen, F.; Wu, Y.; Ding, Z.; Xia, X.; Li, S.; Zheng, H.; Diao, C.; Yue, G.; Zi, Y. A Novel Triboelectric Nanogenerator Based on Electrospun Polyvinylidene Fluoride Nanofibers for Effective Acoustic Energy Harvesting and Self-Powered Multifunctional Sensing. *Nano Energy* **2019**, *56*, 241–251, doi:10.1016/j.nanoen.2018.11.041.
 235. Bhatta, T.; Maharjan, P.; Cho, H.; Park, C.; Yoon, S.H.; Sharma, S.; Salauddin, M.; Rahman, M.T.; Rana, S.S.; Park, J.Y. High-Performance Triboelectric Nanogenerator Based on MXene Functionalized Polyvinylidene Fluoride Composite Nanofibers. *Nano Energy* **2021**, *81*, 105670, doi:10.1016/j.nanoen.2020.105670.
 236. Sun, C.; Zu, G.; Wei, Y.; Song, X.; Yang, X. Flexible Triboelectric Nanogenerators Based on Electrospun Poly (Vinylidene Fluoride) with MoS₂ / Carbon Nanotube Composite Nanofibers. **2022**, doi:10.1021/acs.langmuir.1c02785.
 237. Li, W.; Sengupta, D.; Pei, Y.; Giri, A.; Kottapalli, P. Wearable Nanofiber-Based Triboelectric Nanogenerator for Body Motion Energy Harvesting. **2021**, 18–21.
 238. Huang, J.; Hao, Y.; Zhao, M.; Li, W.; Huang, F.; Wei, Q. All-Fiber-Structured Triboelectric Nanogenerator via One-Pot Electrospinning for Self-Powered Wearable Sensors. *ACS Appl. Mater. Interfaces* **2021**, *13*, 24774–24784, doi:10.1021/acsami.1c03894.
 239. Sun, X.; Feng, Y.; Wang, B.; Liu, Y.; Wu, Z.; Yang, D.; Zheng, Y.; Peng, J.; Feng, M.; Wang, D. A New Method for the Electrostatic Manipulation of Droplet Movement by Triboelectric Nanogenerator. *Nano Energy* **2021**, *86*, 106115, doi:10.1016/j.nanoen.2021.106115.
 240. Zhang, Q.; Mu, J.; Mu, J.; Yang, X.; Zhang, S.; Han, X.; Zhao, Y.; You, Y.; Yu, J.; Chou, X. A Design of Flexible Triboelectric Generator Integrated with High-Efficiency Energy Storage Unit. *Energy Technology* **2021**, *9*, 2000962, doi:10.1002/ente.202000962.
 241. Busolo, T.; Szweczyk, P.K.; Nair, M.; Stachewicz, U.; Kar-Narayan, S. Triboelectric Yarns with Electrospun Functional Polymer Coatings for Highly Durable and Washable Smart Textile

- Applications. *ACS Appl. Mater. Interfaces* **2021**, *13*, 16876–16886, doi:10.1021/acsami.1c00983.
242. Sun, N.; Wang, G.; Zhao, H.; Cai, Y.; Li, J.; Li, G. Nano Energy Waterproof , Breathable and Washable Triboelectric Nanogenerator Based on Electrospun Nanofiber Films for Wearable Electronics. *Nano Energy* **2021**, *90*, 106639–106639, doi:10.1016/j.nanoen.2021.106639.
 243. Tao, X.; Zhou, Y.; Qi, K.; Guo, C.; Dai, Y.; He, J.; Dai, Z. Journal of Colloid and Interface Science Wearable Textile Triboelectric Generator Based on Nanofiber Core-Spun Yarn Coupled with Electret Effect. *Journal of Colloid And Interface Science* **2022**, *608*, 2339–2346, doi:10.1016/j.jcis.2021.10.151.
 244. Cheng, Y.; Zhu, W.; Lu, X.; Wang, C. Mechanically Robust, Stretchable, Autonomously Adhesive, and Environmentally Tolerant Triboelectric Electronic Skin for Self-Powered Healthcare Monitoring and Tactile Sensing. *Nano Energy* **2022**, *102*, 107636, doi:10.1016/j.nanoen.2022.107636.
 245. He, H.; Guo, J.; Illés, B.; Géczy, A.; Istók, B.; Hliva, V.; Török, D.; Kovács, J.G.; Harmati, I.; Molnár, K. Monitoring Multi-Respiratory Indices via a Smart Nanofibrous Mask Filter Based on a Triboelectric Nanogenerator. *Nano Energy* **2021**, *89*, 106418, doi:10.1016/j.nanoen.2021.106418.
 246. Bhatta, T.; Maharjan, P.; Shrestha, K.; Lee, S.; Rahman, M.T.; Rana, S.M.S.; Sharma, S.; Park, C.; Yoon, S.H.; Park, J.Y. A Hybrid Self-Powered Arbitrary Wave Motion Sensing System for Real-Time Wireless Marine Environment Monitoring Application. **2022**, *2102460*, 1–14, doi:10.1002/aenm.202102460.
 247. Yang, D.; Feng, Y.; Wang, B.; Liu, Y.; Zheng, Y.; Sun, X.; Peng, J.; Feng, M.; Wang, D. Nano Energy An Asymmetric AC Electric Field of Triboelectric Nanogenerator for Efficient Water / Oil Emulsion Separation. *Nano Energy* **2021**, *90*, 106641–106641, doi:10.1016/j.nanoen.2021.106641.
 248. Sultana, A.; Ghosh, S.K.; Alam, Md.M.; Sadhukhan, P.; Roy, K.; Xie, M.; Bowen, C.R.; Sarkar, S.; Das, S.; Middya, T.R.; et al. Methylammonium Lead Iodide Incorporated Poly(Vinylidene Fluoride) Nanofibers for Flexible Piezoelectric–Pyroelectric Nanogenerator. *ACS Appl. Mater. Interfaces* **2019**, *11*, 27279–27287, doi:10.1021/acsami.9b04812.
 249. Mahanty, B.; Ghosh, S.K.; Maity, K.; Roy, K.; Sarkar, S.; Mandal, D. All-Fiber Pyro- And Piezo-Electric Nanogenerator for IoT Based Self-Powered Health-Care Monitoring. *Materials Advances* **2021**, *2*, 4370–4379, doi:10.1039/d1ma00131k.
 250. Wang, Y.; Zhu, M.; Wei, X.; Yu, J.; Li, Z.; Ding, B. A Dual-Mode Electronic Skin Textile for Pressure and Temperature Sensing. *Chemical Engineering Journal* **2021**, *425*, 130599, doi:10.1016/j.cej.2021.130599.
 251. Xia, G.; Huang, Y.; Li, F.; Wang, L.; Pang, J.; Li, L.; Wang, K. A Thermally Flexible and Multi-Site Tactile Sensor for Remote 3D Dynamic Sensing Imaging. *Front. Chem. Sci. Eng.* **2020**, *14*, 1039–1051, doi:10.1007/s11705-019-1901-5.
 252. Li, X.; Ji, D.; Yu, B.; Ghosh, R.; He, J.; Qin, X.; Ramakrishna, S. Boosting Piezoelectric and Triboelectric Effects of PVDF Nanofiber through Carbon-Coated Piezoelectric Nanoparticles for Highly Sensitive Wearable Sensors. *Chemical Engineering Journal* **2021**, *426*, 130345, doi:10.1016/j.cej.2021.130345.
 253. Yu, Z.; Chen, M.; Wang, Y.; Zheng, J.; Zhang, Y.; Zhou, H.; Li, D. Nanoporous PVDF Hollow Fiber Employed Piezo-Tribo Nanogenerator for Effective Acoustic Harvesting. *ACS Applied Materials and Interfaces* **2021**, *13*, 26981–26988, doi:10.1021/acsami.1c04489.
 254. Niu, H.; Zhou, H.; Shao, H.; Wang, H.; Ding, X.; Bai, R.; Lin, T. Nano Energy Energy Generation from Airborne Noise : Improving Electrical Outputs of Single-Layer Polyvinylidene Difluoride Nanofiber Membranes by Incorporating a Small Number of Nylon-6 Nanofibers. *Nano Energy* **2021**, *90*, 106618–106618, doi:10.1016/j.nanoen.2021.106618.
 255. Klapstova, A.; Horakova, J.; Tunak, M.; Shynkarenko, A.; Erben, J.; Hlavata, J.; Bulir, P.; Chvojka, J. A PVDF Electrospun Antifibrotic Composite for Use as a Glaucoma Drainage

- Implant. *Materials Science and Engineering: C* **2021**, *119*, 111637, doi:10.1016/j.msec.2020.111637.
256. Agueda, J.R.S.; Madrid, J.; Mondragon, J.M.; Lim, J.; Tan, A.; Wang, I.; Duguran, N.; Bondoc, A. Synthesis and Characterization of Electrospun Polyvinylidene Fluoride-Based (PVDF) Scaffolds for Renal Bioengineering. *J. Phys.: Conf. Ser.* **2021**, *2071*, 012005, doi:10.1088/1742-6596/2071/1/012005.
257. Rajamohan, R.; Sillanpää, M.; Subramania, A. Electrospun Polyvinylidene Fluoride Nanofibrous Mats as the Carrier for Drug Delivery System of Benzocaine and Its Complex with β -Cyclodextrin. *Journal of Molecular Liquids* **2021**, *341*, 117411, doi:10.1016/j.molliq.2021.117411.
258. Victor, F.S.; Kugarajah, V.; Bangaru, M.; Ranjan, S.; Dharmalingam, S. Electrospun Nanofibers of Polyvinylidene Fluoride Incorporated with Titanium Nanotubes for Purifying Air with Bacterial Contamination. *Environ Sci Pollut Res* **2021**, *28*, 37520–37533, doi:10.1007/s11356-021-13202-3.
259. Shuai, D. Development of Electrospun Nanofibrous Filters for Controlling Coronavirus Aerosols. 17.
260. Pascariu, P.; Cojocaru, C.; Samoila, P.; Olaru, N.; Bele, A.; Airinei, A. Novel Electrospun Membranes Based on PVDF Fibers Embedding Lanthanide Doped ZnO for Adsorption and Photocatalytic Degradation of Dye Organic Pollutants. *Materials Research Bulletin* **2021**, *141*, 111376, doi:10.1016/j.materresbull.2021.111376.
261. Yang, Y.; Li, L.; Zhang, Q.; Chen, W.; Lin, S.; Wang, Z.; Li, W. Enhanced Coalescence Separation of Oil-in-Water Emulsions Using Electrospun PVDF Nanofibers. *Chinese Journal of Chemical Engineering* **2021**, *38*, 76–83, doi:10.1016/j.cjche.2020.08.037.
262. Tessema, A.A.; Wu, C.-M.; Matora, K.G.; Naseem, S. Highly-Efficient and Salt-Resistant CsxWO₃@g-C₃N₄/PVDF Fiber Membranes for Interfacial Water Evaporation, Desalination, and Sewage Treatment. *Composites Science and Technology* **2021**, *211*, 108865, doi:10.1016/j.compscitech.2021.108865.
263. Bicy, K.; Gueye, A.B.; Rouxel, D.; Kalarikkal, N.; Thomas, S. Lithium-Ion Battery Separators Based on Electrospun PVDF: A Review. *Surfaces and Interfaces* **2022**, *31*, 101977, doi:10.1016/j.surfin.2022.101977.
264. Barbosa, J.C.; Correia, D.M.; Gonçalves, R.; de Zea Bermudez, V.; Silva, M.M.; Lanceros-Mendez, S.; Costa, C.M. Enhanced Ionic Conductivity in Poly(Vinylidene Fluoride) Electrospun Separator Membranes Blended with Different Ionic Liquids for Lithium Ion Batteries. *Journal of Colloid and Interface Science* **2021**, *582*, 376–386, doi:10.1016/j.jcis.2020.08.046.
265. Qian, J.; Zhang, Z.-M.; Bao, R.-Y.; Liu, Z.-Y.; Yang, M.-B.; Yang, W. Lightweight Poly (Vinylidene Fluoride)/Silver Nanowires Hybrid Membrane with Different Conductive Network Structure for Electromagnetic Interference Shielding. *Polymer Composites* **2021**, *42*, 522–531, doi:10.1002/pc.25844.
266. Rose, A.; P A, F.; S Mural, P.K.; Chandran, A.M. *A Carbon Doped Electrospun Nano Fibre for Effective Emi Shielding*; Social Science Research Network: Rochester, NY, 2021;

)